Oxidative dehydrogenation of hydrocarbons over mixed metal oxides

Thesis Submitted to AcSIR for the award of the

Degree of

Doctor of Philosophy

in

Chemical Sciences

By

Ashok Kumar V

AcSIR No. 10CC11A26050

Under the guidance of

Dr. Thirumalaiswamy Raja

CSIR-National Chemical Laboratory,

Pune-411008

सीएसआयआर–राष्ट्रीय रासायनिक प्रयोगशाला
(वैज्ञानिक तथा औद्योगिक अनुसंधान परिषद)
डॉ. होमी भाभा मार्ग, पुणे – 411 008. भारत
CSIR-NATIONAL CHEMICAL LABORATORY
(Council of Scientific & Industrial Research)
Dr. Homi Bhabha Road, Pune - 411008. India

CERTIFICATE

This is to certify that the work incorporated in this Ph.D. thesis entitled "***Oxidative dehydrogenation of hydrocarbons over mixed metal oxides***" submitted by **Mr. Ashok Kumar V** to Academy of Scientific and Innovative Research (AcSIR) in fulfillment of the requirements for the award of the degree of ***Doctor of Philosophy***, in ***Chemical Sciences***, embodies original research work under my supervision. I further certify that this work has not been submitted to any other University or Institution in part or full for the award of any degree or diploma. Research material obtained from other sources has been duly acknowledged in the thesis. Any text, illustration, table etc., used in the thesis from other sources, have been duly cited and acknowledged.

Ashok Kumar V
(Student)

Dr. T. Raja
(Supervisor)

Communication Channels
NCL Level DID : 2590
NCL Board No. : +91-20-25902000
EPABX : +91-20-25893300
: +91-20-25893400
FAX
Director's Office : +91-20-25902601
COA's Office : +91-20-25902660
COS&P's Office : +91-20-25902664
WEBSITE
www.ncl-india.org

DECLARATION

I, **Ashok Kumar V**, hereby declare that this Ph.D. thesis entitled "***Oxidative dehydrogenation of hydrocarbons over mixed metal oxides***" was carried out by me for the degree of Doctor of Philosophy in Chemical Sciences under the guidance and supervision of Dr. T. Raja, CSIR-National Chemical Laboratory, Pune, India.

I confirm that:

- this work was done wholly by me while in candidature for a research degree at this institution.
- no part of this thesis has previously been submitted for a degree or any other qualification at this institution or any other institution.
- the interpretations put forth are based on my reading and understanding of the original articles and all sources have been duly acknowledged.

V. Ashok

Ashok Kumar V

Research Scholar

Place : PUNE

Date : 07/03/2017

Dedicated to my

Amma and Appa...

Acknowledgements…..

The completion of this thesis is credited to the support and encouragement of numerous people encompassing my family members, friends, colleagues and well wishers. At this point of accomplishment I am privileged to acknowledge all those people who made this thesis possible. It is a pleasant task to reciprocate to the ones who contributed in many ways to the success of this study.

First and foremost, I would like to express my heartfelt and sincere gratitude to my research supervisor **Dr. T. Raja** who gave an invaluable guidance and unconditional support. His constant inspiration and constructive criticism helped me enormously to focus my views in proper perspective. He gave me the freedom to think and work and I shall cherish my learning experience under his guidance. I take this opportunity to express my deepest sense of gratitude and respect towards him for guiding me in the right direction throughout the research tenure.

I extend my sincere thanks to the Director of CSIR-NCL Prof. Ashwini Kumar Nangia, Dr. Sourav Pal (former director) and Dr. D. Srinivas (Chairman, Catalysis Division) for providing me the opportunity to accomplish my research work in this prestigious and well-equipped laboratory. My thanks to Dr. C.V.V. Satyanarayana, Dr. C.S. Gopinath ,Dr. R. Nandini Devi, , Dr. A. T. Biju, Ms. Violet Samuel, and all other scientific and non-scientific staff for their help and support in scientific and technical matters during my tenure as a research student. I take this occasion to thank all my teachers, well-wishers classmates and friends in various stages for their teachings, love, encouragement, kind cooperation and good wishes that I received from them.

I have high regards for Aswathy T V who was my first trainee and with whose support my whole Ph.D work sailed through. I would also like to acknowledge my present and past labmates Manikandan, Prabu[2],Periz, Fahima, Gayathri, Divya, Sruthy, Mudassir,Sumathi akka Prasad, Fawaz, Aditya, Ashamsa for their immense help and support. I would also like to extend my regards to my friends Sreedhala, Anju, Mohan, Lenin, Lakshmi, Pradnya, Suman, Shiva, Trinath for their love and encouragement. Also, I sincerely thank all my divisional friends - Anish and CPV group, CVVS group, CSG group, RND group, NCML group, snacks-Subni for their timely help.

I sincerely thank my seniors Sivaranjini, Senthil, Edwin, Khaja anna, Kanna, Chaitanya, Venu, Devadutta, Rajesh, Hanumant, Prabu and Atul. I would also like to thank Tamil gang, Telugu gang ,all my friends (though I would have missed some) and well wishers in NCL for creating a congenial atmosphere for doing research. I also would like to thank my M.Sc, B.Sc and school friends for their support and encouragement.

My high regards and respect to my parents for their unconditional love and support even when we were in hard situations. It gives me great pleasure to thank them for their love, sacrifice, moral support, blessings, care and constant encouragement that they have shown to me. I would extend my respect and indeed indebted to Anand because of whom I was able to do Ph.D and special thanks to Abi and kavi. I would extend my thanks to my cousins and their family for their love and encouragement.

Above all, I owe it all to Almighty God for granting the wisdom, health and belief to undertake research work for my thesis and enabling me to its completion.

Ashok Kumar V

Table of contents

Chapter 2 : Experimental methods and characterization techniques

Chapter 3: Oxidative dehydrogenation of ethane to ethene over Manganese substituted $Ca(Sr)TiO_3$ perovskite type oxides

Chapter 4 : Oxidative dehydrogenation of ethyl benzene (EB) to styrene (ST)

Chapter 5 : Oxidative dehydrogenation of 1-butene to 1,3-butadiene

List of Figures

List of Tables

List of Abbreviations

HTlcs	Hydrotalcites
PXRD	Powder X-ray diffraction
SEM	Scanning electron microscopy
TEM	Transmission electron microscopy
XPS	X-ray photoelectron spectroscopy
TPD	Temperature programmed desorption
GC	Gas chromatography
FID	Flame ionization detector
TCD	Thermal conductivity detector
BET	Brunauer-Emmett-Teller
EDAX	Energy dispersive X-ray analysis
EB	Ethyl benzene
ST	Styrene
ODH	Oxidative dehydrogenation
TGA	Thermogravimetric analysis
JCPDS	Joint Committee on Powder Diffraction Standards
ICSD	Inorganic crystal structure data
BD	1,3-butadiene
atm. pressure	Atmospheric pressure

Chapter 1

Introduction

1.1. Introduction: Catalysis

In early 19th century when the industrial revolution started there was a huge concern about the control of a chemical reaction. Almost all industrial reactions were carried out at higher temperature and pressure which sometime caused the degradation of reactants as well as energy loss. The major aim was to achieve maximum output of products at milder reaction conditions for the ease of operation. Thus *catalyst* came into the frame of study. J. J. Berzelius, a Swedish chemist, first coined the term catalysis in 1836 after which Redeal and Taylor translated it in English.[1] Later it was Ostwald who was one of the pioneers in chemical thermodynamics, brought in thermodynamics for defining a catalyst where he stated that catalyst is a material that will leave the equilibrium of a reaction unchanged.[2] According to International Union of Pure and Applied Chemistry (IUPAC), catalyst increases the rate of the reaction without modifying the overall standard Gibbs Energy change in the reaction.[3]

The broad regime catalysis is divided into two major categories which are i) Homogeneous catalysis, where catalyst and the reactant molecule will be in same phase and ii) Heterogeneous catalysis, where catalyst and the reactant molecule will be in different phase. Adsorption is the key phenomenon in heterogeneous catalysis and on the catalytic surface there are several sites called active centres, in which adsorption taking place. Majority of the industrial processes employ heterogeneous catalysts as the separation of catalyst from the reaction medium. By the end of nineteenth century the concept of catalysis from academia transferred to industrial processes. The demand for bulk chemicals increased with a focus on reducing the by-products by catalysis which had tremendous economic advantages.[4] In the earlier 20th century the commercial applications of catalysis were done without a firm grasp of the science and principles like equilibrium. When the fundamentals of catalysis were understood majority of the chemical industries started depending upon the catalysts for production of inorganic chemicals such as sulphuric acid, ammonia, and nitric acid. Although the interest was driven by the need for NH_3 as a component in production of agricultural fertilizer also especially for manufacturing

explosives in World War I. Later the usage of catalysts was probed much deeper in socio-economic pathways to minimize the wastage generated.[5] Almost after a century in ammonia synthesis which is now widely applied at very large scale, the molecular basis of catalytic processes has been understood by works of Gerhard Ertl. Later in the mid of 20th century various catalytic processes were developed which includes selective hydrogenation, hydrogenolysis, dehydrogenation, oxidation, isomerization, polymerization. These developments emphasized that catalysis is ubiquitous and the backbone of various chemical synthesis which led to our societal prosperity.

1.2. Dehydrogenation of hydrocarbons

Olefins are the building blocks for the synthesis of variety of polymers and consequently for the production of numerous number of commodities and specialties for day today life. A major part of today's olefin is produced by steam and thermal cracking of respective hydrocarbon or petroleum products. In present day context the worldwide production of olefins is by three processes; they are i) thermal cracking (pyrolysis or steam cracking), ii) catalytic cracking and iii) catalytic dehydrogenation. These processes are highly endothermic and possess thermodynamic limitations.

1.2.1. Steam Cracking

Around 90 % of current olefin production is from thermal cracking of respective hydrocarbon or LPG and naphtha, in which the common process employing steam is referred as pyrolysis or steam cracking. The main products that are obtained in this process are ethene, propene and to some extent higher olefins. The typical dehydrogenation setup[6] is shown in **Fig. 1.1**

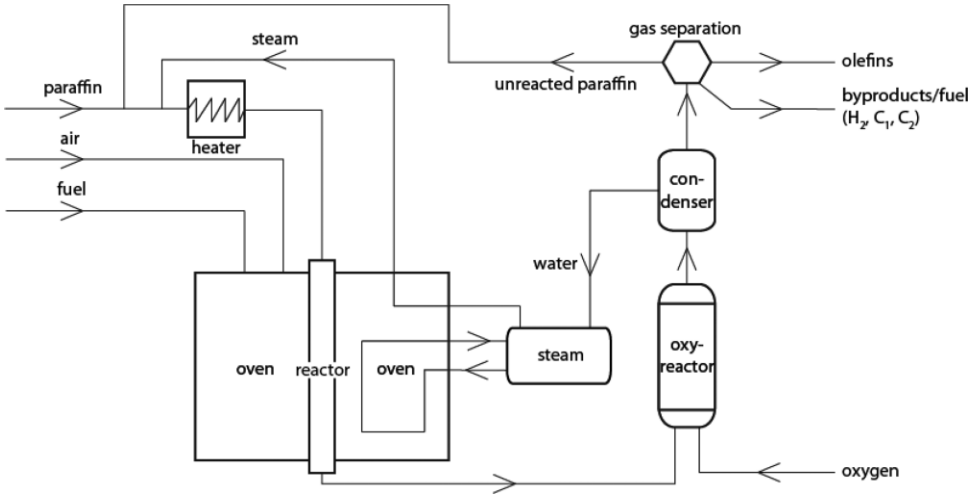

Fig. 1.1. A typical Steam cracking setup

The stream of hydrocarbons and steam are preheated in a convection section. The preheated stream of hydrocarbon is passed through a fired tubular reactor where at desired/controlled reaction parameters like residence time, temperature, and partial pressure, hydrocarbon is cracked. Usually it is heated at the temperature range of 500 - 650 °C to 750 - 875 °C for few milliseconds of contact time and the hydrocarbons in the feedstock are cracked into smaller molecule.

1.2.2. Fluidized catalytic cracking

Fluidized catalytic cracking **(**FCC) is the most common catalytic cracking process. In this process, in a fast moving gas stream, the catalyst powder which by virtue of its inherent properties behaves like a fluid and will be raised in fluidized form through the system. **Fig. 1.2** is the schematic profile of typical FCC process. In this, the catalyst flows down from the regenerator which is combined with feed and steam and elevated up through the riser into the reactor and fluidized by hydrocarbon vapors. The catalyst coming out after reaction is directed towards stripper followed by regenerator where it is regenerated by combustion gases.[6]

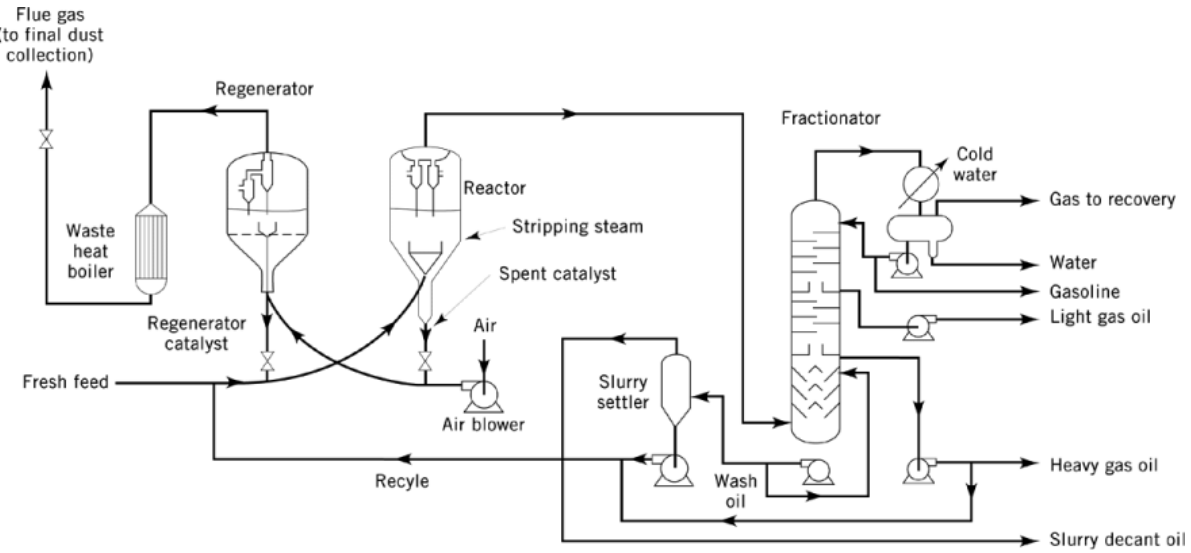

Fig. 1.2. A typical FCC setup used for cracking hydrocarbons

1.2.3. Catalytic dehydrogenation

Dehydrogenation is a typical endothermic equilibrium reaction which is mostly catalyzed by a noble- or toxic heavy-metal catalyst. By the principles of thermodynamics, elevated temperatures and low pressures increase olefin yield. In other hand high process temperatures invariably cause pyrolysis (cracking) of hydrocarbon to coke in addition to olefin. As a consequence of this there is a possibility of feedstock wastage and the coke formed induce rapid catalyst deactivation.

The dehydrogenation of alkane is one of the most complex chemical processes to realize industrially as the thermodynamic equilibrium affects the conversion per pass and due to endothermic nature of this process large amount of heat must be supplied to the reactant system. **Fig. 1.3.** shows the temperature required for equilibrium conversion of alkanes. It is clearly evident that temperatures between 500 and above 700 °C are needed to reach a conversion rate of 50 % in case of short chain alkanes.[7] Moreover high temperatures also enhance an undesired parallel process, i.e., thermal cracking reactions that reduce the selectivity to the desired product.

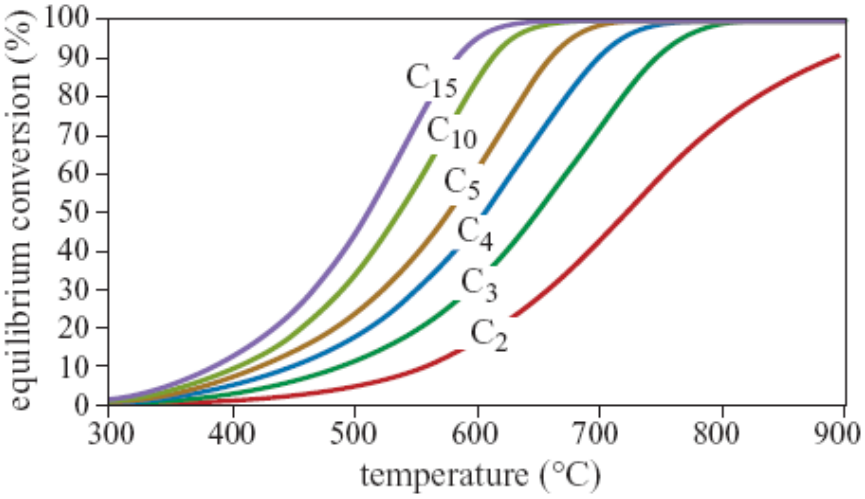

Fig. 1.3. Equilibrium conversion as a function of reaction temperature

1.3. Oxidative dehydrogenation

Oxidative dehydrogenation is usually carried out in the presence of an oxidant or in other words a hydrogen acceptor such as molecular oxygen. This process has the budding advantages to surpass the major technical glitches associated with pure dehydrogenation.[8] In this process there are two added advantages: (1) by the principle of law of mass action as the equilibrium concentration is driven towards products the conversion of reactants to products is increased; (2) the added exothermicity during water formation supplies the needed heat of reaction. Even though it is advantageous over normal dehydrogenation it suffers from technical drawbacks like, i) runaway reactions-like over oxidation and oxygenated intermediates which reduce the overall selectivity, ii) the flammability limits is an important factor which restricts the flow parameters of the reactants and iii) difficulty in removal of the heat of reaction which form hotspots. Till date there are no commercial plants for the oxidative dehydrogenation of hydrocarbons although pilot or demonstration plants have been built and operated.[9] ODH provides an improved energy

efficiency as it is exothermic, while dehydrogenation and cracking are endothermic and process simplicity are effective incentives. To demonstrate the effectiveness of the process with an example, the production of acrylonitrile from propane - a yield of 60 % is sufficient to obtain a cost equivalency with the current technology from propylene (due to the difference in cost between propane and propylene), and also the propylene synthesis by propane ODH should provide better olefin yields than those obtained with current technologies.[8] The present scenario for ODH reactions are given in the table below.[10]

Hydrocarbon	Product	Stage of development
Ethane	1,2-Dichloroethane Vinyl chloride	Pilot scale
Ethane	Acetaldehyde	Lab scale
Ethane	Ethanoic acid	Lab scale
Ethane	Ethene	Lab scale
Propane	Propenal, acrylic acid	Lab scale
Propane	Propanol	Lab scale
Propane	Acrylonitrile	Demonstrative plant
Propane	propene	Lab scale
n-Butane	Ethanoic acid	Lab scale
n-Butane	Maleic anhydride	Lab scale
n-Butane	1,3- Butadiene	Industrial abandoned

Table. 1.1. State of art of ODH processes worldwide

1.3.1. Catalyst system selection and their workability

The catalysts that are been employed for ODH of hydrocarbons can be divided into three broad regimes they are,[9]

1. Metal oxides with redox sites (obviously, d-block metal oxides)- Redox mechanism
2. Non reducible metal oxides i.e. catalysts which are very difficult to reduce under the reaction conditions
3. Metal supported catalyst systems generally noble metals

1.3.2. Mars-Van-Krevelen Mechanism

Majority of ODH reactions follow Mars-Van-Krevelen (MVK) mechanism **(Fig. 1.4)**. According to this mechanism first the reaction happens between the oxide catalysts and the hydrocarbon, in

which the later is oxidized and the former reduced, which is then followed by the reaction of the reduced oxide with oxidant to restore the initial state. The oxygen which is restored back from oxidant is formed via series of electron transfer steps . As shown in **Scheme.1.1.** there are two types of oxygen species usually formed during this process which are electrophilic and nucleophilic species. In this the electrophilic oxygen species like O^{2-}, O_2^{2-}, and O^- are responsible for the total oxidation. The nucleophilic lattice oxygen species (O^{2-}) species is associated with selective oxidation.

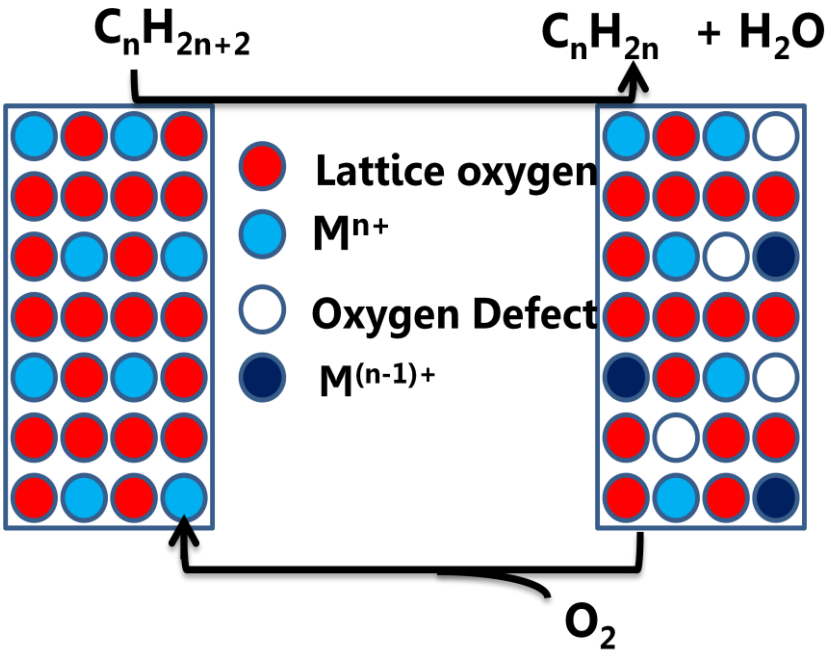

Fig. 1.4. MVK mechanism

$$O_{2(ads)} + e^- \rightarrow O_2^-{}_{(ads)}$$

$$O_2^-{}_{(ads)} + e^- \rightarrow 2O^-{}_{(ads)}$$

$$O^-{}_{(ads)} + e^- \rightarrow O^{2-}{}_{(lattice)}$$

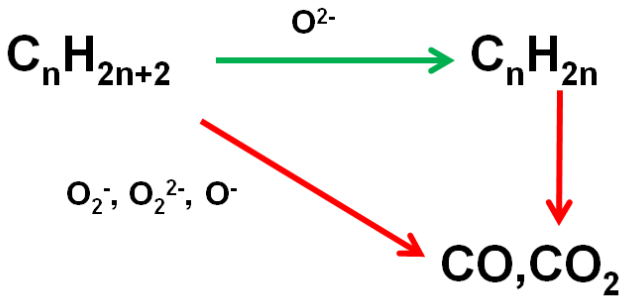

Scheme. 1.1. Different stages of oxygen activation on catalyst surface and their role in product formation

Based on this mechanism it is evident that the metal ion in the catalyst must be in the higher oxidation state to oxidize the hydrocarbon in the first step. In contrast, if a lower oxidation state

for the metal ion is present in the catalyst it corresponds to a surface which is poorer in oxygen ions and these generate more of electrophilic oxygen species when oxygen is adsorbed.

1.3.3. Oxidants

The usual oxidant employed in most of the ODH reactions is oxygen as it possess an added advantage in combusting the coke formed during the reaction. In higher temperatures there is a possibility of oxygen induced over oxidation and cracking. In past two decades the usage of soft oxidants has come into existence where oxidants like N_2O, CO_2, Air, etc. are been employed.

The utilization of carbon dioxide (CO_2), major contributor to the greenhouse effect is an important value addition in focus with principles of green chemistry. Unlike using CO_2 as a carbon source it can be employed as a soft oxidant, which is a non-traditional oxygen transfer agent.

$$C_nH_{2n+2} + CO_2 \longrightarrow C_nH_{2n} + CO + H_2O \qquad 1.1$$

The activation temperature is usually higher for CO_2 when considered to oxygen which is the only drawback in using carbon dioxide as oxidant. Krylov et. al have reported the usage of carbon dioxide as oxidant where the reaction temperature was 830 °C which gave ethane conversion of about 80 % with 76 % selectivity and employed K-Cr/Mn/SiO_2 as catalyst.[11] The above mentioned catalyst was active for ODH of butane also but the reaction temperature was in the range of 600-630 °C which gave conversion around 66 %. In case of propane Ga_2O_3 was effective when compared to other catalysts which gave around 30 % conversion at reaction temperature 600 °C.

In case of Nitrous oxide employed as oxidant the selectivity is usually higher when compared to oxygen because the over oxidation does not happen in the earlier case.[12,13] The reaction happens as given below,

$$C_3H_8 + N_2O \longrightarrow C_3H_6 + H_2O + N_2 \qquad 1.2$$

1.4. Mixed metal oxides

Mixed metal oxides are an important class of catalysts which are extensively employed for various chemical transformations. Generally mixed metal oxides possess two characteristics that distinguish them from metals which are i) absence of metal-metal bonds and ii) non-zero valent metal. Three striking features that describe oxides are (i) oxidation state of metal at the surface, (ii) coordination environment of surface atoms and (iii) redox properties of the oxides.[14] In addition to catalysts as such, metal oxides are widely employed catalyst supports even. In general

metal oxide surfaces are more complex in their structure and are highly heterogeneous. Metal oxide surfaces exhibit redox properties and both basic and acidic characters based on their composition, which is important for some reactions in catalysis. In catalytic oxidation or ODH reactions oxide catalysts have to undergo oxidation-reduction cycles. In selective oxidations or ODH reactions gaseous oxygen reacts with substrate to form oxygenates or water. Incorporation of oxygen from oxidant to reactant molecule takes place in two ways. They are (i) Transfer of electrons to adsorbed oxygen to form the species like O^-, O_2^{2-} and O_2^-, which on the incorporation of oxygen in to a product molecule and its subsequent desorption, return to the solid (ii) the other is direct incorporation of lattice oxygen of the oxide in to product molecule and lattice oxygen getting rejuvenated from oxidant. The later phenomenon is usually referred as Mars-Van-Krevelen mechanism. There are a variety of important factors that influence the redox cycle of the metal oxides which are metal-oxygen bond strength, presence of cation vacancies, ability to form shear structures, optimal density of active oxygen, acid base properties, electron binding energy of lattice oxygen and the crystallographic plane.[15]

1.4.1. Perovskites

Perovskites with general formula ABO_3 are a major group of functional materials which provides a vast scope and varied stoichiometric options making them the most studied mixed oxide system. Perovskite (ABO_3) is the name for a big structural family whose structure is derived from the mineral $CaTiO_3$. The mineral was discovered by German mineralogist Gustav Rose in rural mountain of Russia in 1839 and it is named after Russian mineralogist Lev Perovski. In the ABO_3 structure "A" site is generally a cation with 12-fold coordination which can be a lanthanide, alkaline, or alkaline-earth cation and "B" site is generally a cation with 6-fold co-ordination which can be a transitional metallic ion with 3d, 4d or 5d configuration. The great advantage with perovskites is that it provides a scope for variety of substitution with same or different valences which can be expressed as $A_{1-x}A'_xB_{1-y}B'_yO_{3\pm\delta}$[16] In perovskites the degree of substitution of the A- and/or B-site cation cannot be random because would lead to irregularity of framework and finally collapse the matrix structure. The Goldschmidt tolerance factor decides the possibility of perovskite structure formation which should be $0.75 < t < 1.0$, where $t = (r_A + r_O)/\{\sqrt{2}(r_B + r_O)\}$ is the tolerance factor, and r_A, r_B, and r_O are the radii of the respective ions.[17] The oxygen vacancy can be tuned in a controlled way when desired foreign cation is used and this offers a appropriate and viable way of correlating physicochemical properties with catalytic

performances of the materials.

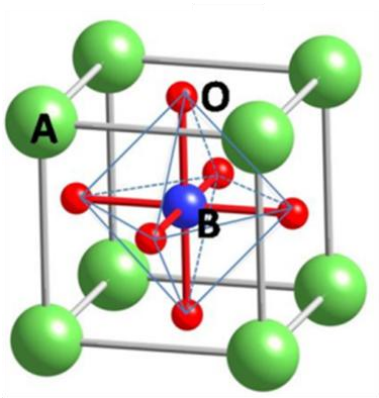

Fig. 1.5. A typical perovskite unit cell

Perovskite type metal oxides are extensively studied for a wide range of reactions like oxidation of NO[18,19], CO[20,21], NH_3[22] and hydrocarbons.[23-26] Many reports with manganese and cobalt-based perovskites have been reported which show a higher catalytic activity for oxidation reactions.[27,28] The 'B' cation in perovskites usually possess a variable oxidation state which makes these materials as better oxidation catalysts. Generally the 'B' cations selected for CO and hydrocarbon oxidation are Mn, Co, Ni, or Fe, which are the most active components in oxidation reactions. The nomenclature usually followed for these perovskites are generally based on the 'B' cation like manganites, cobaltite, ferrites, etc. These perovskites are well studied for total oxidation reactions as it possess a rich oxygen vacancies and oxygen mobility.[29-33] Efforts are being made to tune the properties of perovskites for selective oxidation like oxidative dehydrogenation reactions. The substitution of 'La' with 'K' in $LaMnO_3$ suppressed the formation of superoxide and peroxide species in surface which are responsible for total oxidation of ethane.[34] $PrCoO_3$ and $SmCoO_3$ was investigated for oxidation of ethane in which the former was active for ODH and the latter was active for total oxidation. In this Praseodymium stabilizes Co^{3+} ions and prevents their reduction to Co^{2+} and Co^0 which prevents the increase in oxygen vacancies thereby making it active for ODH reaction.[35] Yi et al. showed that in ODHE when $SrFeO_{3-\delta}$ perovskite was employed 43 % selectivity towards ethylene was obtained.[36] In this same catalyst Dai et al. showed that the selectivity doubled when $La_{1.6}Sr_{0.4}CuO_{3.852}$, $La_{1.6}Sr_{0.4}CuO_{3.855}F_{0.143}$,and $La_{1.6}Sr_{0.4}CuO_{3.856}Cl_{0.126}$ perovskites were studied for oxidative dehydrogenation of ethane. The authors have explained that the incorporation of halide ions, with similar ionic radii to O^{2-} promotes the lattice oxygen mobility and reduces surface oxygen defects.[37]

1.4.1.1. Synthetic routes for preparation of Perovskites

1.4.1.1.1. Ceramic method

The ceramic method which is also known as solid-solid method is based on solid-state diffusion. As the solid state diffusion state is slow in this method the oxide powders of desired metals are calcined at very high temperatures (above 1000 °C) and for long reaction times forms the perovskite structure.[38] Due to this harsh conditions there is grain growth and low specific surface area which are not suitable for catalysis applications.[39] In addition to that repeated heating and grinding must be done to obtain a homogeneous and pure perovskite with a surface area of 1-2 $m^2 g^{-1}$ and the crystal sizes in the range of 10-100 μm.[40]

1.4.1.1.2. Hydroxy acid Complexation method

This is the classic method for the synthesis of perovskites which is also called as Pechini method which was introduced by Pechini back in 1967 for synthesis of niobates and titanates.[41] Chelation of hydroxy acid with metal ions is the key phenomenon in this synthesis. When the water evaporates a gel forms which later forms a foamy material during baking at 180 °C. The foamy material when ground and calcined at temperature ranges between 600-800 °C forms perovskites. Among the hydroxy acids employed citric acid is used extensively for synthesis of perovskites as phase pure materials are obtained when citric acid is employed. Usually the stability of the gel depends upon hydroxycarboxylic acid used and among all citric acid complexes shows best stability toward auto-oxidation in the presence of oxidizing cations. $LaCoO_3$ prepared with little amount of Ethylene glycol along with citric acid showed a improved catalytic activity. This is due to slight modification of material surface crystallinity when EG is added. Also EG acts as a stabilizer of the citric acid-metal chelate which reduces the rate of combustion of the gel.[42] Even though the hydroxylation method using citric acid is a pretty old process but it is an efficient and versatile synthesis route and the materials prepared by this method possess satisfying textural properties.[43]

1.4.1.1.3. Auto combustion Method

The auto combustion route which is called as self-propagating high-temperature synthesis (SHS) is an efficient alternative route to synthesize nanocrystalline mixed oxides. This approach is widely employed for the synthesis of variety of materials like carbides, nitrides, oxides, and mixed oxides. The main striking advantages of this synthesis are i) using chemical energy rather than electrical power, ii) fast synthesis and iii) easy scale up. In an autocombustion reaction after

solvent evaporation the gel is placed on a hot plate or in a muffle furnace. Autocombustion can be done under three different synthesis conditions which are fuel-deficient (oxidizing), stoichiometric and fuel-rich (reducing) conditions. This fuel/oxidizer ratio has a great impact in final material properties as they influence the heat release in the materials and in other way controlling the maximum temperature in the material during combustion.[44-46] Hence the selection of an optimum fuel-to-oxidizer ratio is necessary to ensure formation of a pure crystalline phase **(Fig. 1.6 B).**[47] For example in synthesis of $LaFeO_3$ by the glycine combustion method the surface areas of the prepared materials varied from 6.5 to 27.8 m^2 g^{-1} the highest surface area was obtained at a glycine-to-nitrate ratio of 2.[48,49]

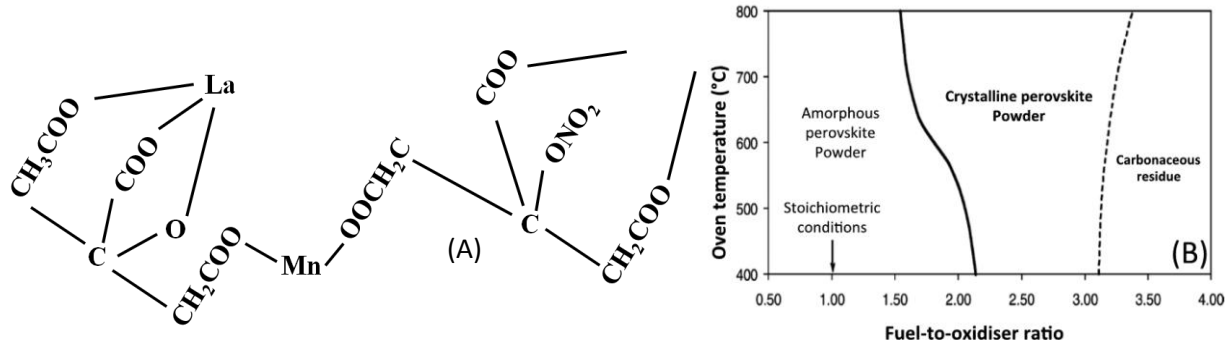

Fig. 1.6. (A) Complexation occurring between manganese and citric acid during precursor formation: case of $LaMnO_3$[50] (B) Impact of the fuel (urea) to oxidizers ratio on formation of $LaMnO_3$.[47]

1.4.1.1.4. Other preparation methods

The other preparation methods are i) Nonaqueous Solvothermal method where a mixture of alcohols like 2-methoxyethanol and benzyl alcohol are employed,[51] ii) Hard templating method to synthesize mesoporous perovskites,[52-54] iii) Periodic macroporous perovskites by using polymer beads and many more.[55,56] These methods are not so well practiced as the earlier methods.

1.4.1.2. Oxygen Vacancy and B-site substitution in Perovskites

It is evident from the structural features of perovskite oxides that the oxygen vacancy can be generated by substituting an external cation without destroying the matrix of the parent structure. The oxygen vacancy or the oxidation state of 'B'-site cation can also be tuned by substituting A^{3+} cation by a A'^{2+} one in the $A^{3+}_{1-x}A'^{2+}_{x}BO_3$ structure. Tuning the oxygen vacancy or the control of the oxidation state of 'B'-site metal cation are important parameters because the catalytic cycle proportionally depends on the redox property of B-site metal cation and in other hand oxygen

vacancy provides the sites for substrate adsorption and activation. The below figure **(Fig. 1.7)** shows the different vacancies generated when 'A' and 'B' site oxidation states changes. **Fig 1.7.** also explains the mode of oxygen activation on the surface of the catalyst.

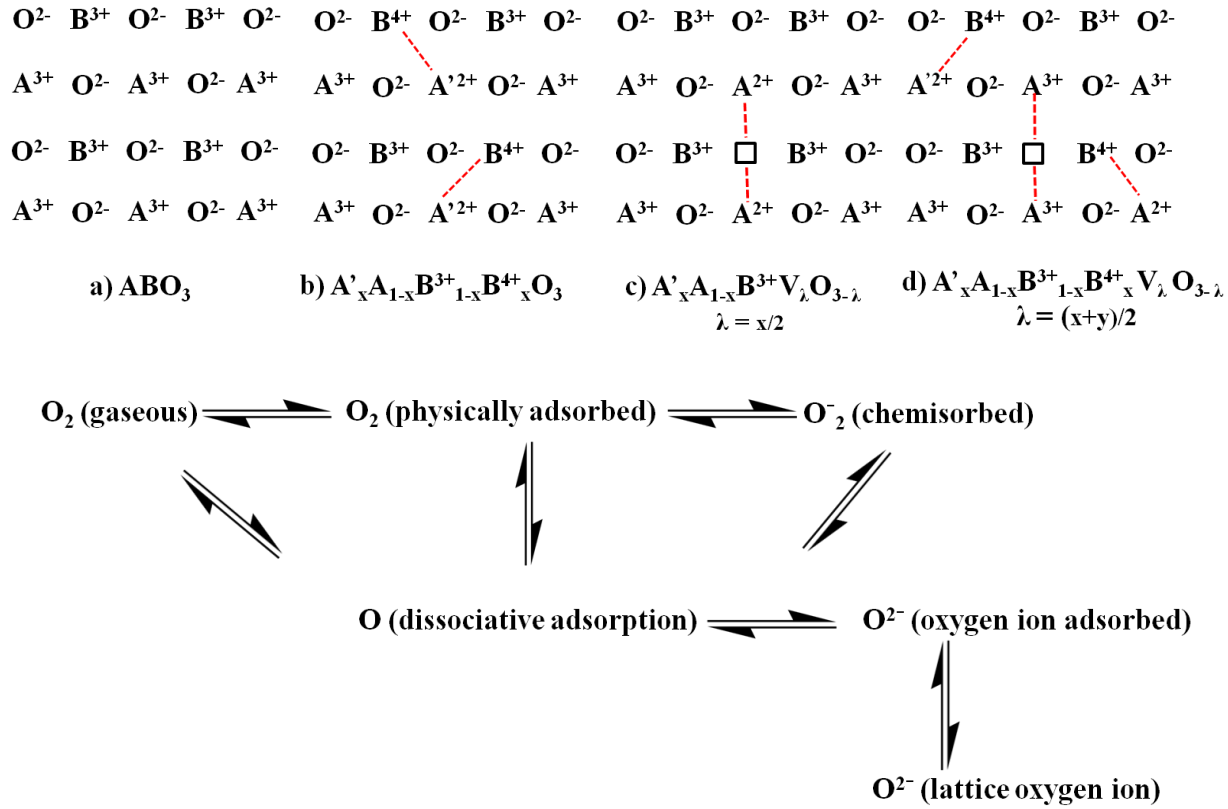

Fig. 1.7. Oxygen vacancy in perovskite on 'B'-site substitution and O_2 activation on its surface[57]

An equilibrium in B^{4+}-(O^{2-})-B^{4+} = B^{3+}-□-B^{3+} + 1/2O_2 ("□" represents oxygen vacancy) is maintained when there is an increase in oxidation state of 'B'-site metal cation. In other words oxygen vacancy can be generated by losing one lattice oxygen, or vice versa. By virtue of this cycle molecular oxygen can be adsorbed and activated (by receiving electrons) on the oxygen vacancy which is subsequently transformed into chemically reactive oxygen species. This substantiates that oxygen vacancy acts as a bridge for the transformation of molecular and lattice oxygen.

1.4.2. Hydrotalcites

Hydrotalcites (HTlcs) which are also called as layered double hydroxides (LDHs) or anionic clays are a vast group of naturally occurring materials which can also be readily synthesized when suitable mixtures of metal salts precipitated with calculated amounts of base. These materials usually possess hydroxide layers of metal cations which possess an overall positive

charge which is counter balanced by the incorporation of anions of exchangeable nature. They have general formula $[M_{1-x}^{2+} M_x^{3+} (OH)_2]^{x+}[A_{x/n}^{n-}]^{x-}$, where M^{2+} and M^{3+} are bi- and trivalent metal cations, respectively, and 'A' is an inter lamellar anion with charge $n-$ and x is equal to the ratio $M^{3+}/(M^{2+}+M^{3+})$.$A_{x/n}^{n-}$is termed as gallery ion. Pure HTlcs are obtained for x values 0.2-0.33. The acid-base properties of these solid bases can be easily controlled by varying its composition.[58] Variations in 'Al' content can modify the basic properties of the material by altering the ratio of acid:base site distribution through the introduction of Al^{3+}, O^{2-} sites which are of moderate Lewis acidity and only medium basicity. Strong basicity of alkali metal oxides can originate from O^{2-}, medium strength from O^- species near hydroxyl groups and weak one from OH groups.[59]

The key parameters which determines the usage of hydrotalcites are its degree of crystallinity and textural properties. The property and nature of the bivalent and trivalent cations and along with their ratio, the nature of the anions, the concentrations of metal salt solution and alkali solution, the rate of addition of metals and alkali solutions, the reaction pH, the aging temperature and time, and the drying temperature of the obtained precipitate affects the above mentioned two properties. The specific surface area, morphology, and particle-size distribution of the hydrotalcite also depend on the synthesis method.[60]

1.4.2.1. Structure of hydrotalcites

The structure of LDHs are similar to brucite ($Mg(OH)_2$) and natural hydrotalcite ($Mg_6Al_2(OH)_{16}CO_3.4H_2O$). Brucite type structure consists of neutral host layers which is composed of M^{2+} centred octahedra coordinated with six hydroxyl groups located in the vertices whereas each OH^- is surrounded by three metal cations**. (Fig: 1.8)** These sheets are kept together by van der Waals force along with hydrogen bonds. It is the basic form of layered double hydroxide and other phases may be considered as derived from this type. Here M^{2+}cations are partially substituted by M^{3+} and the electroneutrality is balanced by anions, usually carbonates, chlorides, nitrates, sulphates, organic anions and water molecules arranged in interlayers.[61] A number of synthetic hydrotalcite like compounds (HTlcs) can be prepared by isomorphous substitution of di- and trivalent metal cations having more or less equivalent ionic radii. This results in an expansion in the dimension along layer stacking direction, whereas the structure framework is still maintained. (**Fig: 1.10**) A number of synthetic hydrotalcite like compounds (HTlcs) can be prepared by isomorphous substitution of di- and trivalent metal cations having

equivalent ionic radii.

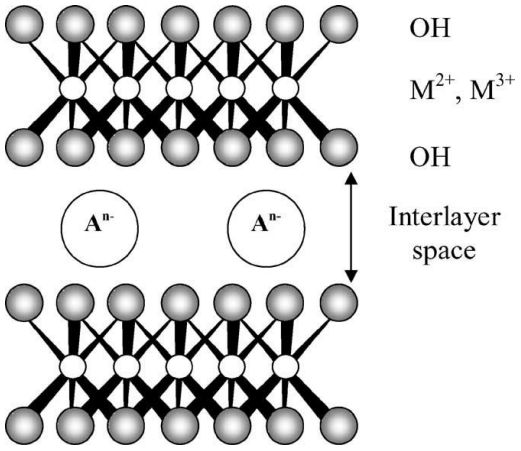

Fig. 1.8. Hydrotalcite structure showing the brucite like layers and interlayer anions[62]

A number of synthetic hydrotalcite like compounds (HTlcs) can be prepared by isomorphous substitution of di- and trivalent metal cations having equivalent ionic radii. These metal cations in LDHs can be Mg^{2+}, Fe^{2+}, Co^{2+}, Ni^{2+}, Zn^{2+}, etc., and Al^{3+}, Fe^{3+}, Cr^{3+}, Ga^{3+}, etc respectively.[63-66] It is also possible to produce hydrotalcites containing large variety of different interlayer anions like SO_4^{2-}, WO_4^{2-} and CrO_4^{2-}. In M^{2+}-Al^{3+} category, particularly Mg^{2+}-$Al^{3+}$is more dominated due to the fact that hydrotalcite $Mg_6\ Al_2\ (OH)_{16}\ (CO_3).4H_2O$ is a widely known anionic clay found in nature. Thus different combination of M^{2+}, M^{3+} and A^{n-} will results in a large family of mixed hydroxides and derived mixed oxides whose physicochemical properties can be tuned for various catalytic reactions.[67,68]

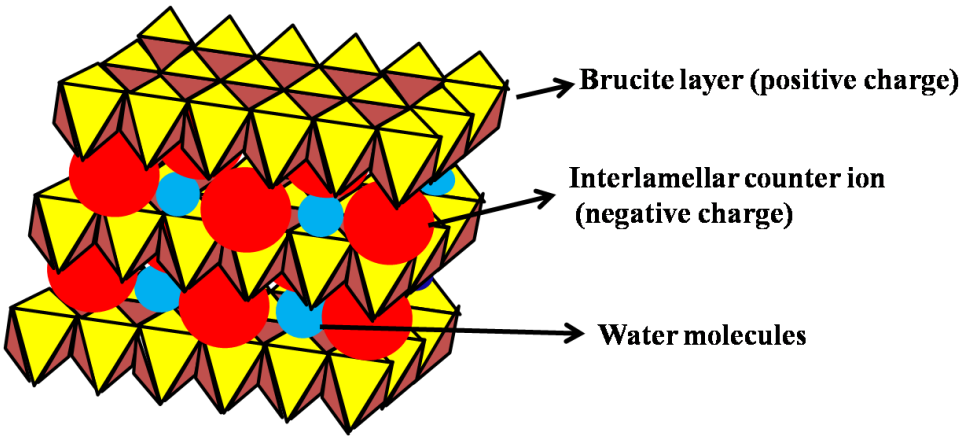

Fig. 1.9. Double layered structure of hydrotalcite[69]

The features of HTlcs therefore are tuned by the inherent properties of the brucite-like sheets, by the nature and position of anions in the interlayer region and by the difference in the stacking of the brucite sheets. The sheets containing cations are built as in brucite, whereas the cations

randomly occupy the octahedral holes in the close-packed configuration of the OH^- ions. Generally M(II) and M(III) ions occupy in the voids of the close packed configuration of hydroxyl group in the brucite-like layers as far as the ionic radii and the valence states are allowed.[70]

1.4.2.2. Methods of preparation

The particle size, crystallinity and the base strength are extremely sensitive to the precise preparative method/conditions. The general properties of hydrotalcites depends on the M(III) and M(II) incorporated in it which comprises the degree of order of distribution of the different cations along with exact mixing procedure and subsequent aging or other treatment which makes it difficult to compare from different groups. In addition, the amphoteric feature of Al^{3+} also plays a very favorable role in promoting the precipitation and crystallization of M^{2+}-Al^{3+}LDHs.[71]

1.4.2.2.1. Direct synthesis

Direct synthesis or co-precipitation is employed for the preparation of hydrotalcites. In this method while precipitating the metal ion solutions by base with required interlamellar anion the nucleation and growth of the metal hydroxide is usually layer by layer. The key restriction in this method is that this method is possible only if the required interlayer anion is held tightly as the counter ion in the metal salts is held. In addition to this the anions which is used in HTlcs should not readily react with constituent cations to form a stable or insoluble salts.[71]

1.4.2.2.2. Co-precipitation in non-aqueous solutions

Mixture of alcohols also can be employed during co-precipitation to form mixed alkoxide/inorganic anion–intercalated HTlcs. On overnight hydrolysis of this solution forms alkoxide anions which form transparent suspension of HTlcs and subsequently forms thin films on drying. This method finds its use in synthesis of pillared anionic clays that which can be utilized as precursors for the synthesis of transparent HTlcs films.[72] These method usually leads to poorly crystallized solids.

1.4.2.2.3. Anion exchange method

The interlamellar anions in the hydrotalcites which are loosely held can be easily replaced with a different anion by simply stirring the HTlcs in an aqueous solution with the replacement anion in excess. Generally HTlcs with nitrate and chloride anions are utilized as starting materials in this synthesis. In principle interlamellar anions of various types like organic and inorganic nature possessing different charges, sizes or shapes are been successfully intercalated into HTlcs.

1.4.2.2.4. Preparation from Oxides and Hydroxides

In this method the metal oxide or hydroxide are hydrated and during this desired anion is taken in the solution which is need to be employed as interlamellar anion. In other way of the same HTlcs which are synthesized with a thermally labile interlamellar anion can be calcined and it can be rehydrated as earlier with different anion.[71]

1.4.2.2.5. Sol-gel Method

The preparation involves hydrolysis followed by polymerization of the sol containing metal alkoxides. Here a mobile colloidal suspension (sol) is formed followed by gel due to internal cross-linking. In a typical synthesis the alkoxides are first homogenised in an solvent usually organic and refluxed. To this solution water is slowly added causing cross-linkage to occur.[58] Hydrotalcites synthesized by this method exhibit good homogeneity, relatively good control of stoichiometry, high surface area and high porosity characteristics.[71]

Hydrotalcites contains aluminium magnesium carbonate hydrate which is an antacid which alters the acidity of stomach juices, by binding to excess acid.[73,74] It has anion exchange capabilities, high surface area, and basic properties and is stable up to 673 K and has memory effect to get back its structure when contacting the mother liquor or atmosphere in prolong time. In hydrotalcites modifications can be brought by di- and trivalent cations, their proportion, and/or the interlayer anions which make them better catalysts. HTlcs find many applications such as ion exchangers, adsorbents, ionic conductors, gene delivery vectors, ceramic precursors, polymer stabilizers, catalysts and catalyst supports.[75-78]

1.4.2.3. Hydrotalcite derived mixed oxides

There has been for the past years an increased interest in using HTlc-like compounds as precursors for mixed oxide catalysts in various reactions.[58] Hydrotalcites are excellent catalysts for Baeyer-Villiger oxidation, epoxidation, Claisen Schmidt condensation, Knovengel condensation, isomerization, alkylation of diketones and oxidative dehydrogenation reactions. Different combination of M^{2+}, M^{3+}, and A^{n-} results in a large family of mixed hydroxides, the physicochemical properties of which derived mixed oxides can thus be finely tuned for various catalytic reactions.[66,67] Layered hydrotalcites on heat treatment will give amorphous mixed oxides and complex spinel type structures. The LDHs and their mixed oxides are potential multifunctional catalysts possessing metals as redox sites and acid-base sites. Methods to transform HTlcs in a controlled pathway to respective mixed oxides retaining the properties of

the parent material is still a point of concern till today. In addition to that, to synthesize a mixed metal oxide catalysts with tailored properties lies in the control at the atomic level rather than at the particle level. Yang et al. found that dehydroxylation is complete before decarbonation of Mg-Al-CO_3-HT[79] and Kameda et al. noted similar decomposition behaviour for Mg-Al-Cl-HT[80] while Xu et.al observed that evolution of NO_3^- in Mg-Al-NO_3-HTlcs usually happens along with dehydroxyalation.[81] Mixed metal oxides are generally formed due to the layer structure collapse during dehydroxylation.[79,81,82] The nature of cation and interlayer anions play a vital role in determining the thermal stability of HTlcs but the relationship is not well understood. Step by step thermolysis of HTlcs was studied by thermal analyses, powder XRD of the products, and in particular in situ from the onset temperature of their formation by many physicochemical techniques.

Co-precipitation of metal salts solution with base at constant pH in the temperature range of 60-70 °C is the commonly used method of synthesis of hydrotalcites. Layered hydrotalcites on heat will give amorphous mixed oxides with complex spinel type structures. The formation of mixed oxides from HTlcs happen generally through thermal decomposition which involves many intermediate steps like dehydration, decomposition of interlayer anions, and dehydroxylation of layer hydroxide groups.[83] Generally dehydration occurs initially at lower temperatures and at higher temperature dehydration and dehydroxylation follow in competition or sequence. Hydrotalcite decomposition to the mixed oxide goes through an intermediate highly disordered layered phase, which is exclusively the product of interlayer water removal, causing a dramatic shrinkage of the space between brucite-like layers.

A TGA-DTG curve of as-synthesized hydrotalcite is reported in the study of memory effect of hydrotalcites by J. P. Ramirez et al. The first weight loss step in the TGA occurs below 500 K and it is due to removal of water which is physically adsorbed and hydrogen bound water in the interlayer which is evidenced by MS analysis.[84] The event corresponding to dehydroxylation of hydroxyl groups along with evolution of interlayer anions in the HT lattice is also observed in the TGA analysis. The endothermic event above 500 °C is due to crystallization of rock salt (MgO) and $MgAl_2O_4$ spinel. As shown in **Fig. 1.10**, it is explicit that the water molecules possess a direct interaction with interlayer anions and hydroxyl groups of the lattice and indirectly with metal cations by electrostatic forces and these interactions determine the dehydration. **Fig. 1.11**

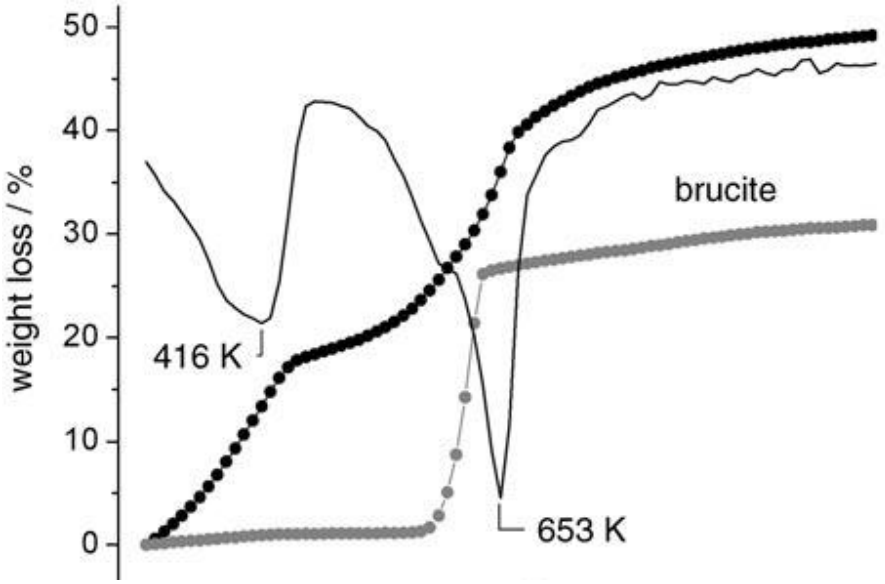

Fig. 1.10. TGA-DTG curve of as-synthesized HT[88]

In situ XRD studies showed that the formation of the mixed oxide $Mg(Al)O_x$ occurs at 623 K with periclase structure. Characteristic reflections of the rock-salt periclase structure were observed. As a consequence of the dehydroxylation of the brucite-like sheets the layered structure collapses to oxide phase. This process occurs in the broad range 473-723 K according to TGA and TPD-MS analysis.[85]

Heating stage Raman microscopy and infrared emission spectroscopy also have been shown very useful tools to study the structural changes and reactions like dehydration, dehydroxylation, and decarbonisation in crystalline materials like hydrotalcites during heat treatment in addition to the conventional techniques as XRD and TG/DTA.[86]

Mixed oxides derived from hydrotalcites have interesting properties like

1. High surface area
2. High thermal stability
3. Good metal dispersion
4. Basic properties
5. Homogeneous mixture formation
6. Small crystal size
7. Memory effect, in which metal oxide resulting from the thermal decomposition of hydrotalcite can be reconstructed into original hydrotalcite structure upon contact with water or aqueous solutions containing certain anions.[87,88,89]

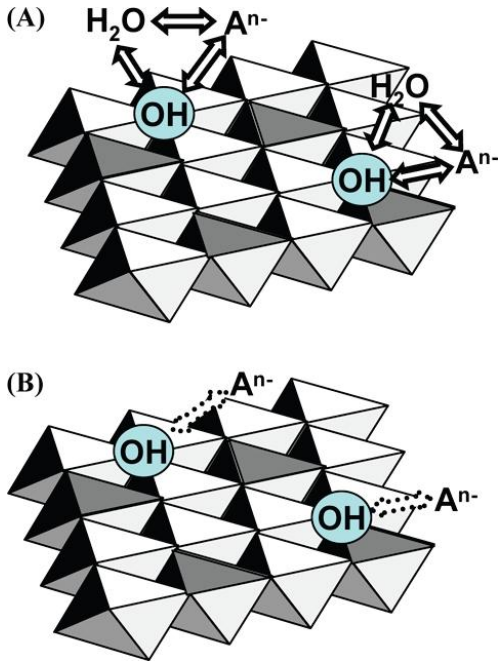

Fig. 1.11. Hydrotalcite prior to hydration (A) and after hydration (B) octahedrons has one cation in the centre. The shaded triangle means an M(III) in the centre; otherwise M(II) is in the center[69]

1.4.3. Ceria

Lanthanides or rare-earth oxides are extensively studied for their unique textural and electronic properties which drive in improving the overall catalytic activity and stability of catalysts. Among the rare earth oxides one of the important and most significant oxides in industrial catalysis is CeO_2.[90] Ceria possess a cubic fluorite structure (FCC) in which each cerium is coordinated with eight oxygen in FCC arrangement and each oxygen has a tetrahedron cerium coordination **(Fig. 1.12).** By the virtue of its oxygen vacancies ceria acts as an oxide ion conducting material. Oxygen vacancies are of two types which are i) intrinsic and ii) extrinsic vacancies. Among this the intrinsic oxygen vacancies are generated due to Ce (III) ions in the fluorite lattice which are formed as a consequence of the reduction equilibrium of Ce^{4+}/Ce^{3+} and the extrinsic oxygen vacancies are generated when a heteroatom is substituted in the lattice of ceria.[91]

Due to the high melting point of ceria (2400 °C) it is employed for high temperature applications like total oxidation and combustion of natural gas.[92] Ceria possess unique properties like high dielectric constant, high reactivity high refractive index and high hardness.[93] A remarkable property of ceria is the extent of redox Ce^{4+}/Ce^{3+} sites which has the ability to adsorb or desorb oxygen (oxygen activation). This property of ceria can be fine tuned by the incorporation of d-

block elements or transitional metal ions in lattice of ceria and also by promoting them by dispersing noble metals. Therefore, ceria can be used as a promoter or support in industrial catalytic processes.[93,94]

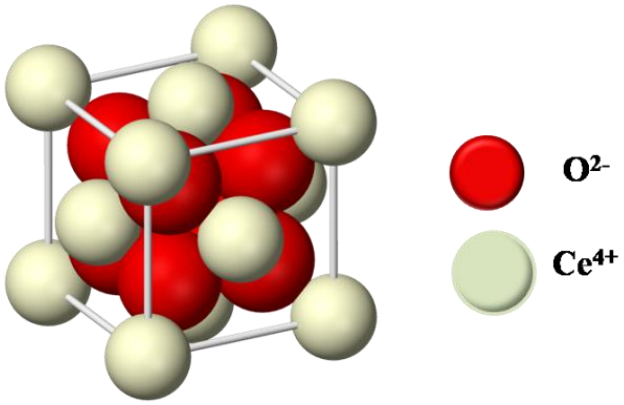

Fig. 1.12. The FCC cell of CeO_2 with fluorite structure

The acidic and basic properties of CeO_2 and CeO_2-based mixed oxide materials are measured by microcalorimetry, by pyridine and CO_2 adsorbed in situ IR study of adsorbed pyridine and model reactions. From these investigations it was evident that the surface acidity is due to surface Ce^{4+} and $OH^{\delta+}$ species and the surface basicity is due to $O^{2-}$and $OH^{\delta-}$ ions. The amount of acid-base sites on the surface is due to surface unsaturated cations and the hydroxyl groups which depends on the method of preparation.[95]

Ceria and ceria based composites are widely applied in oxidation/combustion catalysis, catalytic wet oxidation three way catalysis, water gas shift reaction, and solid oxide fuel cells.[96-101] The acid-base and redox properties of ceria plays a pivotal role in various catalyzed reactions. Ceria possess a superior low temperature reducibility and remarkable oxygen storage/release capacities (OSC) i.e. it has the ability to shift between Ce^{3+} and Ce^{4+} [90] in a stable fluorite structure and hence finds its utility as an additive in three way catalysts (TWC) for automobile exhaust treat.[90,92,102]

In all the applications and catalytic activity studies CeO_2 is not used alone and it is generally used in combination with other oxides or with active metals (generally noble metals) and thermally stable supports. Therefore these properties suggest that ceria may function as a structural/electronic promoter or as a co-catalyst, but not as a true catalyst. The structural instability prevents the usage of ceria in three way catalysis and as fluidized catalysts. Generally there is a drop in specific surface area of ceria at elevated temperatures, although a high degree

of textural stability can be obtained by doping and modifying the preparation procedure. Other notable disadvantage is the cost factor of pure ceria which is comparatively higher than supports like Al_2O_3 and SiO_2. In recent years much efforts are being invested to find appropriate dopants or co-catalysts which increase the high thermal stability of ceria retaining its distinct properties like low temperature redox nature and its high oxygen mobility. In this context usually ceria is evenly mixed with other thermally stable mixed oxides where noble metals also can also be used to boost up the catalyst activity. One such option is mixed oxide derived from hydrotalcite where they possess the ability to accommodate a large variety of di- and trivalent cations, and the formation of high-surface-area and well-dispersed mixed oxides upon thermal decomposition, are key aspects for the successful application of hydrotalcite-like compounds in catalysis.[103,104]

CeO_2 based mixed oxides can effectively catalyze oxidation of various hydrocarbons and remove total organic carbon from polluted waters from different sources. Pure ceria undergoes sintering at high temperatures and loses its OSC characteristics so it is not advantageous to use it as such.[105] By synthesizing appropriate ceria based composite oxides, its textural properties and catalytic properties can be improvised. Ceria are generally employed for oxidation reactions due to its redox nature and presence of labile oxygen species in surface.[106] CeO_2 based or ceria dispersed mixed metal oxides are better catalysts for oxidation of many hydrocarbons and for removing total organic carbon from contaminated waters. CeO_2 present in lower amounts in other oxide systems show a better activity for a wide range of catalytic reactions like CO_2 activation[106], CO oxidation[107,108] and CO/NO removal.[109] Therefore ceria and ceria containing materials are important class of materials due to the uniqueness such as low temperature reducibility and oxygen storage characteristics of ceria ($Ce^{3+}\leftrightarrow Ce^{4+}$) and to accommodate variable levels of bulk and surface oxygen vacancies.[110] Due to these properties they are employed as supports as well as catalysts in the pathways wherein redox reaction conditions are required.

1.4.4. Rare-earth Orthovanadates

Rare earth vanadates are an important class of inorganic materials and owing to their outstanding optical, catalytic, electrical and magnetic properties they have a wide applications as sensors, catalysts and heat-resistant materials.[111,112] Among these rare earth vanadates, $CeVO_4$ is widely studied as these possess a diverse potential applications such as oxidation catalysts, luminescent materials, gas sensors and electrodes.

Vanadium based oxides are known for catalyst using several oxidation reactions.[113] Even though unsupported vanadia is an active catalyst deactivates fast due to which vanadium oxides are generally supported on oxide supports. Ceria shows a promoting effect among various supports like ZrO_2, TiO_2, Al_2O_3, SiO_2, CeO_2, and Nb_2O_5.[114-116] As a consequence of this much efforts was made in studying the characteristics of vanadia and/or ceria catalysts. During in situ spectroscopic studies of V_2O_5 /CeO_2 catalysts it was observed that, there was formation of cerium orthovanadates ($CeVO_4$) upon activation and its formation increases proportionally when vanadia loading increases on the CeO_2 support. The product distribution remained similar at certain vanadia coverage for both V_2O_5/CeO_2 and for pure $CeVO_4$. This observation emphasize that there may be similar active site on both catalysts.[117-120]

1.4.4.1. Structure of Cerium orthovanadates

$CeVO_4$ crystallizes in two types in which the stable phase is a zircon-type body-centred-tetragonal structure with space and a metastable monoclinic huttonite-type structure which are stable above 400 °C. The stable tetragonal structure is usually observed in majority of the synthesis. In a typical tetragonal unit cell of $CeVO_4$ **(Fig. 1.13)**, VO_4 tetrahedral form the sharing corners and edges with CeO_8 dodecahedral chains.[121] Along with that the chains are interrupted by distorted VO_4 units, extended along the 'c'-crystalline axis which are believed to stabilize the Ce^{3+} cations even in an oxidizing conditions. In addition to that the eight 'O' nearest neighbours of Ce are divided into two groups of four atoms each and the bond lengths between them differ slightly (0.09-0.13 Å)[120]

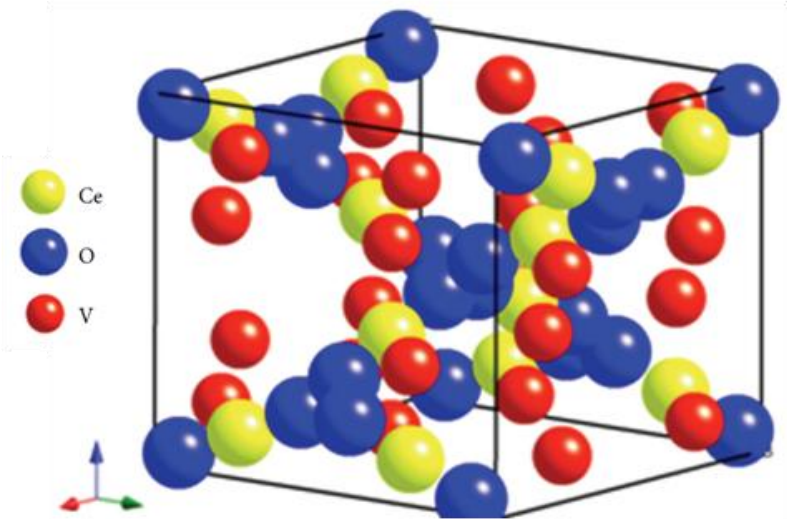

Fig. 1.13. A typical unit cell of cerium orthovanadates

1.4.4.2. Methods of preparation

1.4.4.2.1. Solid State method

In solid state synthesis $CeVO_4$ can be synthesized by two different ways using cerium compounds and V_2O_5. Among the two, one is by reacting cerium oxide with Ce in the III oxidation state (Ce_2O_3) with V_2O_5 at high temperatures. In this method an inert atmosphere is maintained as Ce_2O_3 are highly unstable in air atmosphere at high temperatures.[122]

$$\frac{1}{2}Ce_2O_{3(s)} + \frac{1}{2}V_2O_{5\,(s)} \rightarrow CeVO_{4(s)} \qquad \textbf{1.3}$$

In other method $CeVO_4$ can be synthesized by the solid state reaction of CeO_2 with Ce in the IV oxidation state and V_2O_5 in air atmosphere.[123,124]

$$CeO_{2(s)} + \frac{1}{2}V_2O_{5\,(s)} \rightarrow CeVO_{4\,(s)} + \frac{1}{4}O_{2(g)} \qquad \textbf{1.4}$$

1.4.4.2.2. Hydrothermal method

Hydrothermal method is one of the promising solution chemical methods which is widely employed to synthesize various inorganic materials and is also a quick and useful method to synthesize materials with unique morphology and unusual property. Yan et.al. prepared hollow spheres of $CeVO_4$ using EDTA as a chelating ligand followed by hydrothermal treatment.[112] $CeVO_4$ with different sizes and morphology can be obtained in changing the chelating ligands/ structure directing agents.[125-127] In hydrothermal synthesis the changes in pH induces distinct modifications to bulk and surface compositions. These changes effect the catalytic properties and in particular when the hydrothermal synthesis is done in a strong acidic medium. So during synthesis when pH is reduced to ~1.8, VO^{2+} species forms in which after stabilization cerium precursor and NaOH is added and hydrothermally treated. Due to virtue of this precipitation some amount of ceria phase forms as an impurity.[128]

1.4.4.2.3. Other preparation methods

In addition to the above two methods there are certain methods like chemical vapor deposition (CVD) method, sol-gel method, plasma chemical vapor deposition (PCVD) method and top-seeded solution growth (TSSG) method, microwave synthesis are been employed for synthesis of $CeVO_4$.[129-132]

1.5. Objectives and organization of the thesis

This thesis describes the preparation, physicochemical characterizations and activity studies of different mixed metal oxides towards ODH of hydrocarbons. Substantial efforts were made to investigate structure activity relationships for the selective conversion of the substrates taken. Necessary optimizations and systematic investigation of spent catalysts was also studied by physicochemical techniques.

Organization of thesis

The thesis is divided into six chapters. A brief description of the contents of each chapter is given below.

Chapter 1: Introduction

A general and brief introduction about catalysis, commercial dehydrogenation processes with their shortcomings is given. The importance of ODH pathway and their benefits when compared to conventional and existing processes will be discussed. Overview of the mixed metal oxide systems that was employed for our studies with their structure and synthesis pathways.

Chapter 2: Catalyst synthesis and experimental techniques for characterization

In this chapter the catalyst synthesis methods and the physicochemical techniques used to evaluate the catalysts are discussed in detail. The characterization studies used for studying these materials were carried out by Powder X-ray diffraction, BET surface area measurement, TPD, TGA,XPS,EDAX etc. For each technique, theory and experimental procedure have been described.

Chapter 3: Oxidative dehydrogenation of ethane to ethylene over Manganese substituted $Ca(Sr)TiO_3$ perovskite type oxides

A brief literature overview for ODH of ethane to ethylene with pros and cons of reported catalytic systems. An exhaustive investigation of the perovskite type catalyst using various characterization techniques to study their structure and morphology. XPS was used to find out the surface changes at various temperatures and extending it to correlate with the activity profile obtained.

Chapter 4: Oxidative dehydrogenation of ethyl benzene (EB) to styrene (ST)

A brief literature background of the commercial and existing catalytic systems for ODH of EB to ST is discussed **Part A** of this chapter deals with understanding the role of basicity, reducibility, oxygen storage capacity and metal surface concentration in obtaining a better activity for ceria

incorporated mixed oxide derived from hydrotalcites. **Part B** of this chapter emphasizes the role of manganese substituted in $Ca/SrTiO_3$ perovskites for obtaining a fairly better activity towards EB to ST.

Chapter 5: Oxidative dehydrogenation of 1-butene to 1,3-butadiene over Cerium orthovanadates

In this chapter the importance of 1,3-butadiene and the drawbacks of the reported catalysts in open literature will be discussed. Synthesizing and systematically studying the role of hetero cations in cerium orthovanadates in promoting the activity of the catalyst. Understanding the role of 'Mn' in improving the activity of orthovanadates and tuning other parameters for better and selective activity for ODH of 1-butene to 1,3-butadiene.

Chapter 6: Summary and conclusions

This chapter describes the inferences and conclusions drawn upon the investigations performed with regard to different catalysts used for selective oxidative dehydrogenation of hydrocarbons. The summary and conclusions obtained in the study associated with this thesis which includes some suggestions for further research.

1.6. References

1. J. Berzelius, Ann. *Chim. Phys*. 61 (1836) 146.
2. G. M. Schwab, in J. R. Anderson and M. Boudart (Eds.), *Catalysis Science and Technology*, Vol. 2, Springer, New York, 1981.
3. A.D. Mc Naught, A. Wilkinson, *IUPAC Compendium of Chemical Terminology, 2nd edition, British Royal Society of Chemistry, Cambridge, UK*, 1997.
4. A brief history of catalysis, Bard Lindstroma and Lars J. Petterssonb, *CATTECH*,7 (2003), 130-138.
5. John N. Armor, *Catal. Today*, 163 (2011) 3-9.
6. J. J. H. B. Sattler, J R-Martinez, E S-Jimenez, and B M. Weckhuysen, *Chem. Rev*.,114 (2014), 10613-10653.
7. Synthesis of intermediates for the Petrochemical Industry, Volume II / Refining And Petrochemicals. Pg.No 687-700.
8. F. Cavani , N. Ballarini, A. Cericola, *Catal. Today*, 127 (2007) 113-131.
9. Christian A. Gartner, Andre C. van Veen, Johannes A. Lercher, *ChemCatChem*, 5(2013),1-23.

10. F. Cavani, F. Trifiro, *Catal. Today*, 51 (1999) 561-580.
11. Krylov, O. V, Mamedov, A. K., Mirzabekova, S. R, *Catal. Today*, 24(1995), 371-375.
12. M P. Woods, B Mirkelamoglu, and U S. Ozkan, *J. Phys. Chem. C* ,113(2009),10112-10119.
13. A G-Llamas, C Mirodatos, and J P-Ramirez, *Ind. Eng. Chem.Res*, 44(2005), 455-462.
14. Z. L. Wang; Kang, Z. C., Functional and Smart Materials: Structural Evolution and Structure Analysis. Springer: 1998.
15. R.A. Sheldon; Santen, R. A. V., Catalytic Oxidation: Principles and Applications. World Scientific 1995, 53.
16. S Royer, D Duprez, F Can, X Courtois, C B-Dupeyrat, S Laassiri, H Alamdari, *Chem. Rev*., 114(2014), 10292-10368.
17. Goldschmidt, V. M.,*Die Naturwissenschaften*, 21(1926), 477-485.
18. J Chen, M Shen, X Wang, J Wang, Y Su, Z Zhao, *Catal.Comm.*, 37(2013), 105-108.
19. J Chen, M Shen, X Wang, G Qi, J Wang, W Li, *Appl. Catal. B*,134−135(2013), 251-257.
20. J. J Zhu, Z Zhao, D. H. Xiao, J Li, X. G. Yang, Y. Z. Wu, *Phys. Chem*. 2005, 219, 807-815.
21. H Falcon, M J Martinez-Lope, J A Alonso, J L G Fierro, *Appl. Catal. B*, 26(2000), 131-142.
22. Y. Wu, T. Yu, B.S. Dou, C.X. Wang, X.F. Xie, Z.L. Yu, S.R. Fan, Z.R. Fan, L.C.Wang, *J. Catal.*,120 (1989) 88-107.
23. Zhu, J. J.; Yang, X. G.; Xu, X. L.; Wei, K. M. Z. *Phys. Chem*. 220(2006), 1589-1594.
24. P Ciambelli, S Cimino, G Lasorella, L Lisi, S De Rossi, M Faticanti, G Minelli, P Porta, *Appl. Catal., B*, 37(2002), 231-241.
25. K. S Song, D Klvana, J. Kirchnerova, *Appl. Catal. A*, 213(2001), 113-121.
26. D Klvana, K. S. Song, J. Kirchnerova, *Korean J. Chem. Eng.*, 19(2002), 932-939.
27. In Properties and applications of perovskite-type oxides; Tejuca, L. G., Fierro, J. L. G., Eds.; Marcel Dekker Inc.: New York, 1993.
28. Pena, M. A., Fierro, J. L. G. *Chem. Rev*.101(2001), 1981-2018.
29. J Beckers, G Rothenberg, *ChemPhysChem*, 6(2005), 223-225.
30. V. Roche, E. Siebert, M. C. Steil, J. P. Deloume, C. Roux, T. Pagnier, R. Revel, P. Vernoux *Ionics*, 14(2008), 235-241.
31. N A Merino, B P Barbero, P Grange, L E Cadus, *J. Catal*. 231(2005), 232-244.
32. T Asada, T Kayama, H Kusaba, H Einaga, Y Teraoka, *Catal. Today*, 139(2008), 37-42.
33. A Boreave, H Tan, V Roche, P Vernoux, J-P Deloume, *Solid State Ionics*, 179(2008),

1071-1075.

34. Y. N. Lee, R. M. Lago, J. L.G. Fierro, V Cortes, F Sapina, E Martinez, *Appl. Catal., A* 207(2001), 17-24.
35. M Alifanti, G Bueno, V Parvulescu, V I Parvulescu, V Cortes Corberan, *Catal. Today*,143(2009), 309-314.
36. G. Yi, T. Hayakawa, A. G. Anderson, K. Suzuki, S. Hamakawa, A. P. E York, M Shimizu, K Takehira, *Catal. Lett.,* 38 (1996), 189-195.
37. H. X. Dai, C. F. Ng, C. T. Au, *Catal. Lett.,* 67(2000), 183-192.
38. R. J. H. Voorhoeve, J. P. Remeika, L. E. Trimble, N. Y. Ann, *Acad. Sci.*,272(1976), 3.
39. S. Royer, F. Berube, S. Kaliaguine, *Appl. Catal., A,* 282(2005), 273-284.
40. Y. Teraoka, H. M. Zhang, N. Yamazoe, *Chem. Lett.* 14(1985), 1367-1370.
41. Pechini, M. P. Method for preparing lead and alkaline earth titanates and niobates and coating method using the same to form a capacitor. *U.S. Patent* 3,330,697, (1967).
42. H. Taguchi, S. Yamasaki, A. Itadani, M. Yosinaga, K. Hirota, *Catal. Commun.,* 9(2008), 1913-1915.
43. A. M. Huizaz-Félix, T Hernadez, S. de la Parra, B. Kharisov, *Powder Technol.*,*229(*2012), 290-293.
44. A. G. Merzhanov, J. Mater. *Process. Technol*.,56(1996), 222-241.
45. J. J. Moore, H. J. Feng, *Prog. Mater. Sci.*,39(1995), 243-273.
46. J. J. Moore, H. J. Feng, *Prog. Mater. Sci.*,39(1995), 275-316.
47. S. R. Jain, K. C. Adiga, V. R. P. Verneker, *Combust. Flame,* 40(1981), 71-79.
48. A Civera, M Pavese, G Saracco, V Specchia, *Catal. Today*, 2003, 83, 199-211.
49. R. R. Kondakindi, K. Karan, B. A. Peppley, *Ceram. Int.*, 38(2012), 449-456.
50. M. S. G. Baythoun, F. R. Sale, *J. Mater. Sci.*, 17(1982), 2757-2769.
51. T. M Stawski, S. A.Veldhuis, O. F. Gobel, J. E. ten Elshof, D. H. A. Blank, *J. Am. Ceram. Soc.,* 93(2010), 3443-3448.
52. Z. Sarshar, F. Kleitz, S. Kaliaguine, *Energy Environ. Sci*.,4(2011), 4258-4269.
53. M. M. Nair, F. Kleitz, S. Kaliaguine, *ChemCatChem*, 4(2012), 387-394.
54. Y. Wang, X. Cui, Y. Li, Z. Shu, H Chen, J. Shi, *Micropor. Meso. Mater*.,176(2013), 8-15.
55. E. O. Chi, Y. N. Kim, J. C. Kim, N. H. Hur, *Chem. Mater.,* 15(2003), 1929-1931.
56. Y. N Kim, E. O Chi, J. C Kim, E. K Lee, N. H Hur, *Solid State Comm*. 128(2003),

339-343.

57. J Zhu, H Li, L Zhong, Ping Xiao, X Xu, X Yang, Z Zhao, and J Li, *ACS Catal.,* 4 (2014), 2917-2940.
58. F Cavani, F Trifiro, A Vaccari, *Catal. Today*,11(1991), 173-301.
59. V. K Diez, C. R Apesteguia, J. I Di Cosimo, *J. Catal.*,215(2003), 220-233.
60. S. K.Yun, T. J Pinnavaia, *Chem. Mater.*,7(1995), 348-354.
61. A Tsyganok, A Sayari , *J.Solid State Chem.*,179(2006), 1830-1841.
62. D.G.Cantrell, L. J. Gillie, A. F. Lee, K. Wilson, *Appl. Catal. A,287*(2005), 183-190.
63. R. Allmann, *Acta Crystallogr. Sect. B*, 24(1968), 972-977.
64. P S Braterman, Z P Xu, F Yarberry, In Layered Double Hydroxides (LDHs), *Handbook of Layered Materials*, Auerbach, S. M., Carrado, K. A., Dutta, P. K., Eds.; Marcel Decker, Inc.: New York, 2004, 373-474.
65. V Rives, *Layered Double Hydroxides: Present and Future; Nova Science Publishers, Inc.:* New York, 2006.
66. X Duan, D G Evans, *Layered Double Hydroxides, Structure and Bonding Series; Springer-Verlag:* Berlin, 2006.
67. K Ladewig, Z P Xu, G Q Lu, *Expert Opin. Drug Delivery,* 6(2009), 907.
68. S Bhattacharjee, T. J. Dines, J A. Anderson, *J. Phys. Chem. C,*112(2008),14124-14130.
69. J Zhang, Y F Xu, G Qian, Z P Xu, C Chen, Q Liu, Q. *J. Phys. Chem. C. 114(*2010) 10768-10774.
70. W. T. Reichle, *Solid State Ionics,* 22(1986), 135-141.
71. S M. Auerbach, K A. Carrado, P K. Dutta, P. K. *Handbook of layered materials.* 2004.
72. E. Gardner, K. M. Huntoon, T. J. Pinnavaia, *Adv Mater,*13(2001), 1263-1266.
73. M. Meyn, K. Beneke, G. Lagaly, *Inorg. Chem.*,29(1990), 5201-5207.
74. F. Basile, P. Benito, G. Fornasari, A. Vaccari, *Appl. Clay Sci.*, 48(2010),250-259.
75. C. G.Silva,Y. Bouizi, V. Forns, H. Garca, *J. Am. Chem. Soc.*,131(2009), 13833-13839.
76. K.H. Goh, T.T Lim, Z. L. Dong, *Environ. Sci. Technol.,* 43(2009), 2537-2543.
77. Zhang, H.; Pan, D.; Duan, X. *J. Phys. Chem. C*. 113 (2009), 12140-12148.
78. F. Leroux, J. P. Besse, *Chem. Mater.,* 13(2001), 3507-3515.
79. W. S. Yang, Y. Kima, P. K. T. Liub, M. Sahimia,T. T. Tsotsis, T. T., *Chem. Eng. Sci.,* 57(2002), 2945-2953.

80. T. Kameda,T. Yoshioka, K. Watanabe, M. Uchida, A. Okuwaki, *Appl. Clay Sci.*,35(2007), 173-179.

81. Z. P. Xu, H. C. Zeng, *Chem. Mater.*,13(2001), 4564 - 4572.

82. P. J. Sideris, U. G. Nielsen, Z. H. Gan, C. P. Grey, *Science*, 321(2008), 113-117.

83. J S. Valente, J. Prince, A. M. Maubert, L.L. Rojas, P. D. Angel, G. Ferrat, J. G. Hernandez, E. L. Salinas, *J. Phys. Chem. C*, 113(2009), 5547-5555.

84. J. Rocha, M. Arco,V. Rives, M. A. Ulibarri, *J. Mater. Chem.*, 9(1999), 2499 -2503.

85. J. P. Abello, M. Niek, *Chem. Eur. J.*,13(2007), 870 - 878.

86. J. T. Kloprogge, L. Hickey, R. L. Frost, *Applied Clay Science*., 18(2001), 37-49.

87. V Rives, M. A. Ulibarri, *Coord.Chem. Rev.*, 181(1999), 61-120.

88. A Vaccari, *Appl. Clay Sci.,* 14(1999), 161-198.

89. J. A. Bokhoven, J. C. Roelofs, K. P. Jong, D. C. Koningsberger, *Chem. Eur. J.*,7(2001), 1258 -1265.

90. A Trovarelli, C Leitenburg, M Boaro, G Dolcetti, *Catal. Today*, 50(1999), 353-367.

91. Y. W. Zhang, R Si, C. S. Liao, C.H. Yan, C.X. Xiao, Y. J. Kou, J. *Phys. Chem. B.* 107(2003), 10159-10167.

92. A Trovarelli, *Catalysis by Ceria and Related Materials*. 2002, Catalytic Science Series 2.

93. J. Y. Bai, Z. D. Xu, Y. F. Zheng, H. Y. Yin, *Mater. Lett.*,60(2006),1287-1290.

94. Cabus-Llaurado,M. C.; Cesteros, Y.;Medina, F.; Salagre, P.; Sueiras, J.E. *Micropor.Mesopor. Mater.*,100(2007), 167-172.

95. M. I. Zaki, M. A. Hasan, L Pasupulety, *Langmuir,* 17(2001), 768-774.

96. A Trovarelli, *Catal. Rev. Sci. Eng*.,38(1996), 439-520.

97. S. Imamura, Y. Okumura, T. Nishio, K. Utani, Y. Matsumura, *Ind. Eng. Chem. Res*. 37(1998), 1136-1139.

98. G. Neri, A. Pistone, C. Milone, S. Galvagno, *Appl. Catal. B*,38(2002), 321-329.

99. M Dokiya, *Solid State Ionics*, 383(2002), 152-153.

100. L. Pino, A. Vita, M. Cordaro, V. Recupero, M. S. Hegde, *Appl. Catal.A*,243(2003), 135-146.

101. D Srinivas, C. V. V. Satyanarayana, H. S. Potdar, P Ratnasamy, *Appl. Catal. A,* 246(2003), 323-334.

102. S Bernal, J Kasper, A Trovarelli, *Catal. Today*, 50(1999),173.

103. D. Tichit, B. Coq, *Cat. Tech*, 7(2003), 206-217.

104. W. T Reichle, *J. Catal.*,94(1985), 547-557.

105. A. Trovarelli, C. de Leitenburg, G. Dolcetti, *Chem. Tech.*,27(1997), 32-37.

106. A. Trovarelli, G.Dolcetti,C. de Leitenburg, J. Kaspar, P. Finetti, A.J. Santoni, *J. Chem. Soc., Faraday Trans.*,88(1992), 1311-1319.

107. B. M. Reddy, P. Bharali, P. Saikia, A. Khan, S. Loridant, M. Muhler, W. J.Grunert, *Phys. Chem. C.*,111(2007), 10478-10483.

108. R S Monteiro, L C Dieguez, M Schmal, *Catal. Today*, 65(2001), 77-79.

109. H. Zhang, A. Zhu, X. Wang,T. Wang, C. Shi, *Catal. Commun*., 8(2007), 612-618.

110. C. T. Campbell, C. H. F. Peden, *Science*, 309(2005**)**, 713-714.

111. X Duan, C M Lieber C M., *Adv. Mater*., 12(2000), 298-302.

112. F Luo, C-J Jia, R Liu, L-D Sun, C-H Yan, *Mater. Res. Bull.*, 48 (2013), 1122-1127.

113. B. M. Weckhuysen, D. E. Keller, *Catal. Today*, 78 (2003), 25-46.

114. A. Khodakov, B. Olthof, A. T. Bell, *J. Catal.*,181(1999), 205-216.

115. M. A. Banares, M. V. Martinez-Huerta, X. Gao, J. L. G. Fierro, and I. E. Wachs, *Catal. Today*, 61(2000), 295-301.

116. I. E. Wachs, *Catal. Today*,100 **(**2005), 79-94.

117. W. Daniell, A. Ponchel, S. Kuba, F. Anderle, T. Weingand, D. H. Gregory, and H. Knozinger, *Top. Catal.*, 20 (2002), 65-74.

118. B. M. Reddy, A. Khan, Y. Yamada, T. Kobayashi, S. Loridant, and J.-C. Volta, *J. Phys. Chem. B*, 107 (2003), 5162-5167.

119. M. V. Martinez-Huerta, J. M. Coronado, M. Fernandez-Garcia, A.Iglesias-Juez, G. Deo, J. L. G. Fierro, and M. A. Banares, *J.Catal.*,225(2004), 240-248.

120. J. L. F. Da Silva, M. V. Ganduglia-Pirovano and J. Sauer, *Phys. Rev. B*, 76 (2007), 125117.

121. N. Ekthammathat, T. Thongtem, A. Phuruangrat, and S. Thongtem, J. Nanomater. 2013 (2013), 1-7.

122. L. H. Brixner and E. Abramson, *J. Electrochem. Soc.*,112 (1965), 70 .

123. M. Yoshimura and T. Sata, *Bull. Chem. Soc. Jpn.*,42 (1969), 3195.

124. A. Watanabe, *J.Solid State Chem*., 153(2000), 174-179.

125. J. Liu and Y. Li, *J.Mater. Chem.*, 17 (2007), 1797-1803.

126. L. Fengzhen , S. Xin , Y. Yibin , Z Limin , S Qiaozhen ,S Zhuwei , L Xuehua , M Xianhua ,

J. Rare Earths, 29(2011), 97-100

127. Z-G Yan and C-H Yan, *J. Mater. Chem*., 18 (2008), 5046-5059.
128. S. Gillot, J-P Dacquin, C. Dujardin, P. Granger, *Top. Catal*, 59(2016) , 987-995
129. W. L. Fan, W. Zhao , L. P. You, X. Y. Song, W. M. Zhang, H. Y. Yu, S. X. Sun, *Solid State Chem*.,177(2004), 4399-4403.
130. N Wang, W Chen, Q F Zhang, Y Dai, *Mater. Lett*., 62 (2008), 109-112.
131. H. Wang, Y. Q. Meng and H. Yan, Inorg. *Chem. Comm*., 2004, 7, 553-555.
132. H. Y. Xu, H. Wang, T. N. Jin and H. Yan, *Nanotechnology*, 16(2005), 65-69.

Chapter 2

Experimental methods and characterization techniques

2.1. Introduction

In this chapter, detailed method of preparation of all the catalyst systems will be described along with the characterization techniques that was employed to investigate the catalyst properties. The proper selection and preparation of materials which are reproducible and easily scalable methods are important for stabilizing a catalytic process. Three catalytic systems namely perovskite type oxides, mixed oxides derived from hydrotalcites and cerium orthovanadates were taken for our study for converting the desired hydrocarbons to their respective olefins. An extensive physicochemical characterization of any material is required to investigate and understand the specific properties of the catalyst. The textural properties of the materials like phase composition, crystallinity, surface area, the acid base properties and catalyst morphology with particle size are of considerable importance in tuning the activity. Techniques like powder X-ray diffraction, Nitrogen adsorption, Temperature programmed techniques and Microscopic studies help in probing these properties. Techniques like photoelectron spectroscopy provide a greater insight to the nature and properties of surface of the catalyst. These physicochemical techniques help in drawing out a structure activity relationship based on which various properties of catalyst or reaction parameters can be modified or optimized.

2.2. Catalyst Synthesis

2.2.1. Preparation of Perovskite type oxides

2.2.1.1. Citrate gel method

Stronium nitrate (Alfa aesar), Calcium nitrate (Alfa aesar), Titanium iso-propoxide (Spectrochem) and Manganese nitrate (Alfa aesar) were employed as metal precursors for catalyst synthesis and Citric acid (Thomas Baker) as the gelation agent. The metal precursors were dissolved in minimum amount of water along with citric acid (metal: citric acid in 1:3 ratio). After evaporation of water, the gel was kept in oven at 180 °C after which the dry gel was

ground and calcined at 800 °C. Series of catalysts with different ratios of metal cations in 'A' and 'B' sites were prepared and denoted as given in table below.

S.No	Molar ratio	Code
1	$CaTiO_3$	CT
2	$CaTi_{0.9}Mn_{0.1}O_3$	CTM
3	$Sr_{0.3}Ca_{0.7}Ti_{0.9}Mn_{0.1}O_3$	SC7TM
4	$Sr_{0.4}Ca_{0.6}Ti_{0.9}Mn_{0.1}O_3$	SC6TM
5	$Sr_{0.5}Ca_{0.5}Ti_{0.9}Mn_{0.1}O_3$	SC5TM
6	$Sr_{0.6}Ca_{0.4}Ti_{0.9}Mn_{0.1}O_3$	SC4TM
7	$Sr_{0.7}Ca_{0.3}Ti_{0.9}Mn_{0.1}O_3$	SC3TM
8	$Sr_{0.5}Ca_{0.5}Ti_{0.925}Mn_{0.075}O_3$	SC5TM-075
9	$Sr_{0.5}Ca_{0.5}Ti_{0.75}Mn_{0.25}O_3$	SC5TM-25
10	$SrTi_{0.9}Mn_{0.1}O_3$	STM
11	$SrTiO_3$	ST
12	$CaMnO_3$	CM

Table. 2.1. Perovskite type catalyst composition and their codes

2.2.1.2. Glycine combustion method

Perovskites were also prepared by glycine combustion method in which metal ions to glycine ratio was maintained as 1:2. Appropriate amount of glycine was dissolved in 50 ml of distilled water and to this solution a stoichiometric amount of metal precursors were added. The mixtures were thoroughly stirred by magnetic mixer to eliminate the water at 80 °C until the homogeneous sol-like solution was formed. Then the solution was ignited in air and then calcined at 800 °C for 6 hours. The obtained catalysts were ground and weighed.

2.2.2. Preparation of mixed oxide derived from hydrotalcite

The cerium containing hydrotalcites were prepared by a modified conventional co-precipitation method.[1] Aluminium nitrate, magnesium nitrate (Merck), cerium(III) nitrate (Alfa Aesar), sodium hydroxide and sodium carbonate (Merck) were employed as precursors for catalyst preparation. The metal nitrate precursors (Mg^{2+}, Al^{3+}, Ce^{3+}) were dissolved in water and the precipitating agent containing NaOH and Na_2CO_3 were added simultaneously drop wise at a

constant pH (9.5 ± 0.2). After this, it was hydrothermally treated, where the precipitated solution was taken in a teflon lined autoclave and placed in an oven maintained at 150 °C for 12 hours without stirring. The precipitate was filtered and washed to remove excess base which was then dried overnight at 110 °C followed by calcination at 450 °C for 6 hours. The cerium containing mixed oxide ($Mg_3Al_{1-x}Ce_xO_y$) was prepared with various molar amounts of cerium (x = 0.01, 0.03, 0.05, and 0.5). The above catalysts are labelled as MAC-1, MAC-2, MAC-3 and MAC-4 respectively and MAC stands for magnesium, aluminium and cerium.

Mg:Al:Ce mole ratio	**Code**
Mg(Al)O (3:1)	-
(3:0.99:0.01)	MAC-1
(3:0.97:0.03)	MAC-2
(3:0.95:0.05)	MAC-3
(3:0.5:0.5)	MAC-4
CeO_2	-

Table. 2.2. Mixed oxide catalyst compositions and their codes

2.2.3. Preparation of orthovanadates

$CeVO_4$ was prepared by a pH modified hydrothermal route. Cerium (III) nitrate (Alfa Aesar), Ammonium metavanadate (Merck), Manganese (II) nitrate (Alfa Aesar), Chromium(III) nitrate (Alfa Aesar), Iron(II) nitrate (Alfa Aesar), Cobalt nitrate (Alfa Aesar) were used as metal precursors, Nitric acid (Merck) for stabilization and NaOH during precipitation. Ammonium metavanadate was dissolved in 50 mL of warm distilled water under vigorous stirring and to this solution drops of dilute HNO_3 was added to reduce the pH to 1.8. After maintaining the pH cerium nitrate was added to this solution. After homogenizing the metal salts, NaOH (1 M) was added dropwise to precipitate cerium and vanadium ions as $CeVO_4$. This solution with precipitate was transferred to teflon lined autoclave and placed in oven for 24 hours which was maintained at 180 °C. After cooling the precipitate was centrifuged and washed several times to remove excess base. This precipitate was dried in oven for 12 hours after which it was calcined at 600 °C. By this method during homogenizing metal ions other transitional metals like Cr, Mn,

Fe and Co were added. The $CeVO_4$ were prepared with various heteroatoms were prepared and denoted as given in table below.

S.No	Catalyst (molar ratio)	Code
1	$CeVO_4$ (1:1)	CV
2	$CeCrVO_4$ (0.8:0.2:1)	CCrV
3	$CeMnVO_4$ (0.8:0.2:1)	CMV1
4	$CeMnVO_4$ (0.88:0.12:1)	CMV2
5	$CeMnVO_4$(0.94:0.06:1)	CMV3
6	$CeFeVO_4$ (0.8:0.2:1)	CFV
7	$CeCoVO_4$(0.8:0.2:1)	CCV

Table. 2.3. Orthovanadate type catalyst composition and their codes

2.3. Characterization techniques

The structure activity relationship can be understood and activity can be tuned based on the properties of the catalyst. This emphasizes the importance of the characterization techniques which play a pivotal role in understanding and tuning the activity. The theory and working principle of the various characterization techniques are given below along with the detailed procedure that we employed to study the materials mentioned above.

2.3.1. Powder X-Ray diffraction

In the early 20th century, Max Theodor Felix von Laue showed that crystalline materials behave as 3D-diffraction gratings at particular X-ray wavelengths which are similar to that of d-spacing of two planes in a crystal lattice.[1] Later W. H. Bragg and W. L. Bragg derived Bragg's law according to which, when a X-ray possessing a wavelength similar to the d-spacing upon incident on a sample that is crystalline and by the virtue of atom scattering undergo constructive interference. The mathematical expression of the Bragg's Law is,

$$n\lambda = 2\,d\sin\theta \qquad 2.1$$

in which **λ**-is the wavelength of the X-ray, **d**- is the spacing between the planes, **n**-is the order and **θ**-angle between incident ray and scattering planes.[2]

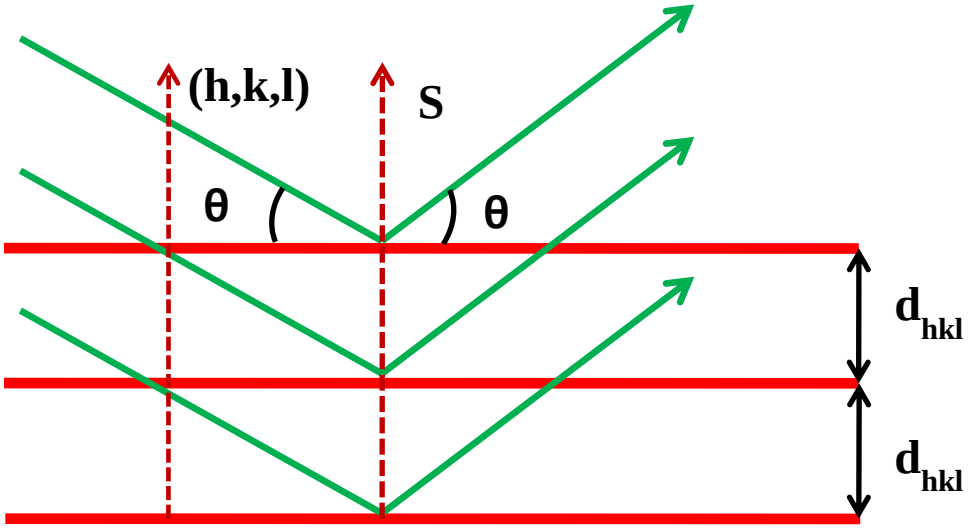

Fig. 2.1. Principle of Bragg's law

After diffraction the detected X-rays are processed and counted. When the sample is scanned in a wide range of 2θ angles it provides the details of powdered sample based on all possible diffraction directions of the lattice because of the random orientation of the material. Mathematically deriving the d-spacings from the diffraction peaks to d-spacings helps in identifying the material as each material has their own unique d-spacings. Usually the above conformation is made by comparing it with standard reference pattern. PXRD is an important tool that is used for determining the structure of materials that are characterized by long-range order.[3] The width of the peaks obtained gives information about the dimension of the reflecting planes. When the size of the crystallite is below 100 nm range the diffraction peak broadens and based on this relation XRD patterns can be utilized to calculate the average crystallite size using the Scherrer formula.

$$t = 0.9\lambda / \beta \cos\theta \qquad 2.2$$

where **t** = thickness of the crystallite (Å), **λ**-is the wavelength of the X-ray, **θ**-angle between incident ray and scattering planes and **β**- is the full width half maximum of the diffraction peak that is considered.

Powder X-ray diffraction (PXRD) data of materials that are reported in this thesis were collected using a PANanalyticalX'pert Pro dual goniometer diffractometer. The data were collected with a step size of 0.008° and a scan rate of 0.5° min^{-1}. The radiation used was Cu-Kα (1.5418 Å) with

a Ni filter and data collection was carried out using a flat holder in Bragg-Brentango geometry. In this geometry, the diffraction vector (s) is always normal to the surface of the material.

2.3.2. N_2 Physisorption

The N_2 physisorption is one of the most important techniques for measuring the surface area and porosity of materials. Usually B.E.T analysis method is the standard method for deriving surface areas from nitrogen adsorption isotherms and was initially determined for multilayer gas adsorption on flat surfaces. The concept and calculations were made by the application of the theory developed by Brunauer, Emmett, and Teller to nitrogen adsorption isotherms. The B.E.T equation is derived based on certain assumptions like

(i) adsorbate physically adsorb on a solid in layers infinitely (ii) From zero coverage to full coverage for all the layers of adsorbate, the adsorption energy remain the same (ii) there is no inter molecular interaction between the adsorbate layers (iii) a new layer starts adsorbing when the earlier layer is not completely covered.

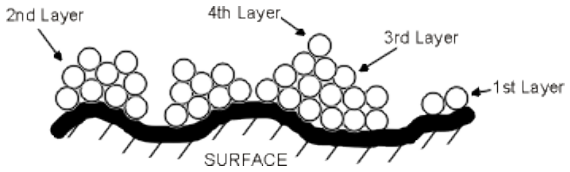

Fig. 2.2. Surface adsorption

The B.E.T equation[4] is,

$$\frac{1}{v\left[(p_0/p)-1\right]} = \frac{c-1}{v_m c}\left(\frac{p}{p_0}\right) + \frac{1}{v_m c} \qquad \textbf{2.3}$$

where,

$\mathbf{v_m}$ is the volume of amount of gas adsorbed after a complete monolayer formation

p is the equilibrium pressure of adsorbate

$\mathbf{p_0}$ is the saturation pressure of adsorbate

c is the BET constant

and **v** is the total amount of gas absorbed

Mathematically the above equation based on experimental results can be plotted as a straight line with1/v [(p_0/p) -1] on the y-axis and φ in x-axis (φ- p/p_0) and this plot is called as BET plot. In order to calculate the amount of Nitrogen adsorbed a linear relationship between 1/v [(p_0/p) -1] and P/P_0 is needed. Generally a limited portion of the total isotherm is used for this i.e. 0.05-0.30. As

shown in plot below **(Fig. 2.3)** The monolayer volume which is denoted as V_m is calculated by 1/(S+I), in which S is the slope and is equal to $(C-1)/CV_m$ and I is the intercept and is equal to $1/CV_m$.[4]

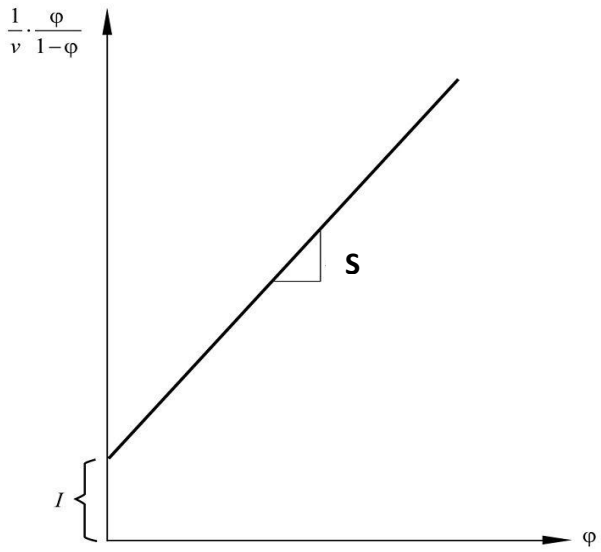

Fig. 2.3. Graphical plot of B.E.T equation

By B.E.T method the total and specific surface area can be obtained. Specific surface area obtained is generally expressed in units of area per mass of sample (m^2/g). This is calculated by,

$$S_{total} = (v_m * Ns)/V \quad \textbf{2.4}$$

$$S_{ssa} = S_{total}/a \quad \textbf{2.5}$$

in which, $S_{total}$is the total surface area and $S_{ssa}$is the specific surface area,

N-Avogadro Number, s-adsorption cross section, V- molar volume of the adsorbate and a- mass of the adsorbent.

Nitrogen adsorption-desorption isotherms for the materials were collected from an Quantachrome autosorb IQ analyzer. After degassing the samples at 200 °C the adsorption was done at liquid nitrogen temperature (77 K). The isotherms were obtained in the relative pressure range, P/P_0= 0.005 to 1.0. The Brunauer-Emmett-Teller (BET) equation was used to calculate the surface area from the adsorption branch.

2.3.3. Thermal Analysis

The process in which the change in property of the material measured with respect to temperature is generally called as thermal analysis. Among thermal analysis methods thermo

gravimetric analysis (TGA) is an important tool to study the change in mass of the solid in response to change in temperature. This technique is widely employed for studying various behavior of materials like its thermal stability, determining the volatile content in sample, degradation characteristics, sintering behavior, etc. Thermogram obtained as a function of temperature provides both qualitative and quantitative information. Thermogram curve provides a relationship between the mass change and to the stoichiometry involved.

TGA of all the samples reported in this thesis were done using a METTLER-TOLEDO TGA/SDTA851e instrument. For weight loss measurements the sample was heated from room temperature to 800 °C in presence of air and the weight loss was monitored. For Oxygen uptake measurement the catalysts was activated in presence of Helium up to 800 °C and cooled. In next step the catalyst was heated from room temperature to 700 °C in presence of oxygen.

2.3.4. Temperature Programmed Desorption

Understanding the nature of the surface and its adsorption properties, it is important in tuning the properties of the catalyst as interaction of reactants with the catalyst surface which is an important step in heterogeneous catalysis. Many techniques are usually employed for this purpose and one among that is temperature programmed desorption (TPD). In this after cleaning the sample surface a probe molecule is adsorbed in room temperature and desorbed at higher temperatures. The desorbed molecules are detected by thermal conductivity detector and can be quantified using a standard calibration.[5,6] TPD is generally used to determine the acidity or basicity of the material taken for study. For evaluating the acidity the usual probe molecule used is ammonia and in some special cases primary and branched amines are also employed. For evaluating the basicity the common probe used is CO_2. Quantities desorbed under different T_{max} provide information on the number, strength and heterogeneity of the adsorption sites. The amount of NH_3/CO_2 desorbed is proportional to the acidity/basicity.

The basicity of the catalysts was measured by TPD of CO_2 using a Micromeritics Autochem-2920 instrument. Prior to the experiment, the sample was activated at 450 °C in Helium flow (40 mL/min) for 1 h and was cooled down to room temperature. After which CO_2 was adsorbed by exposing the sample to10 % CO_2 in Helium (30 mL/min) for 30 minutes. In order to remove the physisorbed CO_2 the temperature was raised to 100 °C and flushed with He for 1 h. Desorption of CO_2 was carried out in Helium flow (40 mL/min) by rising the temperature from 100 to 800

°C at a heating rate of 10 °C/min. The amount of CO_2 desorbed was estimated quantitatively by a TCD which was calibrated before the TPD study.

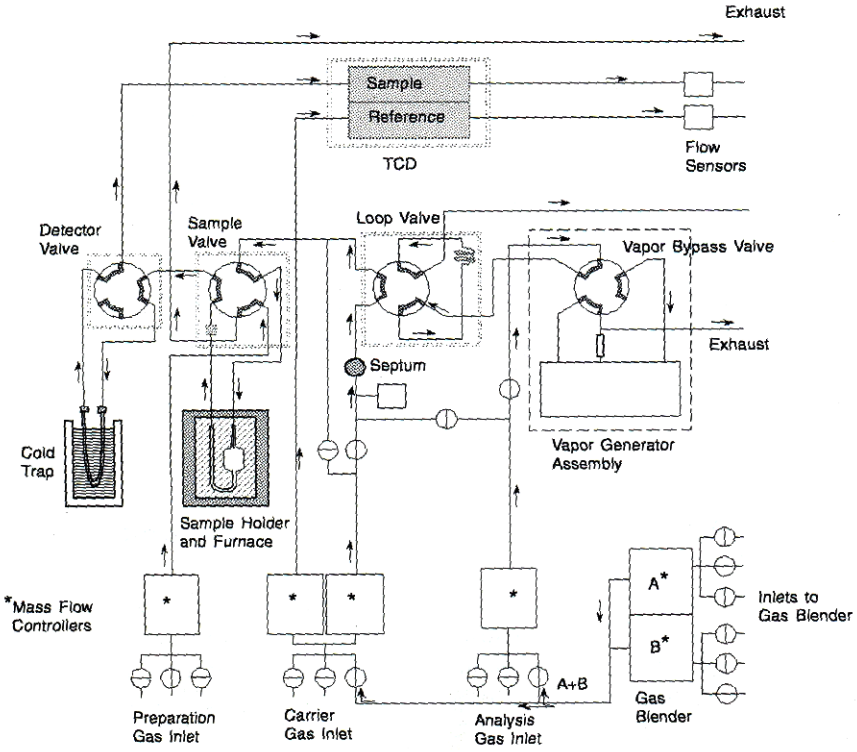

Fig. 2.4. Schematic diagram of TPD instrument

2.3.5. Raman Spectroscopy

Raman spectroscopy is based on the findings of Sir C.V. Raman which was published in 1928.[7] It can be used for both qualitative as well as quantitative purposes. This technique can be qualitative by identifying the frequency of scattered radiations and also can be quantitative if the peak of scattered radiations is integrated. This technique is a scattering technique which follows the principles of Raman Effect which states that frequency of a small fraction of scattered radiation is different from frequency of monochromatic incident radiation. This is due to the inelastic scattering of radiation and its interaction with molecules which are vibrating. By this scattering the molecular vibrations can be probed.[8,9]

In a typical experiment a monochromatic laser beam strikes the sample after which due to the interaction of this light with molecules in a material taken a scattering occurs. This light that is scattered which is of different frequency from that of incident light is employed to construct a Raman spectrum. The spectra is obtained due to an inelastic collision between incident monochromatic radiation and molecules of sample. Most of the scattered radiation has a

frequency which is equal to frequency of incident radiation (Rayleigh scattering). A very less fraction of this scattered radiation possesses a frequency different from frequency of incident radiation (Raman scattering). In this there are two types of radiation in which the frequency of incident radiation is more than frequency of scattered radiation (Stokes lines) and the frequency of incident radiation lower than frequency of scattered radiation (anti-Stokes lines). Generally Stokes lines are highly intense when compared to anti-Stokes bands. Thus stokes lines are used in conventional Raman spectroscopy and anti-Stokes bands are generally used for fluorescing samples as this fluorescence causes interference with Stokes bands.[10] The selection rule for Raman spectroscopy is that the sample should show a change in polarizability during molecular vibration.

Raman spectra were recorded using a Horiba JY LabRAMHR800 Raman spectrometer coupled with a microscope in reflectance mode with a 514 nm and 635 nm excitation laser sources and a spectral resolution of 0.3 cm^{-1}. The sample was pelletized into small discs for analysis.

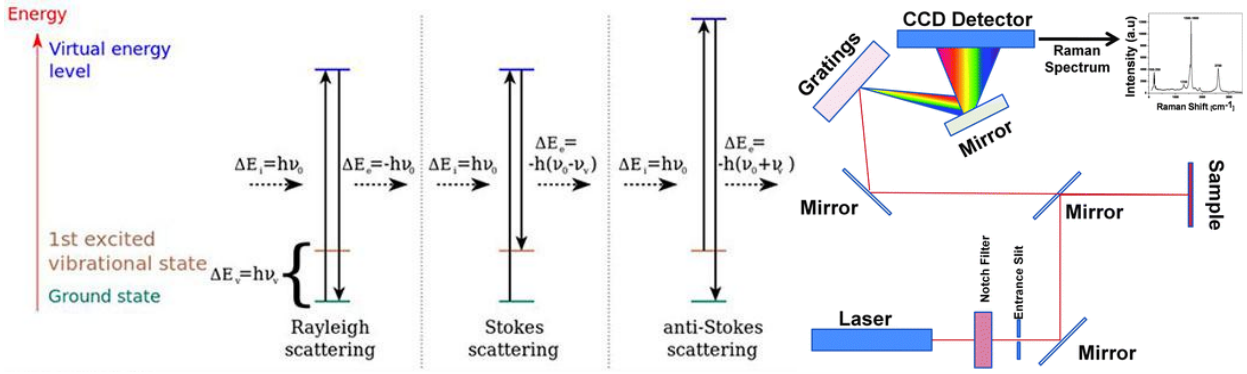

Fig. 2.5. Different types of light scattering and Raman spectroscopy instrument schematic

2.3.6. Scanning Electron microscopy and Energy Dispersive X-ray Analysis (EDAX)

From Scanning Electron Microscope (SEM) information regarding the morphology and surface topology of the material can be obtained by tracing a sample in a raster scan pattern with a beam of electrons. Detection of the secondary electrons that are emitted from atoms in specimen is the common method of analysis in SEM. The topography of the surface of the sample is created by scanning and collecting the secondary electrons which are emitted by employing a special detector. In a typical analysis the electron beam is focused with the help of probe and lenses which scans the surface of material with the help of scanning coils. When the electrons strikes the material it emits signal as electromagnetic radiation. This radiation which is generally

secondary and backscattered electrons are received by the detector and later this resulting signal is amplified and displayed.[11]

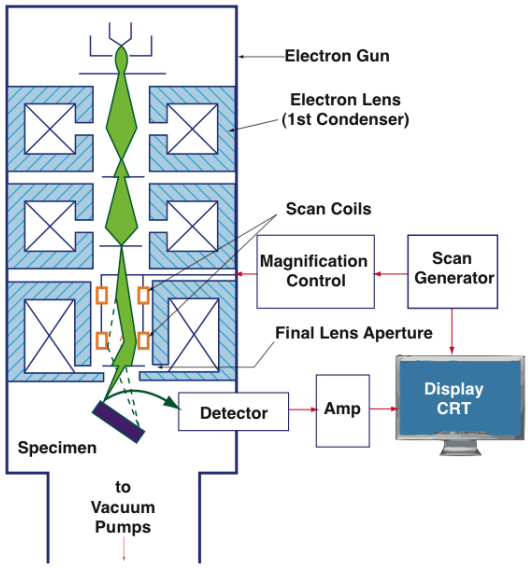

Fig. 2.6. Schematic diagram of SEM instrument

Energy Dispersive X-ray Analysis (EDAX) is generally employed for elemental analysis and finding the chemical composition. Usually high-energy electrons strikes and interacts with atoms in a material in a number of ways and one among is the emission of X-rays. In this process an electron strikes an atom which ejects an electron which was originally positioned in an inner shell. To retain the atom to its original low energy state this vacancy is filled by an electron from high energy shell. During this the electron releases some of its energy as X-rays and this energy released is almost equal to the energy difference between the two levels. All elements in periodic table except hydrogen and helium produce characteristic X-rays which can be used to identify and to calculate the elemental compositions.[12] Usually the EDAX is coupled with microscopic techniques as these are electron beam based techniques which can be used to scan for EDAX also.

The SEM images and EDAX of our materials were obtained using a FEI, Model Quanta 200 3D. The catalyst were dispersed in 2-propanol by ultrasonication and drop casted on silicon wafer.

2.3.7. Transmission Electron microscopy

Transmission electron microscopy is one of the most important and powerful tool for investigation of any material. In this technique a beam of electrons from the electron gun is condensed into focused coherent beam by using multiple condenser lenses and these lenses also

exclude high angle electrons. This electron beam later strikes the materials and is transmitted depending upon the thickness and electron transparency of the specimen. By using objective lens this transmitted electron beam is focused into an image on charge coupled device (CCD) camera. High resolution Transmission Electron Microscope (HRTEM) is used to obtain information in nanomaterials in atomic scale.

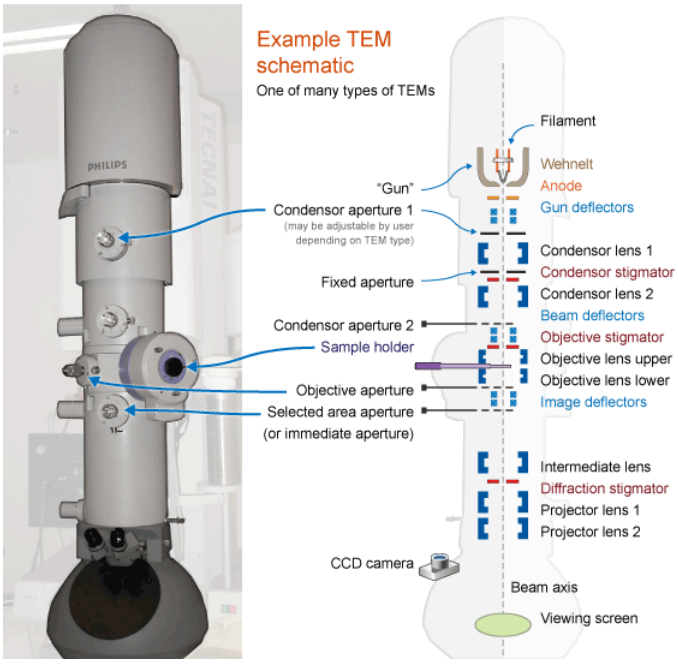

Fig. 2.7. TEM Instrument schematic

An FEI TECNAI F30 electron microscope operating at 300 kV was used for recording high resolution transmission electron microscopy (HRTEM) images of all materials. Samples were powdered and dispersed in isopropanol before depositing onto a holey carbon grid.

2.3.8. X-ray Photoelectron Spectroscopy (XPS)

XPS is one of the powerful surface sensitive technique which helps in analyzing elemental composition, chemical state and electronic state of a material. The XPS works on the Einstein's photoelectric effect where when a beam of photons of desirable threshold frequency strikes a material electrons are emitted. In XPS a beam of X-ray are shone over surface of the solid surface and the kinetic energies of electrons are measured and counted which usually are emitted from few nanometer depth of the surface. A typical XPS spectra is thus obtained by counting the electron over a varied kinetic energies of electron. The peaks that appearing at particular kinetic energy gives the qualitative information and on integration gives the quantitative information. The chemical state and binding energy of a particular electron can be determined by measuring

the kinetic energy of the emitted electrons. The binding energy depends upon i) The parent element from which the electron is emitted along with the orbital from which it is ejected and ii) The chemical environment of the atom from which the electron was emitted.

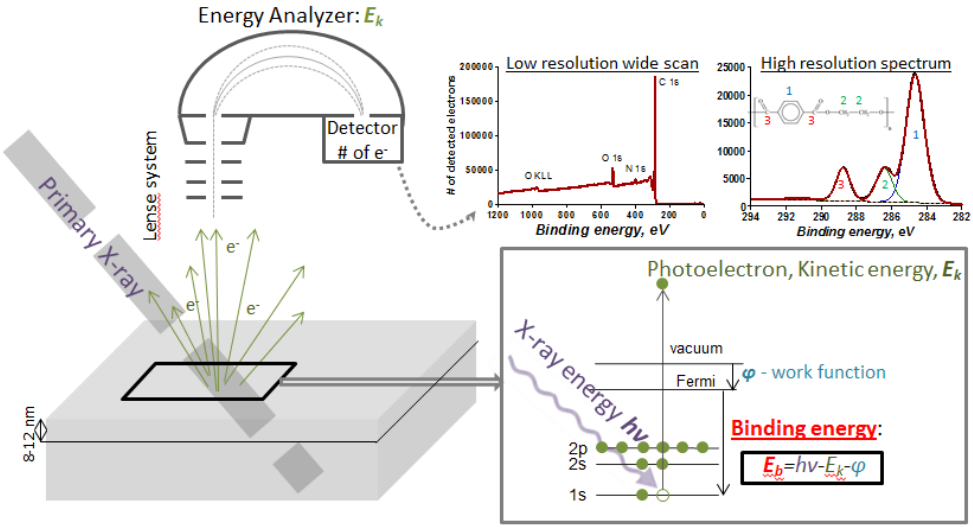

Fig. 2.8. XPS principle and instrument schematic

XPS of our samples were analysed in a custom built near-ambient pressure photoelectron spectrometer (NAPPES) (Prevac, Poland). This instrument has a monochromatic Al Kα X-ray source (VG Scienta, MX 650), a dual anode (Al Kα, Mg Kα) source and a Helium UV discharge lamp. The analysis chamber is equipped with a differentially pumped high pressure electron analyzer (VG Scienta, R3000 HP). The analyzer aperture cone is of 0.8 mm and in this setup XPS can be performed up to 1mbar.[13]

2.4. Catalytic Activity

The catalytic activity of all the materials prepared were tested using a fixed bed reactor (FBR) having two furnace zones. For ODH of EB, an inconel reactor tube with 13 mm internal diameter and 510 mm length was used to pack the catalyst. For ODH of ethane and 1-butene an inconel reactor tube with 8 mm internal diameter and 480 mm length was used. The temperature on the wall of the reactor and in the catalyst bed was measured using a K-type coaxially centered thermocouple. The catalyst was pelletized and sieved through the mesh size of 1.6-1.7 mm. The catalyst charge was 1 cm^3 of sieved materials and was placed in the middle of the reactor using glass wool. On the top and bottom of the catalyst bed the reactor was filled with inert ceramic beads which does not possess any catalytic activity. The pre-heater zone is important to facilitate

complete vaporization in case of ethyl benzene. The catalyst tests were conducted at different temperatures and with various flow rates of oxidant and substrate. Ethyl benzene was pumped using a precision isocratic pump (Lab Alliance Series II) and the gases flow was controlled using a Brook's make Mass Flow Controller (5890E series) of respective gases. The reactants flow was up flow in case of EB and down flow in case of shorter chain alkanes. The liquid and gaseous products were separated in a gas-liquid separator where the gaseous products were analyzed by online GC.

Fig. 2.9. Multiple fixed bed reactor used for testing the catalysts

The liquid products were analyzed offline using an Agilent 6890N gas chromatograph with a BP-5 (5.5% phenyl methyl siloxane) column along with an FID detector. The gaseous sample was analyzed by Thermofischer 1110 Gas chromatography instrument equipped with chromeleon 7 software. In a typical online GC analysis the hydrocarbons were eluted by Restek Alumina plot-Q column followed by detection in FID detector and the permanent gases were eluted by Porapak Q and Molecular Sieves column connected in series followed by detection in TCD. A combined gas chromatograph from dual channel analysis in reference to response from calibration mixture gave the concentrations in the reaction mixture.

GC results were analyzed for the conversion as well as selectivity and yield of the product. Conversion is defined as the fraction of reactant transformed and given by the relation:

$$\text{Hydrocarbon (HC) conversion (mol \%)} = 100\times (HC_{in}-HC_{out})/HC_{in} \quad \textbf{2.6}$$

Selectivity has been determined from the peak area as[14],

$$\text{Selectivity}_i \text{ (wt \%)} = 100 \times \text{area}_i / (\text{sum of all areas}) \quad \textbf{2.7}$$

It is calculated for each product based on its formation.

Reaction yield or partial conversion for a given product is therefore,

$$\text{Yield}_i = (\text{conversion}_i \times \text{selectivity}_i)/100 \quad \textbf{2.8}$$

The concept of space velocity[15] is the ratio of flow rate to the size of the catalyst bed. Some versions of space velocities are,

Gas hourly space velocity (GHSV) = Volume of feed as gas/volume of catalyst **2.9**

Liquid hourly space velocity (LHSV) = Volume of liquid feed/volume of reactor or catalyst **2.10**

2.5. References

1. C. Kittel, Introduction to Solid State Physics, New York: John Wiley & Sons (1976). ISBN 0-471-49024-5.
2. W.L. Bragg, "The Diffraction of Short Electromagnetic Waves by a Crystal", Proceedings of the Cambridge Philosophical Society, 17 (1913), 43-57.
3. N. F. M. Henry, J. Lipson and W. A. Wooster, *The interpretation of x-ray diffraction photographs*, Macmillan and Co Ltd., London, (1951).
4. S Brunauer, P. H. Emmett, E Teller, *J. Am. Chem. Soc.*, 60 (1938), 309-319
5. D. A. King, *Surface Science*, 17(1975), 384
6. E. Habenschaden and J. Küppers, *Surface Science*, 138 (1984), 147.
7. C.V. Raman, K.S. Krishnan, Nature, 121 (1928), 501-502
8. D.A. Skoog, F.J. Holler, S.R. Crouch, Principles of instrumental analysis, (6th ed.) Cengage Learning (2006)
9. J.M. Chalmers, H.G.M. Edwards, M.D. Hargreaves, Infrared and Raman spectroscopy in forensic science, (1st ed.) John Wiley & Sons Ltd., United Kingdom (2012)
10. E. Smith, G. Dent, Modern Raman spectroscopy: a practical approach, John Wiley & Sons, England, Chichester (2005)
11. J. I. Goldstein and H. Yakowitz, Practical Scanning Electron Microscopy, Plenum Press, New York.
12. Energy Dispersive Analysis, Spectroscopy and Separations EKB Series, John Wiley & Sons Ltd, 2015.
13. K. Roy, C. P. Vinod and C. S. Gopinath, *J. Phys. Chem. C*, 117(2013), 4717- 4726.
14. F Malherbe, C Forano, B Sharma, M. P Atkins, J. P. Besse, *Appl. Clay Science*, 13 (1998), 381-399.
15. V. G. Jenson, G. V. Jeffreys, *Mathematical methods in chemical enginnering*. 2nd Edition, Academic press, *6*, 1977.

Chapter 3

Oxidative dehydrogenation of ethane to ethene over Manganese substituted $Ca(Sr)TiO_3$ perovskite type oxides

Synopsis

- Various molar ratios of manganese substituted calcium/strontium based perovskites were prepared by simple citric acid gel method

- Structural refining and lattice parameters were derived for all the synthesized samples

- From XPS analysis of $Sr_{0.5}Ca_{0.5}Ti_{0.9}Mn_{0.1}$(SC5TM), it was evident that the "Mn" species exist in lower oxidation state at the temperature range of 450-550 °C which drive in more of total combustion of ethane which was also evidenced in catalytic activity

- Based on the optimization studies the catalyst with optimum amounts of Sr,Ca,Ti,Mn (SC5TM) shows the best catalytic activity towards ODHE

- SC5TM shows a stable catalytic activity for long time on stream without any significant loss

3.1. Introduction

The strategic bloom of shale gas has provided a vast opportunity in probing ways to utilize them for more value added products. Owing to the great increase in demand for the shorter chain olefins there is a wide scope to look for better catalysts to convert shorter chain alkanes to their respective olefins. High operational costs and environmental issues have made this conversion profitable only on a very large scale. Brazdil[1] has pointed out that ‘‘the direct conversion of ethane and propane to commodity chemical intermediates has the potential to radically transform the chemical industries. The effectiveness of the catalyst, that is the activity for alkane conversion and the selectivity to desired products, will ultimately determine the economics of an alkane-based chemical process. The successful commercial technologies will be those that link catalyst performance characteristics with “innovative process designs”. **Table. 3.1** shows that there is a plenty of ethane available in shale gas which are a comparatively economical starting material for the production of ethene and other value added chemicals.

S. No	Compound	Mol %
1	Methane	77.60
2	Ethane	13.20
3	Propane	5.00
4	n- butane	1.30
5	Isobutane	1.10
6	Natural Gasoline	1.00
7	Inerts (N_2, CO_2)	0.80

Table. 3.1. Composition of the shale gas obtained from Eagle ford drill in US[2]

3.2. Commercial importance of ethene

Ethene is one of the most important building block chemical and it ranks first in production among the organic chemicals (**Table. 3.2**).[3-5] It is also one of the important platform chemicals for the synthesis of variety of fine chemicals as shown in **Fig. 3.1**. Ethene may be polymerized directly to produce polyethylene, which is world's most widely used plastic. Ethene is

chlorinated to form 1,2-dichloroethane which is a precursor for the production of plastic polyvinyl chloride, or combined with benzene to produce ethyl benzene which in turn is used for production of polystyrene. Ethene is also oxidized to produce chemicals like ethylene oxide, ethanol, and polyvinyl acetate. It is also the base material for the production of variety of chemicals like low, linear low and high dense polyethylenes (LDPE, LLDPE, HDPE respectively, Ethylene dichloride (EDC), Vinyl compounds like Vinyl chloride, poly vinyl chloride (PVC), Vinyl acetate (VAM), Styrene and many functionalized compounds **(Fig 3.2)**.

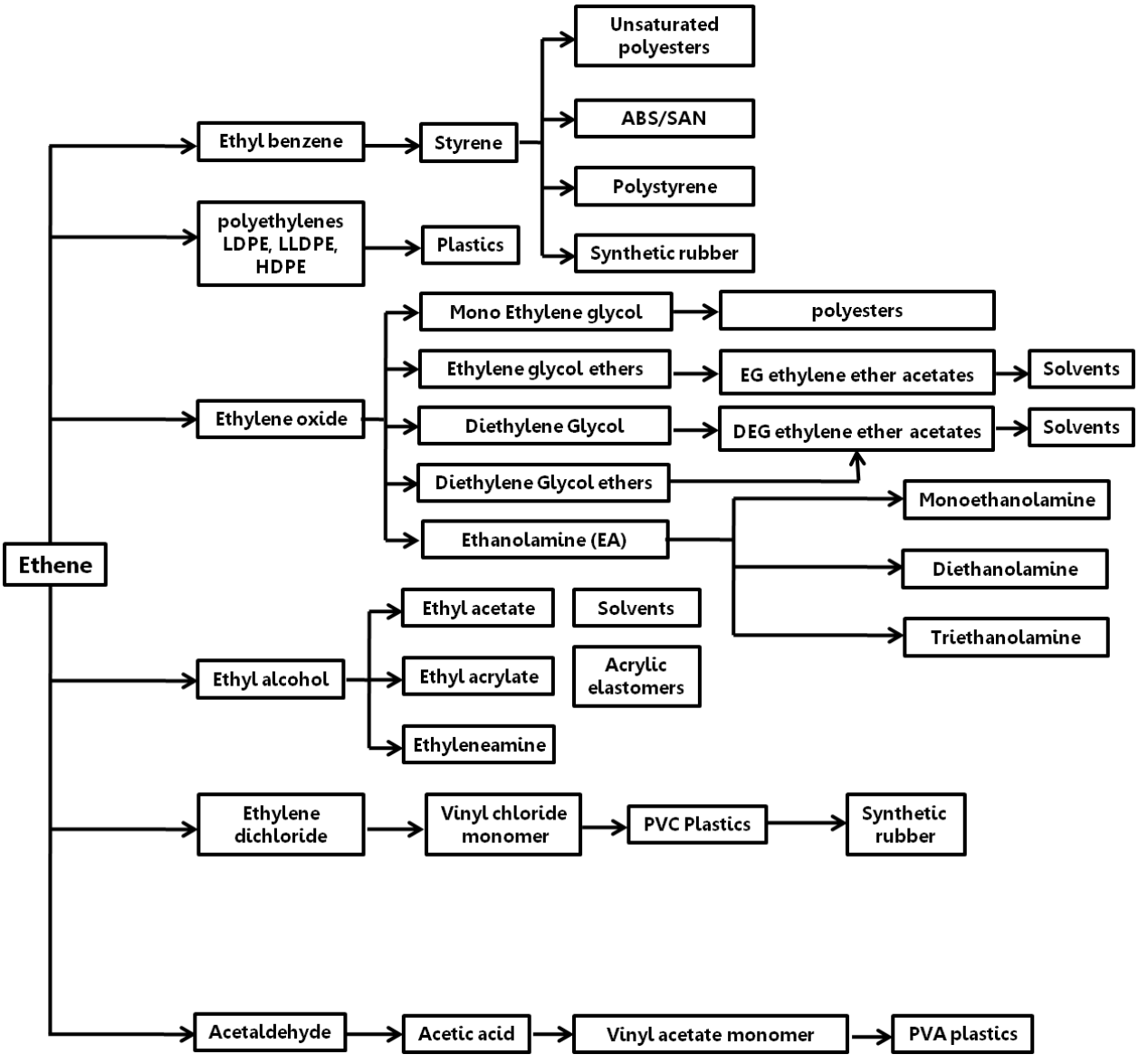

Fig. 3.1. Value added products from Ethene[5]

Chemical	**U.S.A**	**Asia[a]**	**China**	**Europe**
Ethene	23975	18237	14188	19968
Propene	14085	14295	n.a[b]	14758
Ethylene dichloride	8810	3222[c]	n.a	1323
Benzene	6862[d]	10889	5530	5107
Ethyl benzene	4240	n.a	n.a	1226
Cumene	3478	n.a	n.a	n.a
Ethylene dioxide	2664	845[c]	n.a	2619
Butadiene	1580	2715	n.a	2020
Methanol	n.a	n.a	15740	n.a
(a) Japan, South Korea, Taiwan. (b) Info. Not available. (c) Japan only. (d) Thousands of liters				

Table. 3.2. Production of Organic Chemicals in 2010 in Thousands of Metric Tons[4]

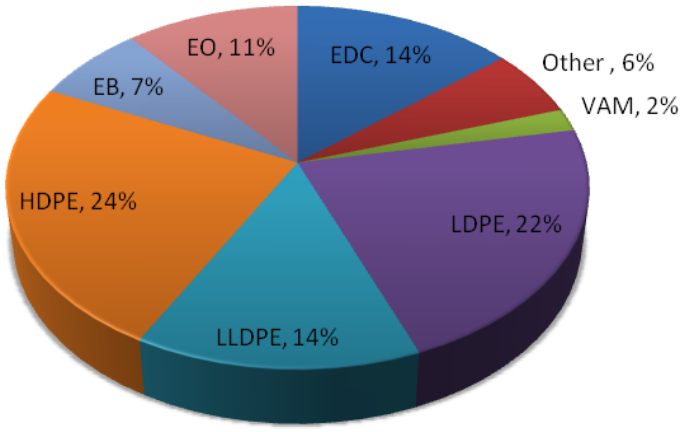

Fig. 3.2. Commercially important products from Ethene as on 2013[5]

3.3. Current commercial production of Ethene

Commercially ethene is produced from three important methods they are i) Steam cracking, ii) Catalytic dehydrogenation of ethane, and iii) Dehydration of Bioethanol

3.3.1 Steam cracking

For the industrial production of ethene, steam cracking is the widely practiced process for the past 50 years. This process is carried out with two different types of feedstock; one is ethane as such and other is naphtha. In a typical process **(Fig. 3.3)**, initially a diluted alkane feed is preheated to a temperature between 550 and 650 °C by homogenizing with higher ratio of steam. This preheated mixture is passed through a high temperature reactor which is maintained in a temperature between 800-900 °C and at shorter residence time to undergo controlled pyrolysis to produce olefins and di-olefins.[3] A rapid quenching of stream coming out of reactor is necessary to avoid product degradation.

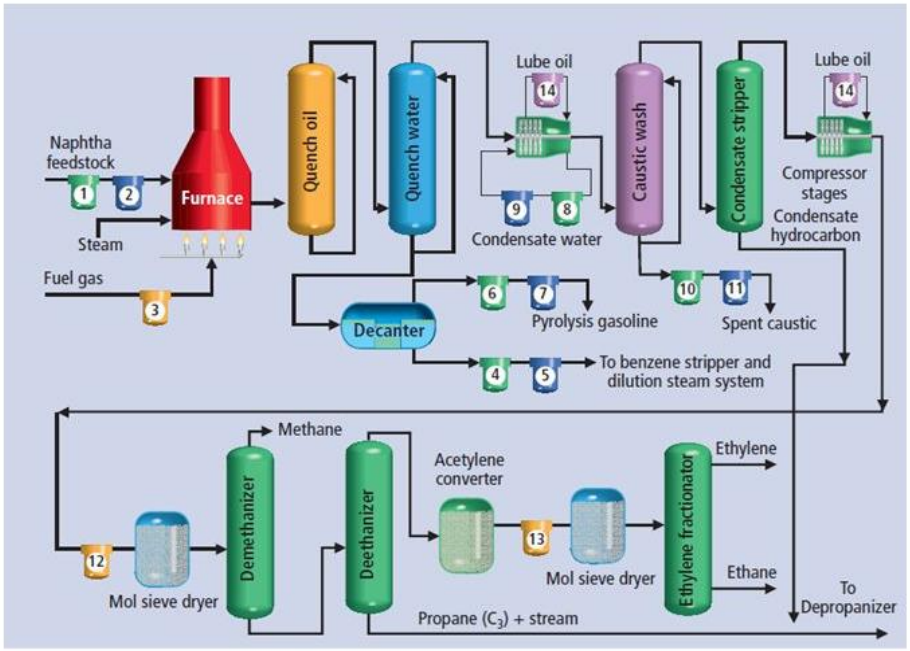

Fig. 3.3. A typical Naphtha cracker

In a steam cracking when ethane is used as feedstock process per pass conversion around 70 % with almost 50 % yield of ethene is obtained.[3] This process suffers from many operational difficulties and drawbacks. As the temperature for cracking is high the actual temperatures in reaction tubes reach up to 1100 °C so the materials designed for the process should be heat resistant. A major concern in an industrial process is the energy economy and heat integration of the process. In this context the total energy required for ethene production is 16 GJ $t^{-1}$when ethane is the feedstock and 23 GJ t^{-1} when naphtha is the feedstock.[3] Along with this considerable amounts of coke are deposited on the reactor walls which is removed by gasification using steam due to which plants has to be shutdown frequently.

3.3.2. Catalytic dehydrogenation of ethane

Dehydrogenation process is an endothermic limited pathway wherein high temperatures and low pressures are required. In a typical dehydrogenation to obtain a equilibrium ethane conversion of 40 % around 700 °C is needed and also at high pressures the equilibrium shift towards ethane.[6,7]

$$C_2H_6 \leftrightarrow C_2H_4 + H_2,\ \Delta_rH_{298} = 136\ kJ\ mol^{-1} \qquad \textbf{3.1}$$

The catalysts which are based on 'Cr' or 'Pt' were employed for above said process but this catalyst gets deactivated by the formation of coke and due to side reactions (dienes, polymers etc.). Many processes and their modified versions (Catadiene, Catofin, UOP oleflex, etc) were developed but none of the process could compete with steam cracking due to their poor per pass yields.

3.3.3. Dehydration of Bioethanol

The bioethanol obtained from biomass can be dehydrated to ethene under mild endothermic conditions in presence of solid acid catalysts. In a typical dehydration process ethanol is preheated and passed through a catalytic reactor and after reaction from the product, liquid stream containing ethanol and water are separated from the gas stream in which ethene is the main constituent.[8] This the economical process but the availability of ethanol limits the process.

$$C_2H_5OH \leftrightarrow C_2H_4 + H_2O,\ \Delta_rH_{298} = 45.6\ kJ\ mol^{-1} \qquad \textbf{3.2}$$

Along with the above three major processes some processes like Oxidative coupling of methane (OCM), Methanol to olefins (MTO), Fischer Tropsch synthesis are also been explored to replace the steam cracking.

3.4. Oxidative dehydrogenation of ethane

When compared to all the above processes oxidative dehydrogenation of ethane (ODHE) possess many conceptual advantages like high ethane conversion and the added exothermicity which helps in decreasing the reaction temperature in the range of 400 to 650 °C. Even though it has many benefits over traditional processes there are some drawbacks like the thermal runaway or over oxidation. Tuning a suitable catalyst is challenging as the olefin formed are more reactive than the alkanes.

Usually there are two groups of catalysts that are studied for ODHE in which one is based on redox type catalyst and other of non-redox type. In this the redox type catalysts usually are mixed oxides with transition metals like V, Mo, Fe ,etc and mostly these catalysts show MVK mechanism type behavior during the reaction. The latter one non-redox type catalysts are

materials like noble metals and other metals which work on virtue of their characteristics. Vanadium (V) and molybdenum (Mo) oxides are the main constituents that are usually present in catalysts used for selective oxidation of alkanes.[9] $MoVTeNbO_x$ mixed-oxide is the best catalyst among all catalysts reported till date for ODHE but the synthesis and phase formation/identification is complex for this catalyst. This catalyst gives a maximum ethane conversion of 87 % and ethene selectivity 84 %.[10] The electrophilic oxygen species also plays a prominent role in determining the total activity of the catalyst. For example, in case of Ni-NbO in which 'Ni' acts as the redox centre whereas 'Nb' helps in preventing the re-oxidation of 'Ni' ions which helps in decreasing the electrophilic oxygen species thereby increasing the selectivity of ethene.[11] Yi et al. showed that in ODHE when $SrFeO_{3-\delta}$ perovskite was employed 43 % selectivity towards ethene was achieved.[12] Over the same catalyst Dai et al. showed that the selectivity doubled when $La_{1.6}Sr_{0.4}CuO_{3.852}$, $La_{1.6}Sr_{0.4}CuO_{3.855}F_{0.143}$,and $La_{1.6}Sr_{0.4}CuO_{3.856}Cl_{0.126}$ perovskites were studied for oxidative dehydrogenation of ethane. The authors have explained that the incorporation of halide ions, with similar ionic radii to O^{2-} promotes the lattice oxygen mobility and reduces surface oxygen defects.[13] $La_xSr_{2-x}FeO_{4-\delta}$ on Li promotion gives a higher selectivity towards ethene at 700 °C but there is a deactivation in the activity after the initial activity.[14] Generally in ODHE high selectivity towards ethene are limited due to the high olefin reactivity and also by virtue of thermodynamics of paraffin and olefin oxidation.

3.5. Results and Discussion

3.5.1. Powder X-Ray diffraction

Fig. 3.4 shows the PXRD patterns obtained for the all the synthesized catalysts. To understand the lattice changes in detail, Rietveld refinement was done using GSAS software.[15] The end group entries $CaTiO_3$, $CaMnO_3$ and $SrTiO_3$ can be indexed as orthorhombic (CT and CM) and Cubic (ST) unit cells. These patterns match well with the ICSD data with no. 82487 (CT), 80874 (ST) and 35218 (CM). From the Rietveld refining of end group entries CT,ST (**Fig. 3.6.a & b**) and CM (**Fig. 3.7**.) lattice parameters were derived. The manganese substituted CT and ST showed similar patterns as that of respective parent material with slight shift in peaks to higher angle which is due to the smaller size of manganese. From Rietveld analysis (**Fig. 3.6. c & d**) it was evident that there was a small decrease in lattice parameters which leads to slight shift in peaks to higher 2θ. In case of SC3TM to SC7TM as the calcium loading increases due to lattice contraction when 'Sr' is replaced by 'Ca' with a smaller ionic radius, the peaks shift to higher

angle. In addition, peak intensity of the peak at 2θ - 39° corresponding to reflection of 211 plane and characteristic of orthorhombic unit cell (CT) increases as the calcium loading increases. To understand the changes in the system further Rietveld analysis of the materials from SC3TM-SC7TM was carried out and there was a drastic change in the space group from cubic to tetragonal and later to orthorhombic as calcium loading was increased. SC3TM matched well with tetragonal system (I4/mcm, ICSD No. 94572) and later in case of SC4TM and SC5TM it matches with the orthorhombic system (Bmmb, ICSD No. 51124). On further increase in calcium loading (SC6TM,SC7TM) it crystallizes in orthorhombic system (Pbnm, ICSD No. 94569). Lattice parameters derived from refinement are tabulated in Table. 3.2 which shows the change in unit cell dimensions when manganese was substituted in the parent Ca(Sr)TiO_3 materials. From our study it was evident that the change in structure from cubic to orthorhombic on calcium loading was from Pm-3m-I4/mcm-Bmmb-Pbnm. The cell volume also increases as the calcium content increases and it is maximum for SC4TM and SC5TM which decreases on further calcium loading.

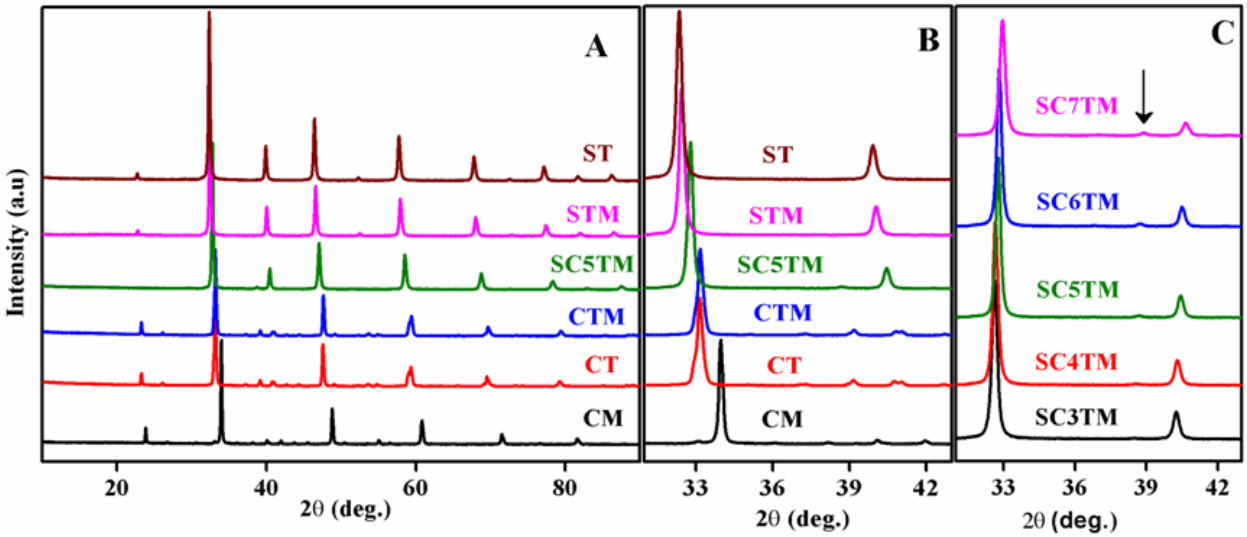

Fig. 3.4. PXRD patterns (A, B & C) of all the catalysts synthesized

High temperature PXRD in presence of air was done for SC5TM which showed a change in pattern as temperature increased (**Fig. 3.5.)**. At 650 °C the pattern was more or less similar as ST which matches well with the cubic structure (Pm-3m, ICSD No. 80874) but with a slight decrease in the lattice parameters. The refinement parameters of the PXRD pattern at 650 °C is given in **Table 3.3**. This kind of change in parameters and space group are common for

perovskite type oxides at higher temperatures.[16] On cooling to room temperature the pattern was similar as the earlier observed with orthorhombic structure (Bmmb, ICSD No. 51124)

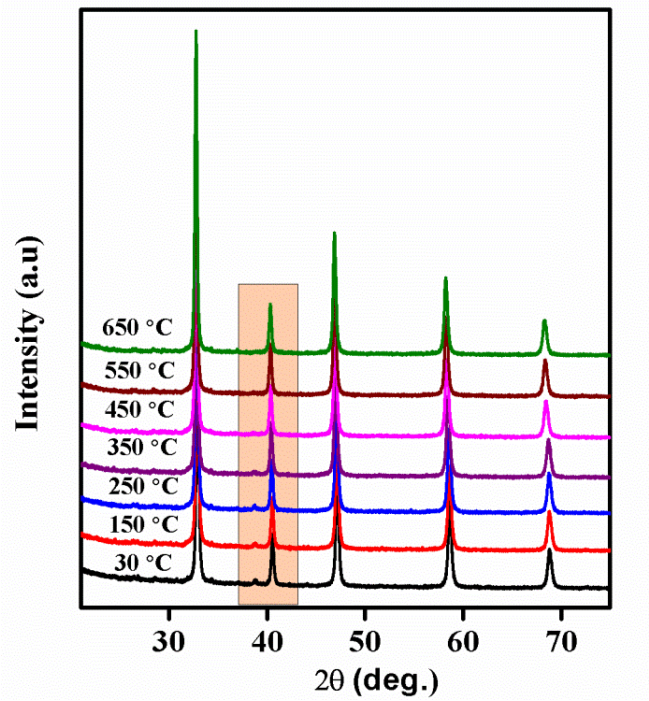

Fig. 3.5. High temperature PXRD pattern of SC5TM in presence of air

Sample	a/Å	b/Å	c/Å	χ^2	R_p	Space group	Cell Volume/ Å^3
ST ($SrTiO_3$)	3.90290(1)	3.90290(1)	3.90290(1)	1.34	0.018	*Pm-3m*	59.452(1)
STM ($SrTi_{0.9}Mn_{0.1}O_3$)	3.89138(1)	3.89138(1)	3.89138(1)	1.67	0.028	*Pm-3m*	58.927(1)
SC3TM ($Sr_{0.7}Ca_{0.3}Ti_{0.9}Mn_{0.1}O_3$)	5.4757(2)	5.4757(2)	7.7368(5)	2.29	0.052	*I4/mcm*	231.973(3)
SC4TM ($Sr_{0.6}Ca_{0.4}Ti_{0.9}Mn_{0.1}O_3$)	7.7116(2)	7.7345(2)	7.7217(3)	2.29	0.038	*Bmmb*	460.560(7)
SC5TM ($Sr_{0.5}Ca_{0.5}Ti_{0.9}Mn_{0.1}O_3$)	7.7162(12)	7.7180(11)	7.7187(3)	2.26	0.067	*Bmmb*	459.675(7)
SC6TM ($Sr_{0.4}Ca_{0.6}Ti_{0.9}Mn_{0.1}O_3$)	5.4438(3)	5.4438(4)	7.6971(8)	2.21	0.055	*Pbnm*	228.104(3)
SC7TM ($Sr_{0.3}Ca_{0.7}Ti_{0.9}Mn_{0.1}O_3$)	5.4318(4)	5.4371(4)	7.6853(8)	1.83	0.056	*Pbnm*	226.976(3)
CTM ($CaTi_{0.9}Mn_{0.1}O_3$)	5.36983(6)	5.41950(6)	7.62039(9)	1.28	0.029	*Pbnm*	221.767(2)

CT ($CaTiO_3$)	5.38366(5)	5.43960(5)	7.64238(7)	1.29	0.032	*Pbnm*	223.807(2)
CM ($CaMnO_3$)	5.2731(2)	7.4491(3)	5.2644(2)	1.45	0.086	*Pnma*	206.785(3)
SC5TM at 650 °C ($Sr_{0.5}Ca_{0.5}Ti_{0.9}Mn_{0.1}O_3$)	3.89506(2)	3.89506(2)	3.89506(2)	1.60	0.126	*Pm-3m*	59.094(1)

Table. 3.3. Lattice parameters of all the catalysts studied along with space group and unit cell

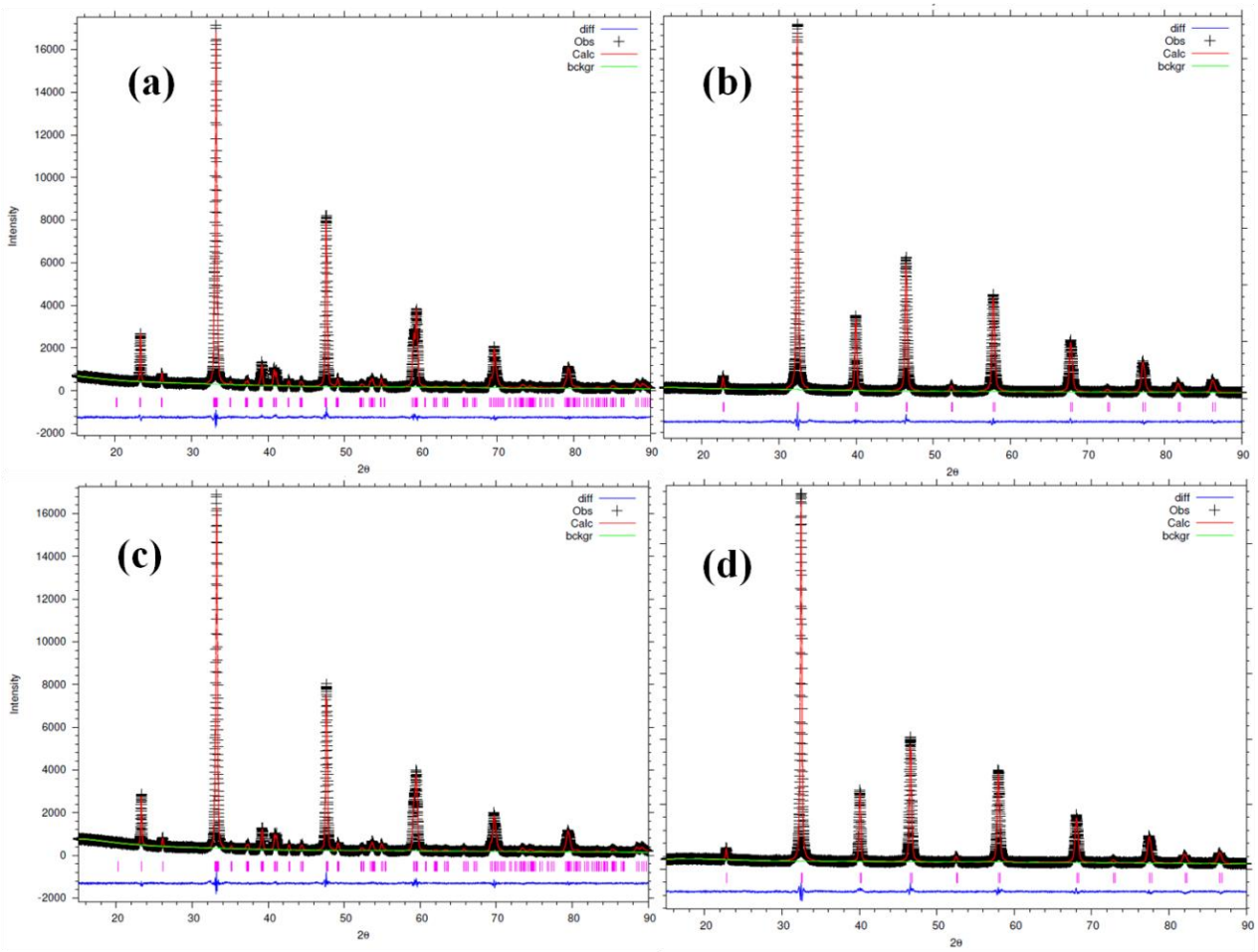

Fig. 3.6. Rietveld refinement patterns of a) CT, b) ST, c) CTM and d) STM

Surface area of all the catalysts were calculated by using Brunauer-Emmett-Teller (BET) equation and the results are shown in **Table. 3.4**. CT and SC5TM have comparable surface areas and SMT have more surface area than other ones whereas SC5TM shows high activity for ODHE. This indicates that the surface area has slight or no effect in this reaction when these perovskites are being employed.

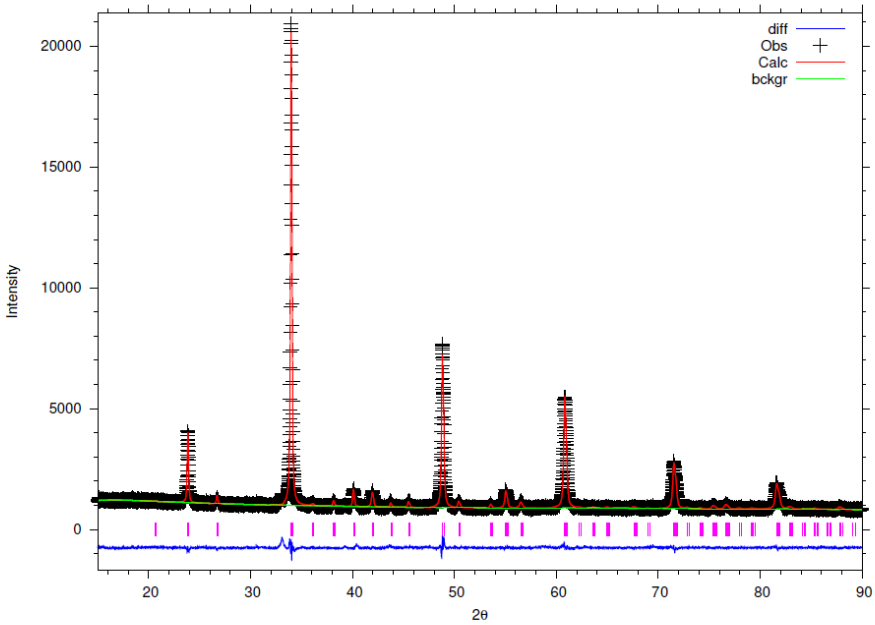

Fig. 3.7. Rietveld refinement pattern of CM

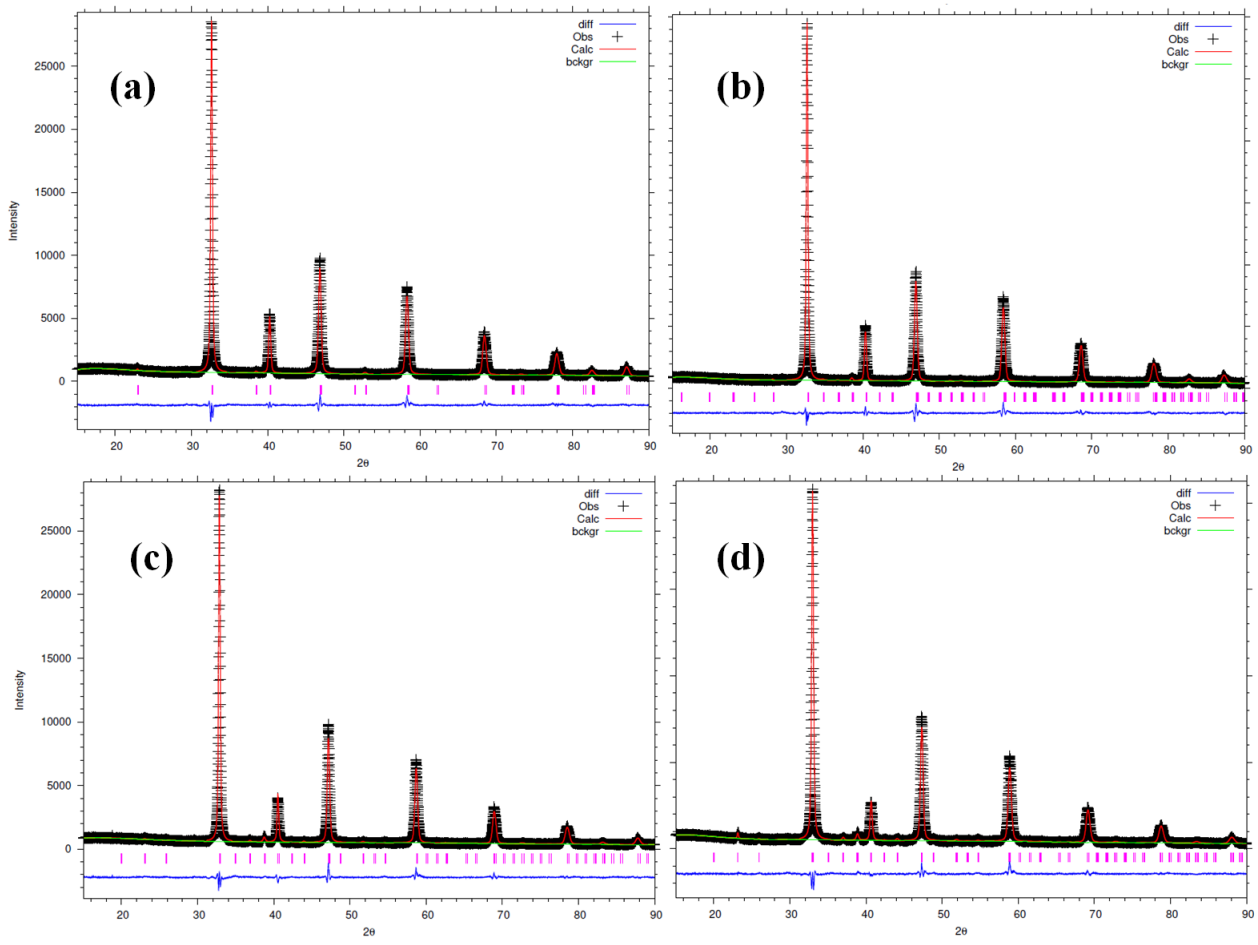

Fig. 3.8. Rietveld refinement patterns of a)SC3TM, b)SC4TM, c)SC6TM and d)SC7TM

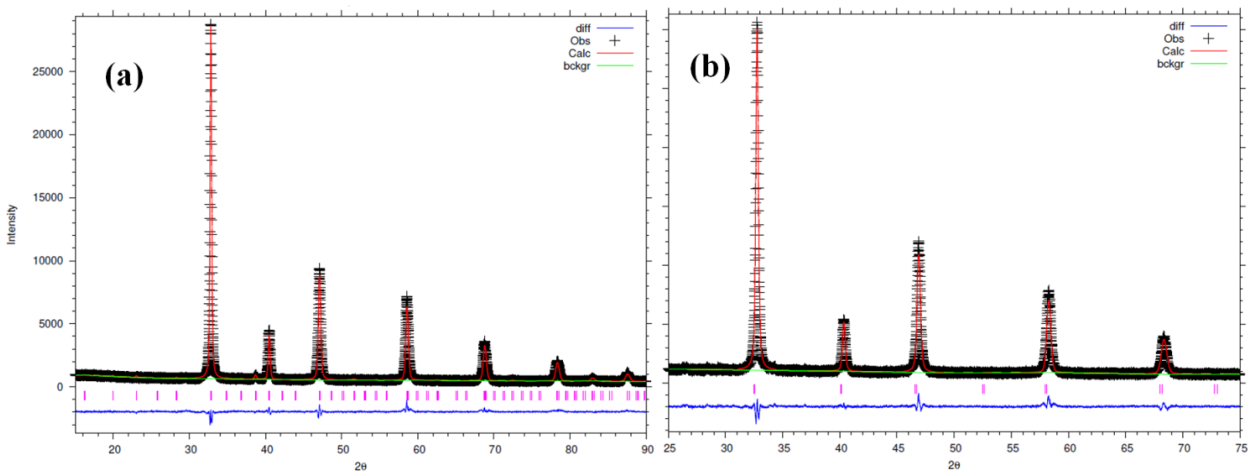

Fig. 3.9. Rietveld refinement patterns of a)SC5TM and b) SC5TM at 650 °C

S.No	Molar ratio	Code	Surface area (m^2/g)
1	$CaTiO_3$	CT	7
2	$CaTi_{0.9}Mn_{0.1}O_3$	CTM	9
3	$Sr_{0.3}Ca_{0.7}Ti_{0.9}Mn_{0.1}O_3$	SC7TM	12
4	$Sr_{0.4}Ca_{0.6}Ti_{0.9}Mn_{0.1}O_3$	SC6TM	11
5	$Sr_{0.5}Ca_{0.5}Ti_{0.9}Mn_{0.1}O_3$	SC5TM	8
6	$Sr_{0.6}Ca_{0.4}Ti_{0.9}Mn_{0.1}O_3$	SC4TM	9
7	$Sr_{0.7}Ca_{0.3}Ti_{0.9}Mn_{0.1}O_3$	SC3TM	10
8	$Sr_{0.8}Ca_{0.2}Ti_{0.9}Mn_{0.1}O_3$	SC2TM	12
8	$Sr_{0.5}Ca_{0.5}Ti_{0.925}Mn_{0.075}O_3$	SC5TM-075	11
9	$Sr_{0.5}Ca_{0.5}Ti_{0.75}Mn_{0.25}O_3$	SC5TM-25	7
10	$SrTi_{0.9}Mn_{0.1}O_3$	STM	11
11	$SrTiO_3$	ST	19
12	$CaMnO_3$	CM	6

Table. 3.4. Catalyst compositions along with their codes and total surface area

3.5.2. Microscopic analysis

Fig. 3.10 shows the SEM and TEM micrographs of SC5TM. In SEM the morphology of the material was evident which shows a spongy macroporous nature which is typical for a perovskite type material. In TEM analysis also similar morphology was observed in which individual

domains of the structure measured around 60 - 70 nm. In high resolution TEM the lattice fringes with inter planar distance 0.27 nm matches well with the d-spacing obtained from the 121 plane of the perovskites observed in PXRD. No other fringes or domains of individual oxides were observed which emphasize the even distribution of metal ions and purity of the perovskite structure formed.

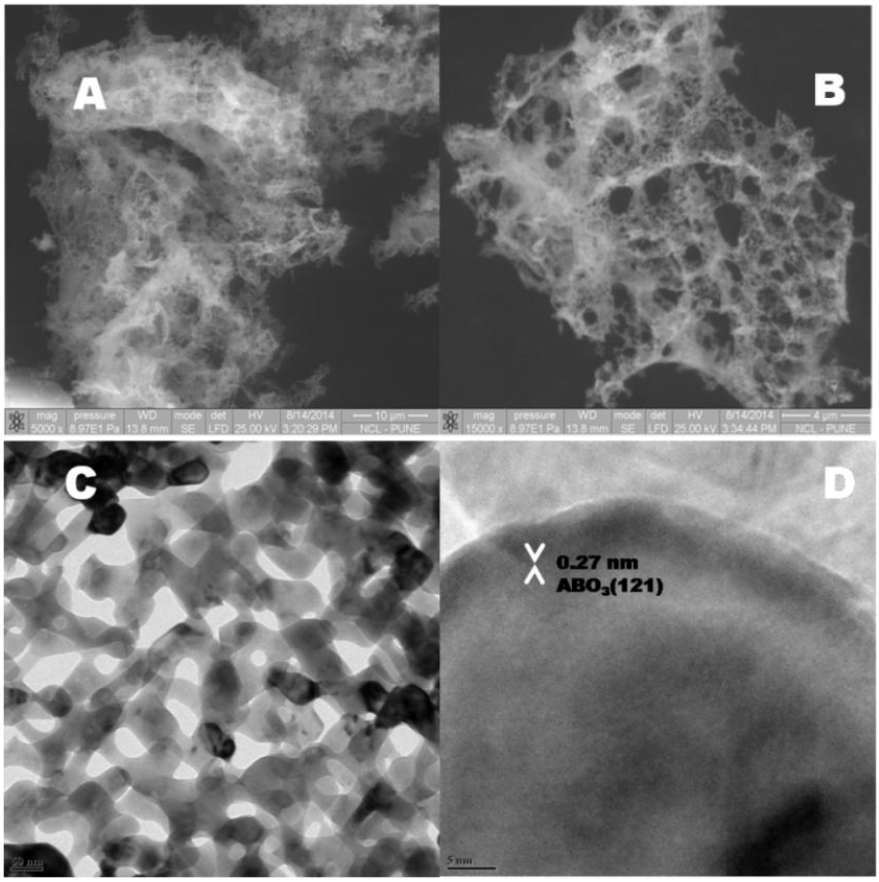

Fig. 3.10. A & B) SEM images of SC5TM, C & D) TEM images of SC5TM

3.5.3. Oxygen uptake analysis

Oxygen uptake analysis by TGA was done after incorporation of 'Mn' in 'B' site of CT and ST (**Fig. 3.11**). The weight gain after oxygen treatment is a direct evidence for the oxygen uptake ability of a material as such. Among the three catalysts in CTM the weight gain was more which implies that this catalyst possess more oxygen uptake capacity when compared to STM. This uptake ability is due to the oxygen vacancies available on the surface of the catalyst which suggests that CTM possess more oxygen vacancy in comparison with STM. In case of SC5TM the weight gain is comparatively less than CTM and STM which suggests that the oxygen vacancies are still reduced which in turn reduces the electrophilic oxygen species formed in

catalyst surface during O_2 adsorption. The first step in ODHE is the C-H bond cleavage which is rate determining step and it is done by electrophilic oxygen species present on the surface. In turn this species are responsible for C-C bond cleavage which thrives in complete oxidation of ethane. In general, a nominal amount of electrophilic oxygen species are required for a better conversion and to minimize over oxidation.[17] This property of SC5TM helps in achieving a better selective ODHE when compared to other catalysts.

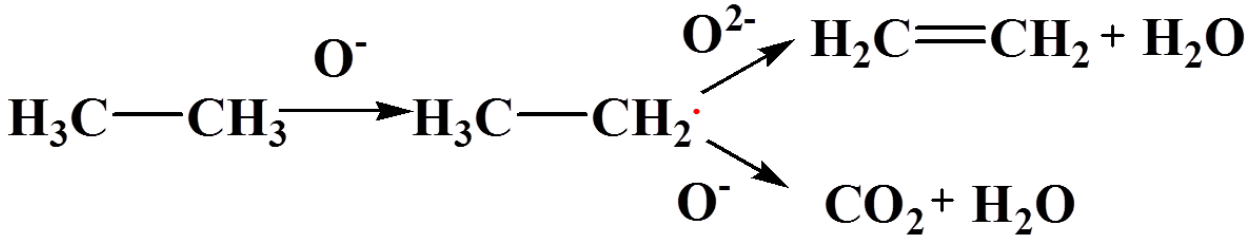

Scheme 1: Reaction mechanism of ODH

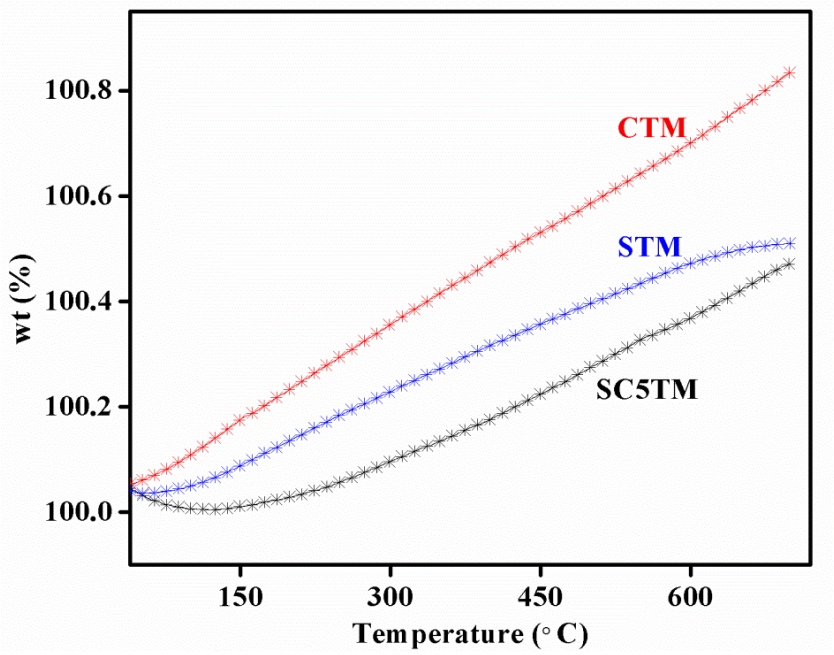

Fig. 3.11. Oxygen uptake ability of STM, CTM and SC5TM

3.5.4. X-ray photoelectron spectroscopy

XPS at various temperatures was recorded to study the changes in surface of the catalyst in presence of oxygen at 0.1 mbar pressure (**Fig. 3.12**). In Ti 2p at UHV peaks corresponding to Ti^{4+} with a small percentage of Ti^{3+} was observed. On introduction of 0.1 mbar of oxygen and starting from room temperature the peak maxima started shifting towards higher binding energy (458.6 eV) indicating that Ti exists in its highest oxidation state (Ti^{4+}) with binding energy for Ti

$2p_{3/2}$ and Ti $2p_{1/2}$ peaks at 458.8 and 464.6 ± eV respectively.[18] In the case of manganese at UHV and room temperature, peak corresponding to Mn^{4+} (642.6 ± 0.3 eV) was observed in maximum with a small shoulder at 641.4 ± 0.2 eV corresponding to Mn^{3+}/Mn^{2+}.[19-22] This shows that as such the catalyst possess manganese in mixed valence state. As oxygen (0.1 mbar) was introduced and temperature was increased there was an increase in the shoulder peak (641.4 ± 0.2 eV) which emphasize that the surface getting enriched with $Mn^{3+/}Mn^{2+}$ ions. This increases the surface defects which in turn increases the electrophilic oxygen formation which thrive in total oxidation of hydrocarbons.[11] The intensity of this shoulder peak is maximum in temperature range of 400-550 °C. This is observed in activity profiles wherein at lower temperatures the selectivity of CO_2 is higher. As the temperature is increased due to more oxygen diffusion the intensity of peak at 642.7 ± 0.2 eV increases which suggests that Mn^{4+} concentration increases which in turn are responsible for increase in selectivity of ethene.

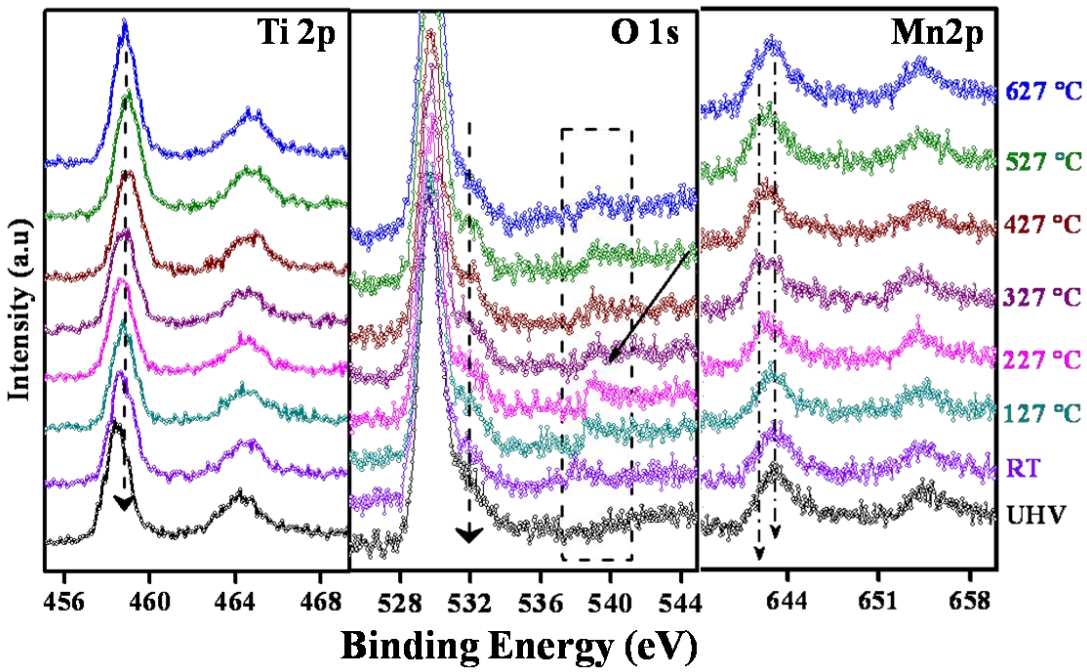

Fig. 3.12. XPS profiles of Ti 2p, O 1s and Mn 2p at UHV and different temperatures in presence of 0.1 mbar O_2

In O1s XPS spectra the peak at 529.6 ± 0.2 eV is due to the lattice oxygen and the surface adsorbed oxygen species or electrophilic oxygen appear at 532 ± 0.2 eV.[21,22] The intensity of the later peak is more predominant between temperature range of 350 - 500 °C which is obvious as the manganese is in lower oxidation states due to which the amount of electrophilic oxygen

species increases. This peak decreases at higher temperatures when manganese oxidizes back to Mn^{4+}. The peak due to adsorbed molecular oxygen (538.5 ± 0.2 eV) decreases as temperature increases, which suggests that oxygen absorption increases when defects are formed and replenishes the oxygen defective sites at very high temperatures.[23]

3.5.5. Catalytic Activity

3.5.5.1. Effect of Manganese

To understand the effect of manganese in ODHE was done with catalysts CT, ST, CTM and STM at 650 °C with GHSV 6000 h^{-1} reactant flow (**Fig. 3.13.)**. The selectivity towards ethene was less in case of ST and CT (28 and 21 % respectively) as these oxides are with more oxygen defects which drives in total oxidation of ethane. When 'Mn' was substituted in "B" site the selectivity increased by 10 % which is likely due to the redox nature of manganese which did the purpose. The selectivity towards ethene was 34 % and 37 % for CTM and STM respectively. In extension of that CM was also tested in which the combustion nature of these perovskites were predominant due to which selectivity of ethene was only 19 % with 80 % conversion of ethane. This is obvious as these manganates type perovskites are known for complete combustion of hydrocarbons.[19,24,25]

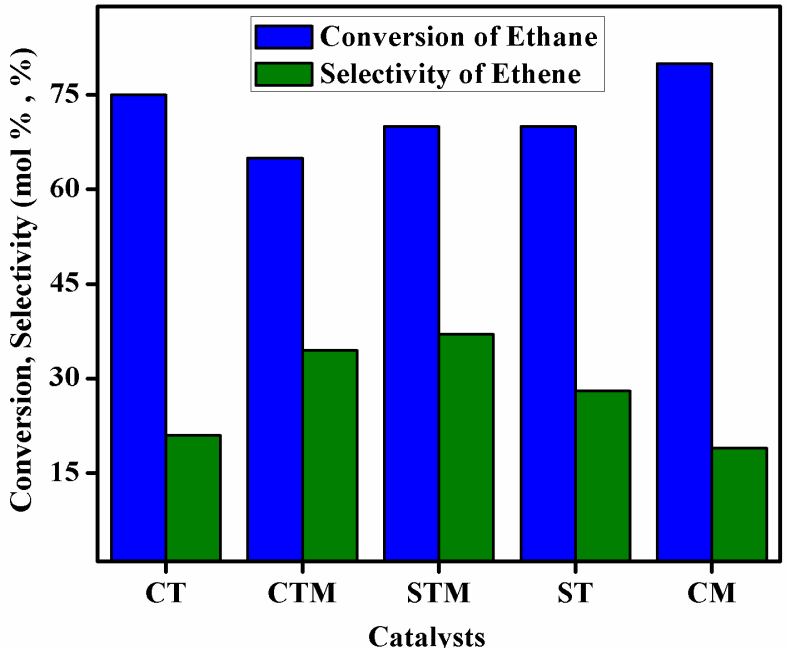

Fig. 3.13. ODHE activity of end group catalysts and manganese substituted CT and ST

Reaction conditions: *Atm pressure, 650 °C, 1 cc catalyst, total reactant flow: 6000* h^{-1} *(O_2/ethane =1.5)*

3.5.5.2. Effect of calcium loading in STM

To investigate the synergism of 'Ca' and 'Sr' and to observe the change in activity when there is a change in the unit cell of perovskites, in STM when different ratios of 'Ca' was substituted in "A" site. As the 'Ca' was substituted, initially in SC2TM the conversion of ethane decreased slightly and gradually activity increased as calcium loading increased. In case of SC5TM the yield of ethene was highest with a selectivity of 61 % which was almost twice that of STM and CTM. The selectivity decreased as calcium loading was increased above 0.5 molar ratio and the conversion was more with over oxidation which was more or less similar to that of CTM. This is likely due to the increase in oxygen defects which generate electrophilic oxygen species similar to CTM which helps in over oxidation of ethane which decreases the selectivity of ethene. An optimal amount of calcium loading which in turn generates a optimal amount of electrophilic oxygen species are required for a better conversion of ethane and an improved selectivity of ethene.

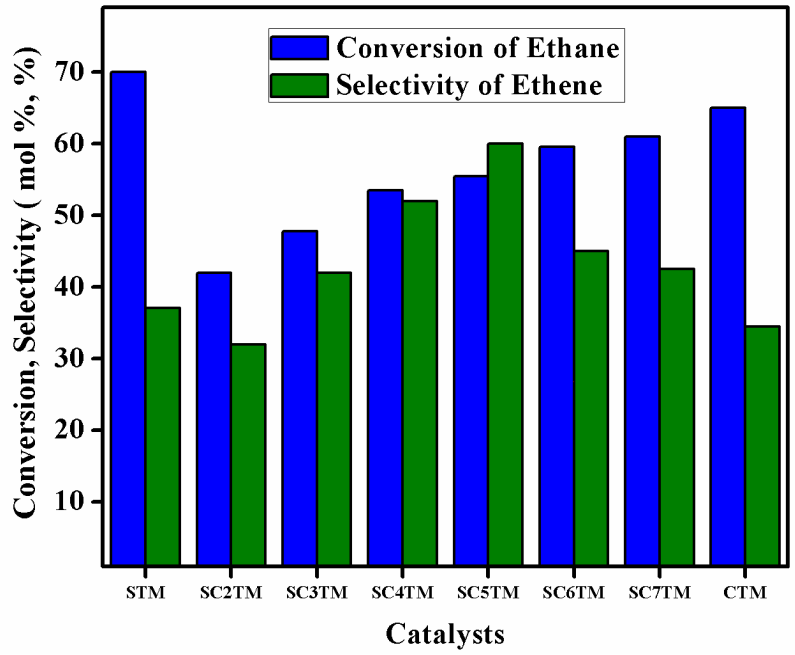

Fig. 3.14. Comparison of ODHE activity for different Ca/Sr catalysts

Reaction conditions: *Atm pressure, 650 °C, 1 cc catalyst, total reactant flow: 6000 h^{-1} (O_2/ethane =1.5)*

3.5.5.3. Effect of reaction temperature

To understand the role of temperature the reaction was carried out at a wide range of temperature from 450 - 700 °C using SC5TM as catalyst at 6000 h^{-1} total reactant flow. Below 450 °C there

was no appreciable activity in all these catalysts. The selectivity towards ethene was low at lower temperature range (450 -550 °C) in all the catalysts (**Fig. 3.15 a**) which is due to more electrophilic oxygen species at lower temperatures which leads to combustion and favors lower selectivity towards ethene and more of CO_2 was formed. The amount of electrophilic oxygen increase is due to the formation of more oxygen defects in the surface which was evident in XPS analysis. As the temperature is increased the electrophilic oxygen species decreases (O_2^-, O^-) and the lattice oxygen which are nucleophilic (O^{2-}) participate in the reaction by Mars Van Krevelen mechanism (MVK) as a consequence of that the over oxidation reduces and the selectivity increases at higher temperatures. Among all the temperature conditions at 650 °C maximum selectivity of ethene (61 %) was observed and this was considered as the optimized temperature for further studies (**Fig.3.15 b**). Above 650 °C the ethane cracking was more due to which the main products formed were hydrogen and methane.

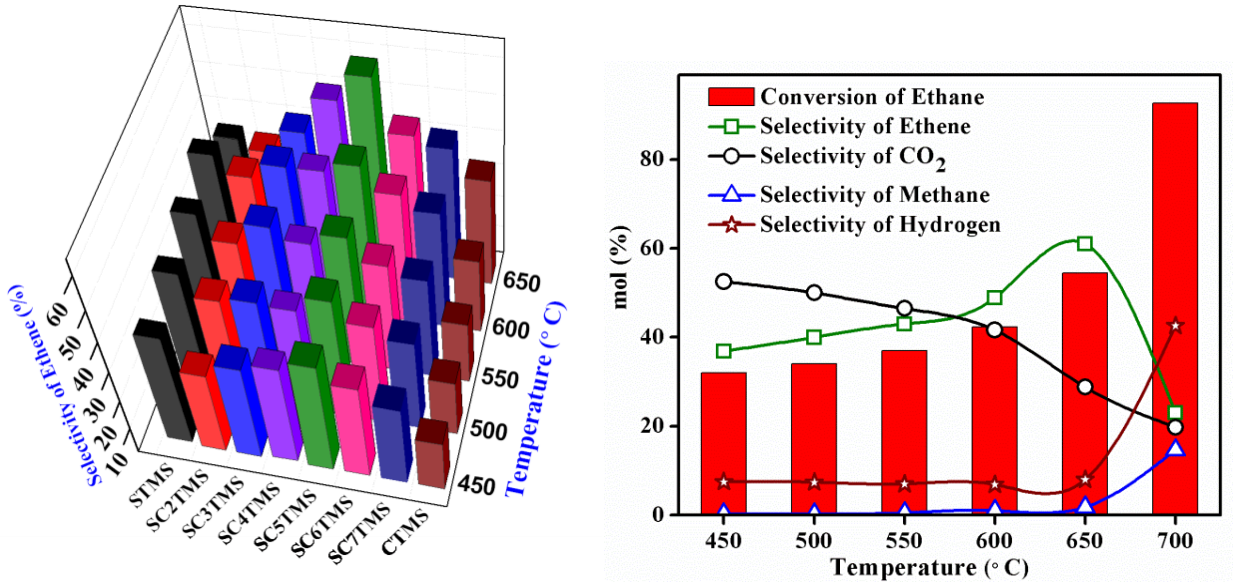

Fig. 3.15. a) Selectivity profiles of catalysts with different calcium loadings at selected temperature range and b) Reaction profile of SC5TM with selectivity of all products at different temperatures. ***Reaction conditions:*** *Atm pressure, 1 cc catalyst, total reactant flow: 6000* h^{-1} *(O_2/ethane =1.5)*

3.5.5.4. Optimization of manganese content

To optimize the amount of manganese three different molar ratios (0.075, 0.1, 0.25) of manganese substituted SC5TM was prepared and investigated for ODHE (**Fig. 3.16**). At lower manganese loading the selectivity of ethene was low when compared to other two catalysts

which were due to the decrease in active redox sites in the catalyst. When the amount of manganese was increased, at 0.1 molar ratio of manganese the selectivity was highest (61 %) when compared to other two loadings of manganese. In continuation, when the manganese amount was increased the conversion increased with decrease in selectivity (50 %) and with overall similar yield as SC5TM. As time on stream increases the overall activity decreases for SC5TM-25 due to the coke deposition over the catalyst which was observed in spent catalyst TGA. This is obvious as the manganese amount increases there likely to be more of combustion and coke deposition over the catalyst. Based on these studies SC5TM with 0.1 molar ratio of manganese was considered to be the optimized catalyst composition for a better selectivity towards ethene.

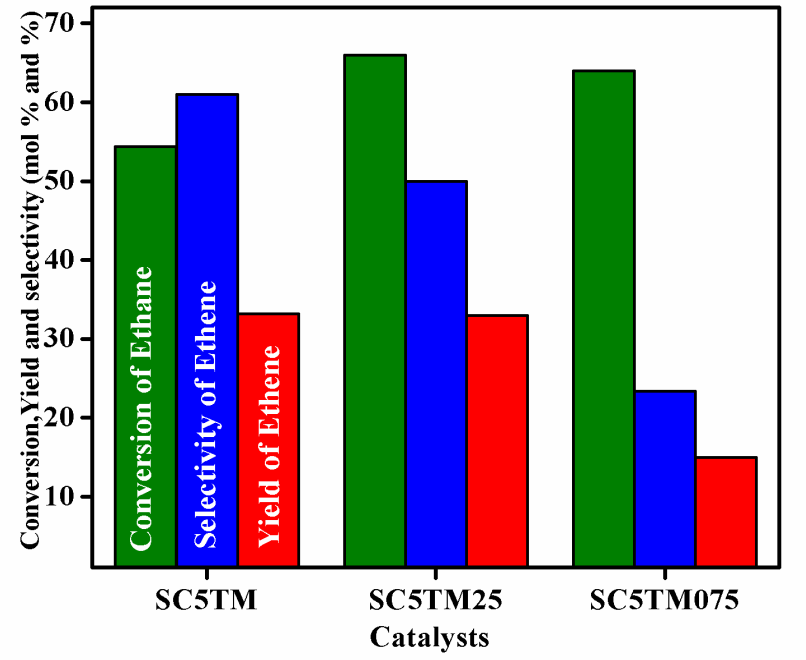

Fig. 3.16. Effect of Manganese loading in SC5TM

Reaction conditions: *Atm pressure, 650 °C, 1 cc catalyst, total reactant flow: 6000 h^{-1} (O_2/ethane =1.5)*

3.5.5.5. Durability studies-Time on stream

To demonstrate the stability of the catalyst, this reaction was carried out for long time on stream conditions at optimized reaction conditions i.e. 6000 h^{-1}, 650 °C and SC5TM as catalyst (**Fig 3.17**). After an initial decrease in conversion and increase in selectivity the activity remained stable for 24 hours. The minor decrease in activity was observed after 24 hours which was same as the initial activity when the catalyst was regenerated with oxygen flow. By this study it was

explicit that the catalyst is durable and stable for longer time on stream and also decrease in activity can be subdued by the activation of the catalyst with oxygen.

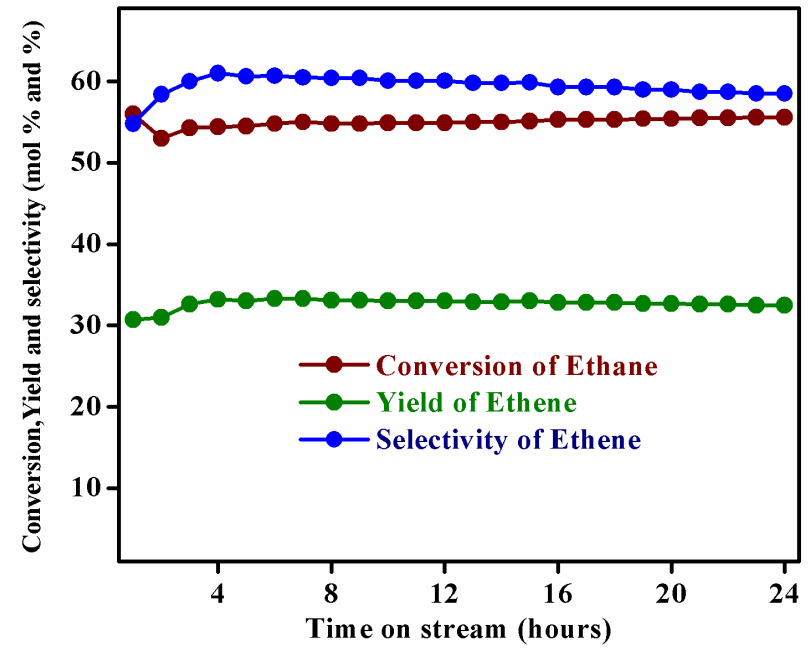

Fig. 3.17. Time on stream study on SC5TM for 24 hours

Reaction conditions: *Atm pressure, 650 °C, 1 cc catalyst, total reactant flow: 6000 h^{-1} (O_2/ethane =1.5)*

3.5.5.6. Spent catalyst Analysis

PXRD pattern of spent SC5TM did not show much variation after reaction which emphasizes the sturdiness of the catalyst to withstand at high temperatures. To estimate the amount of coke formed after the reaction, the spent catalysts (CTM, STM, SC5TM, CM and SC5TM-25) were subjected to thermo gravimetric analysis. **Fig. 3.18** shows the weight loss profiles of all the catalysts analyzed in TGA. SC5TM showed a minimum weight loss when compared to all other catalysts which supports the uniqueness of the catalyst.

This interesting feature helps in driving the catalytic activity for long time on stream reaction conditions. Among the other catalysts the CM showed highest amount of coke (20 %) deposition which foreground the activity profile of this catalyst. SC5TM-25 which gave a similar yield as SC5TM with less selectivity possessed around 4 % of coke which is the reason for the decline in activity of these catalyst as time progresses.

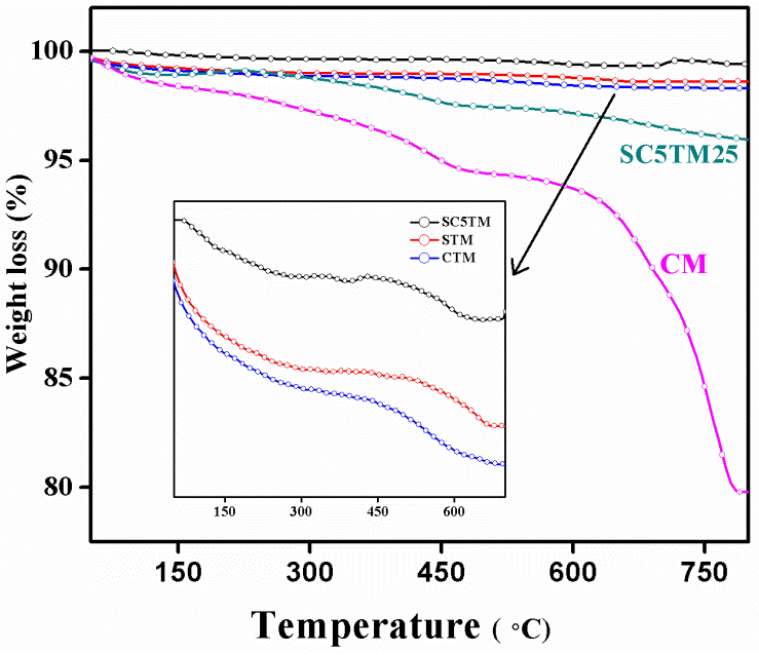

Fig. 3.18. TGA analysis of spent catalysts

3.6. Conclusion

Various molar ratios of manganese substituted calcium/strontium based perovskites were prepared by simple citric acid gel method. Physicochemical analysis like PXRD and TEM show the purity of the perovskite formed. From the oxygen uptake experiment it was evident that the SC5TM has less and nominal amount of oxygen vacancies which gives a better selectivity towards ethene. From XPS analysis of SC5TM it was evident that the "Mn" species exist in lower oxidation state at temperature range of 450-550 °C which drive in for more of total combustion of ethane which was also observed in activity profile. Based on the optimization studies the catalyst with optimum amounts of Sr, Ca, Ti, Mn (SC5TM) shows the best activity towards ODHE. This catalyst shows a stable activity up to 24 hours without significant loss in its activity which emphasizes the sturdiness of the catalyst. The spent catalyst analysis supports the above property which also shows minimal coke deposition.

3.7. References

1. J.F. Brazdil, *Top. Catal*. 38(2006), 289.
2. Composition of Eagle ford drilling well, US - information from Oil and gas financial Journal (News article)
3. H. Zimmermann, R. Walzl, in Ullmann's Encyclopedia of Industrial Chemistry, Wiley-

VCH, Weinheim, 2000.

4. McCoy, M., *Ed. Chem. Eng. News*, 89(2011), 55-56.
5. H M. T Galvis, K P. de Jong, *ACS Catal*., 3(2013), 2130-2149.
6. A. S. Bodke, D. A. Olschki, L. D. Schmidt, E. Ranzi, *Science*, 285(1999), 712.
7. M. M. Bhasin, J. H. McCain, B. V. Vora, T. Imai, P. R. Pujado, *Appl. Catal.A*,221(2001), 397.
8. F. M. Ashmawy, *J. Appl. Chem. Biochem*.,27(1977), 137.
9. F. Cavani, N. Ballarini, A. Cericola, *Catal. Today*, 127(2007), 113.
10. P. Botella, E. Garcia-Gonzalez, A. Dejoz, J.M. Lopez Nieto, M. I. Vazquez, J. Gonzalez-Calbet, *J. Catal*., 225(2004), 428.
11. Z. Skoufa, E. Heracleous, A. A. Lemonidou, *Catal. Today*,192(2012), 169.
12. G. Yi, T. Hayakawa, A. G. Anderson, K. Suzuki, S. Hamakawa, A. P. E York,M Shimizu, K Takehira, *Catal. Lett.*, 38 (1996), 189-195.
13. H. X. Dai, C. F. Ng, C. T. Au, *Catal. Lett.*, 67(2000), 183-192.
14. Y Gao, L M. Neal, F Li, *ACS Catal*.,6(2016), 7293-7302
15. A.C. Larson and R.B. Von Dreele, "General Structure Analysis System (GSAS)", Los Alamos National Laboratory Report LAUR 86-748 (1994).
16. S Qin, A I. Becerro, F Seifert, J Gottsmanna, J Jiang, *J. Mater. Chem*., 10(2000), 1609-1615
17. H Zhu, D C. Rosenfeld, M Harb, D H. Anjum, M Nejib Hedhili, S Ould-Chikh, J-M Basset, *ACS Catal*., 6(2016), 2852-2866.
18. S Azad, M H. Engelhard, L-Q Wang, *J. Phys. Chem. B*, 109(2005), 10327-10331.
19. T.V. Choudhary, S. Banerjee, V.R. Choudhary, *Appl. Catal. A*, 234 (2002) 1-23.
20. V. Di Castro, C. Furlani, M. Gargano, M. Rossi, *Appl. Surf. Sci*., 28 (1987) 270-278
21. J S Yoon, Y-S Lim, B H Choi, H J Hwang, *Int. J. Hydrogen Energy*, 39 (2014), 7955-7962.
22. M C. Biesingera, B P. Payne, A P. Grosvenor, L W.M. Laua, A R. Gerson, R St.C. Smart, *Appl. Surf. Sci*., 257 (2011), 2717-2730.
23. J.L. Hueso, D. Martinez-Martinez, A. Caballero, A.R. Gonzalez-Elipe, B.S. Mun, M. Salmeron, *Catal. Comm*., 10 (2009) 1898-1902.

24. L Giebeler, D Kießling, G Wendt, *Chem. Eng. Technol*., 30(2007), 889-894.
25. M. Alifanti , J. Kirchnerova, B. Delmon, D. Klvana, *Appl. Catal. A,* 262 (2004) 167-176

Chapter 4

Oxidative dehydrogenation of ethyl benzene (EB) to styrene (ST)

Synopsis

- Cerium containing mixed oxides derived from a hydrotalcite precursor was prepared which shows a better catalytic activity for the conversion of Ethyl benzene (EB) to styrene (ST)

- The morphological studies show evenly distributed ceria crystallites at lower loading of cerium

- The catalyst with 0.03 mol % of cerium shows the highest conversion (49.4 %) when compared to all the compositions prepared and showed long term stable activity

- Manganese substituted Ca(Sr)TiO_3 perovskite type oxides showed a better activity when compared to catalyst without manganese

- $Sr_{0.5}Ca_{0.5}Ti_{0.9}Mn_{0.1}$(SC5TM) prepared by glycine combustion method showed slightly higher activity when compared to citrate gel method

4.1.Introduction

Oxidative dehydrogenation (ODH) of ethyl benzene (EB) to styrene (ST) is one of the commercially important transformations, as styrene is an important monomer for the synthesis of polystyrene and various other copolymers. ST is an important platform chemical in petrochemical industry which is utilized for the production of polystyrene (PS) and several polymers, copolymers and reinforced plastics including acrylonitrile-butadiene-styrene (ABS) resins, styrene-acrylonitrile (SAN) resins, styrene-butadiene rubber (SBR) and styrene-butadiene latex **(Fig. 4.1)**.[1] This emphasizes the importance of styrene as it finds its usage in production of end products like food containers and packaging materials to cars, boats, computers and its peripherals. Production of styrene is the fourth major important industrial process. Nearly about 23 million tons of styrene was produced in 2010 and this demand keeps on increasing exponentially every year.[2]

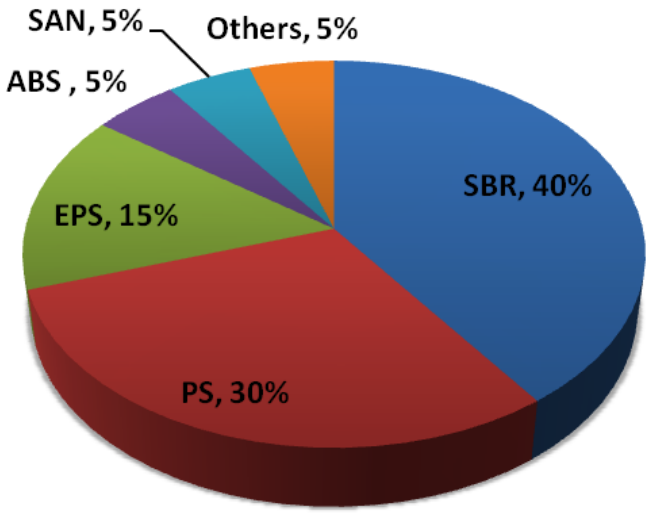

Fig. 4.1. Products of commercial importance obtained from styrene[1]

4.2.Commercial process for production of styrene

Commercially styrene is been produced by two major processes which are,

(i) dehydrogenation of ethyl benzene in presence of steam and

(ii) styrene which is obtained as a by-product in the epoxidation of propylene with ethyl benzene hydroperoxide

4.2.1.Dehydrogenation of EB

This pathway accounts for almost 90 % of styrene production which employs Fe-K based catalyst in presence of steam. The reaction is carried out at high endothermic conditions (550 to

700 °C), pressure around 2 atm along with steam/EB molar ratio from 4 to 20. The typical composition of the catalyst employed is shown in the table below (**Table 4.1.**).[3] The development or aim of the existing processes is to decrease the steam/EB molar ratio. The usage of the steam is to provide increased selectivity and to maintain the heat of reaction.

$$C_6H_5CH_2CH_3 \rightarrow C_6H_5CH{=}CH_2 + H_2 \quad \Delta H°_{298K} = 129.4 \text{ kJ mol}^{-1} \qquad \textbf{4.1}$$

Component	Percentage composition
Ferric oxide	45-77 %
Potassium oxide	10-27 %
Chromium(III) oxide	0-3 %
Cerium (III) oxide	0-5 %
Molybdenum oxide	0-3 %
Magnesium oxide	0-10 %
Aluminium oxide	0-0.1 %
Vanadium pentoxide	0-2.5 %
Calcium oxide	0-2.5 %

Table.4.1. Catalyst composition of commercial EB dehydrogenation catalyst

In this Iron based catalyst potassium acts as a promoter which increases activity by one fold and also enhances the selectivity towards ST. The increase in the activity after potassium addition is due to the formation of $KFeO_2$ species in the surface of the catalyst. One more advantage of using potassium is the formation of potassium oxide along with steam to rejuvenate the catalyst surface by burning the carbonaceous deposits.[4,5] Other promoters have their respective enhancing properties for example chromium and aluminium oxides act as structural promoters, magnesium oxide acts as a support, cerium increases the activity and molybdenum oxide increases the selectivity.[4,6] The major drawback of dehydrogenation reaction is the thermodynamic limitation where the hydrogen accumulation reverses the reaction. UOP in earlier days developed a process to overcome the drawback by introducing a dual catalytic reactor setup where one catalyst performs dehydrogenation and the other oxidizes the hydrogen formed. This process underwent many changes and process developments.[7,8] A process combining Lummus technology and UOP setup of oxidative reheating by selective catalytic oxidation of hydrogen was found effective.

This process is called as Styrene Monomer Advanced Reheat Technology (SMART process).[9] Commercially many reactors were modified to SMART process where it has an advantage of increasing the EB feed rate by 10 % as there is an increased ethyl benzene conversion which in other hand reduces the recycle stream of unreacted mixture.[3]

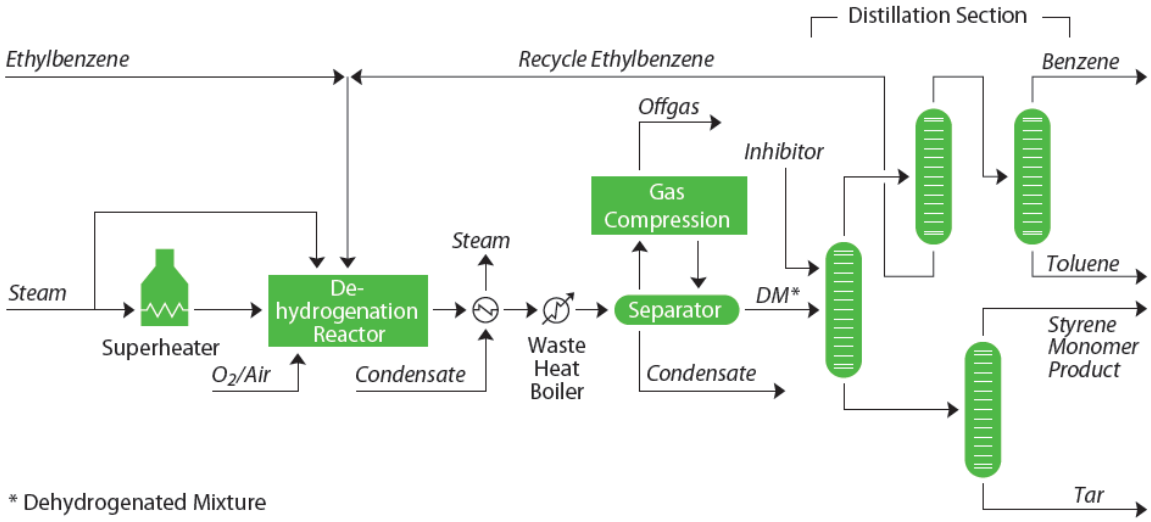

Fig. 4.2. Reactor setup for SMART process[3]

Dehydrogenation process suffers from various disadvantages like

- Energy intensive process due to high endothermic nature of the reaction
- Rapid coking leads to severe catalyst deactivation
- Achieves less than 50% EB conversion per pass
- Needs high steam to hydrocarbon ratio
- Large amount of steam used increases the cost of operation

4.2.2. Epoxidation of propylene

In the propylene oxide process EB is converted to EB hydroperoxide using oxygen which reacts with propylene to form propylene oxide and 1-phenyl ethanol. 1-phenyl ethanol which is formed as by-product is dehydrated to form styrene. It is estimated that per tonne of propylene oxide production 2.2 tonnes of styrene is been formed as by-product. Mo- complex based catalysts are employed for this reaction generally and this process is commercialized by ARCO and Shell. This process is not so efficient when compared to the conventional dehydrogenation process.[9-12]

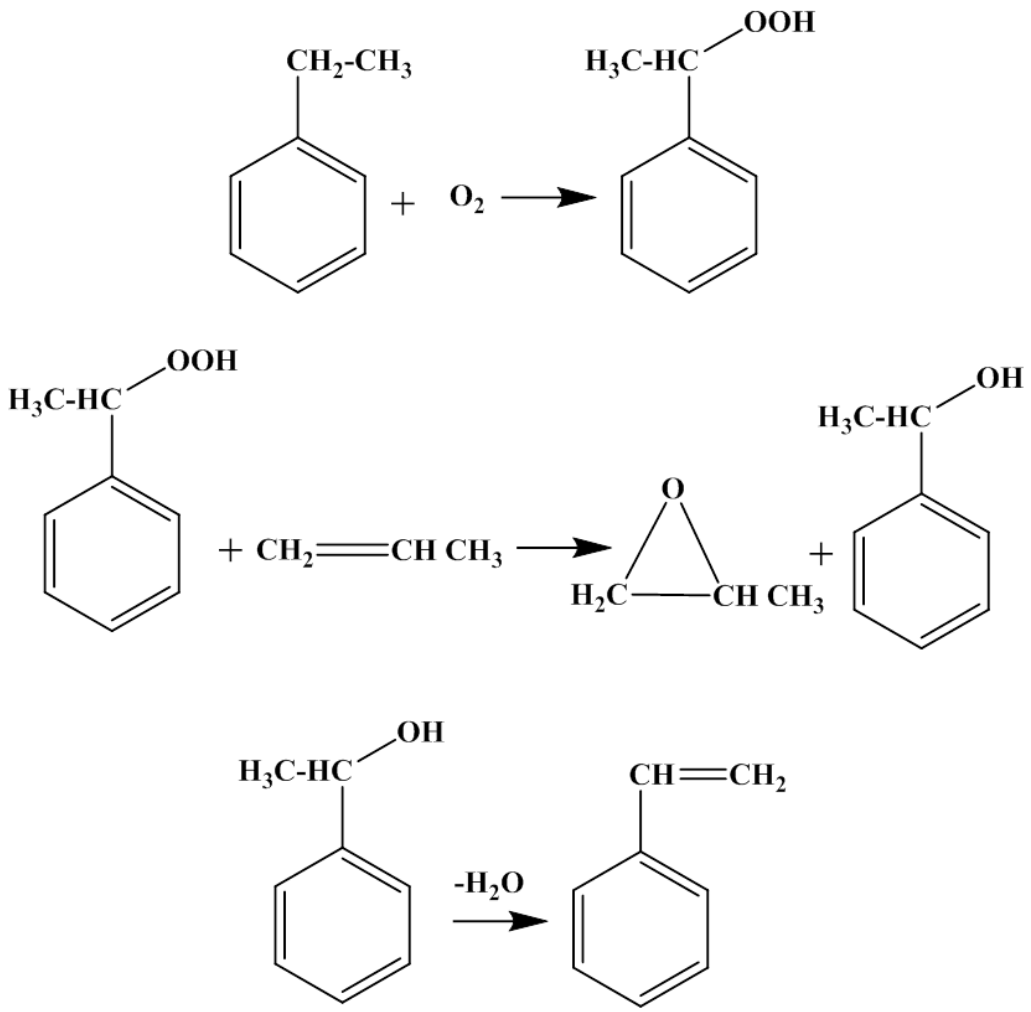

Scheme.4.1. Synthesis of styrene as byproducts in propylene oxide synthesis

4.3.Oxidative dehydrogenation of EB to ST

ODH is a thermodynamically favorable exothermic pathway which can be carried out at lower temperatures compared to the commercial dehydrogenation process. ODH can be carried out with various oxidants like oxygen, air, N_2O, carbon dioxide, etc.

$$C_6H_5C_2H_5 + 0.5\ O_2 \rightarrow C_6H_5C_2H_3 + H_2O \quad \Delta H^{o}_{298K} = -124.2\ kJ\ mol^{-1} \qquad \textbf{4.2}$$

An extensive research is in progress to develop an efficient catalyst and economic process for this particular conversion. A wide range of metal oxides, mixed metal oxides and carbon material have been reported in peer reviewed literature. It is generally observed that mixed metal oxides show more catalytic activity than individual oxides due to the high acid base bi-functionality. Among all the catalyst system studied metal oxides of vanadium and iron based catalysts show better catalytic activity. Reddy et al. have investigated the EB to ST reaction using air as an

oxidant on CeO_2/Al_2O_3 and $V_2O_5/CeO_2/Al_2O_3$ as catalysts.[13] Sivaranjani et al. studied the ODH of EB using oxygen or air as an oxidant with vanadium incorporated in the TiO_2 lattice. Successful 'V' incorporation in TiO_2 lattice ($Ti_{1-x}V_xO_2$) leads to stable styrene yield at around 500 °C.[14] Xiao et al. have reported that the ODH of EB using hierarchical porous carbon spheres using molecular oxygen giving around 43% conversion.[15] Takehira and co-workers employed Mg-Fe-Al mixed oxide derived from a hydrotalcite precursor as a catalyst with a mixture of CO_2 and O_2 as an oxidant.[16] Shiju et al. have utilized N_2O as a mild oxidant for the conversion of EB to styrene with V/Al_2O_3.[17] The $La_{0.8}Ba_{0.2}Fe_{0.4}Mn_{0.6}O_{3-\delta}$ Perovskite catalyst achieves above 60% conversion of ethylbenzene and about 51% yield of styrene yield and has high stability.[18] Basic sites are required to give an irreversible conversion of EB. Balasamy et al. have studied the role of MgO sites in the hydrogen abstraction during dehydrogenation of EB.[19] Fan et al. have reported 34% conversion of EB with 87% selectivity towards ST with mesostructured ceria.[20] Mesostructured Ni-doped ceria shows an improved activity compared to ceria.[21]

PART-A

4.4.ODH of EB to ST over hydrotalcite derived cerium containing mixed metal oxides

4.4.1 Catalyst Characterization

4.4.1.1 Powder X-ray Diffraction (PXRD)

Fig. 4.3 shows the PXRD profiles of series of MAC catalysts along with reference materials before and after calcinations. PXRD of as synthesized catalysts show diffraction patterns corresponding to hydrotalcite layered structure with a small amount of ceria diffraction features. There is no change in the 2θ value of periclase phase after CeO_2 incorporation, which indicates that there is no intercalation of CeO_2 between the HT layers, rather it disperses. The intensity of reflections corresponding to the layered structure decreases as the amount of cerium increases (**Fig. 4.3a**). PXRD patterns of calcined catalysts are depicted in **Fig. 4.3b**. The diffraction features corresponding to both periclase phase of Mg(Al)O (JCPDS. No. 4-829) and ceria (JCPDS. No. 78-0694) were seen predominantly. Absence of layered HT features indicates disintegration of the layered structure into mixed oxides. It is observed that the peak width corresponding to the (111) plane of ceria increases as the cerium loading decreases which suggests that the ceria is well dispersed on Mg-Al oxide. At higher cerium loading, the features corresponding to periclase phase decreases. It is mainly due to the blocking of ceria which is agglomerated on the surface of the catalyst.

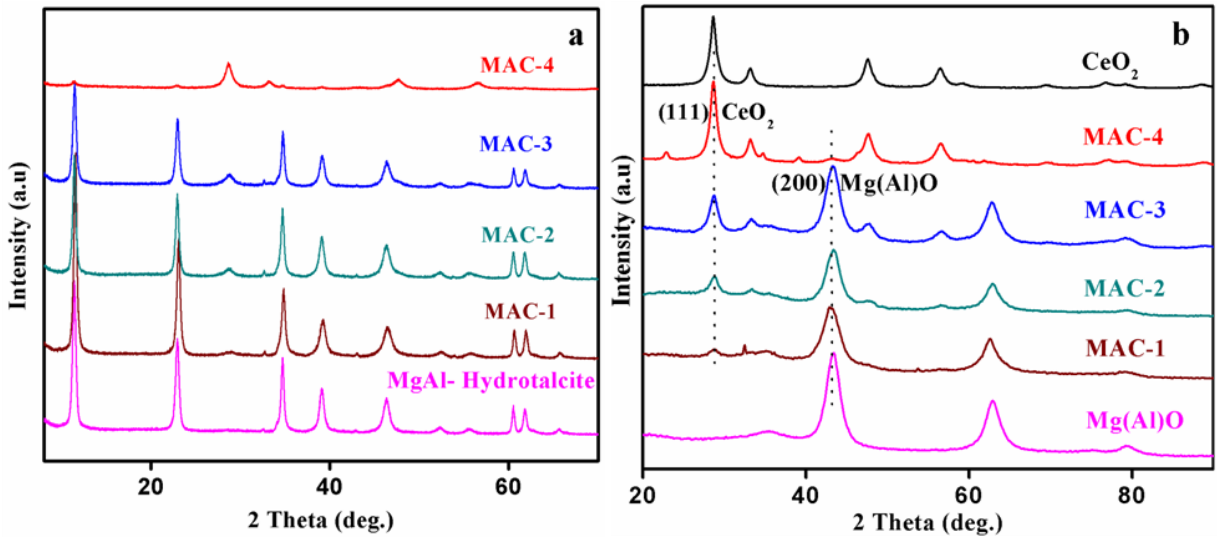

Fig. 4.3.PXRD patterns of (a) as synthesized and (b) calcined MAC catalysts. XRD results for CeO_2 and Mg(Al)O are given for comparison.

The BET surface areas of all the calcined catalysts are given in **Table 4.2**. The lower cerium containing catalysts showed more or less similar surface areas. When the cerium loading increases, the surface area decreases, and in MAC-4 the surface area decreases to a greater extent because of the ceria agglomeration over Mg(Al)O. The basicity of the catalysts were analyzed by temperature programmed desorption of CO_2. As the cerium loading increases the basicity increases when compared to pristine Mg-Al oxide and at higher loading of ceria the basicity drastically decreases.

S.No	Mg:Al:Ce mole ratio	Crystallite size(nm) [a]	Surface Area (m^2/g)	Amount of cerium[b] (wt %)	Basicity[c] (µmol/g)
1	Mg(Al)O (3:1)	--	189	--	363
2	MAC-1 (3:0.99:0.01)	8.66	218	0.61	384
3	MAC-2 (3:0.97:0.03)	9.11	214	1.70	398
4	MAC-3 (3:0.95:0.05)	9.90	180	3.03	402
5	MAC-4 (3:0.5:0.5)	12.7	42	26.16	243
6	CeO_2	13.5	137	--	23

[a] Average crystallite size calculated from Scherrer equation using (111) plane of CeO_2 in PXRD.
[b] Average wt % obtained from EDX analysis carried out over a wide area of 500 μm^2
[c] Obtained by TPD of CO_2

Table.4.2. Physicochemical properties of all catalysts

4.4.1.2. Thermal Analysis

The thermal stability of the catalysts was studied by thermogravimetric analysis. TGA showed that hydrotalcite goes through a series of weight loss involving: adsorbed water, interlamellar water molecules, dehydroxylation of the brucite-like sheets and finally decomposition of the carbonate anions which results in the formation of stable mixed oxide. The maximum

temperature generally used to activate hydrotalcite-like compounds is around 450 °C, as at higher temperatures the hydrotalcite will be transformed into periclase phase. The data from thermal analysis was taken as a reference and the catalysts were calcined at 450 °C at which all the hydrotalcite phases would have been removed to give an evenly distributed mixed oxide.

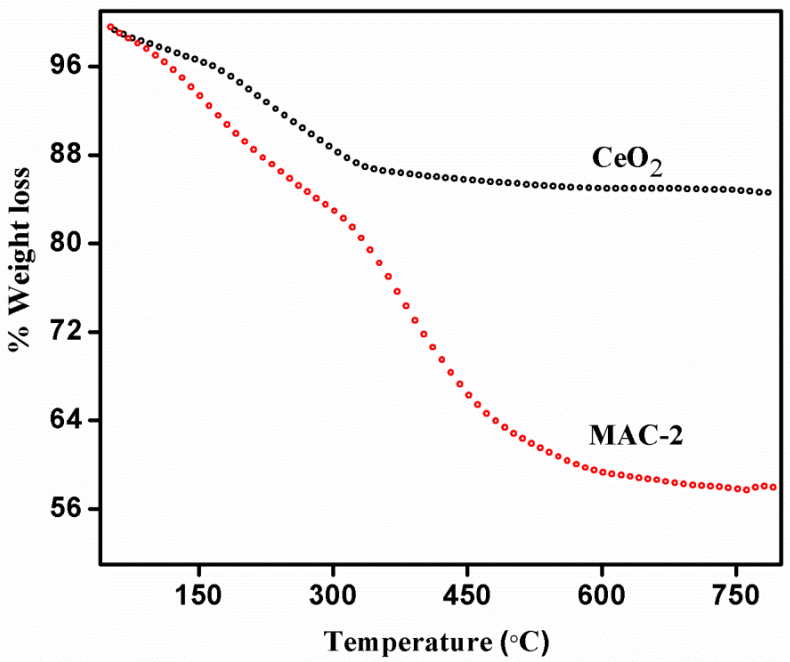

Fig. 4.4. TGA profile of as synthesized MAC-2 and CeO_2

4.4.1.3. Raman spectroscopy

Fig. 4.5 shows Raman spectra for all the series of catalysts along with pristine ceria, which shows a prominent peak at 463 cm^{-1} corresponding to the vibrational mode of the cubic fluorite (F_{2g}) CeO_2 lattice.[22] The peak broadens at less cerium loading which confirms the nanocrystallite size of ceria. At lower loading a peak appears around 546 cm^{-1} due to oxygen vacancies generated and the associated charge imbalance caused by Ce^{3+} ions in ceria.[23] This oxygen vacancy is not so prominent at higher cerium loading. These oxygen vacancies help in achieving good oxygen mobility and an increase in these defect sites has a direct relationship with the rate of conversion

of EB.[24]

4.4.1.4. X-ray photoelectron spectroscopy (XPS)

XPS was recorded to explore the electronic structure of MAC catalysts. The binding energy values for the Mg 2p core level at 50.5 eV and the Al 2p core level at 75 eV respectively were observed (**Fig. 4.6**) which are in good agreement with the literature.[25]Ce 3d and O 1s core level

XPS spectra are shown in **Fig. 4.7**. The O 1s and Ce 3d core level of MAC-2 was compared with the spectra of pure ceria in order to observe the changes in the catalyst surface. **Fig. 4.7 a** shows the O 1s core level spectrum of pure ceria which shows two peaks: (i) 529.3 eV corresponding to lattice oxygen and (ii) 531.3 eV corresponding to surface hydroxyl groups.[26,27] **Fig. 4.7 b** shows the O 1s spectrum of MAC-2 which shows three peaks: (i) a peak at 529.7 eV corresponding to lattice oxygen of ceria, (ii) a peak at 531.3 eV corresponding to lattice oxygen of Mg(Al)O and (iii) a peak at 533 eV corresponding to the surface hydroxyl and carbonate impurities. The BE value shift for O 1s for surface impurities increases by 1.7 eV which might be due to surface defects caused in MAC-2 catalyst along with surface impurities.

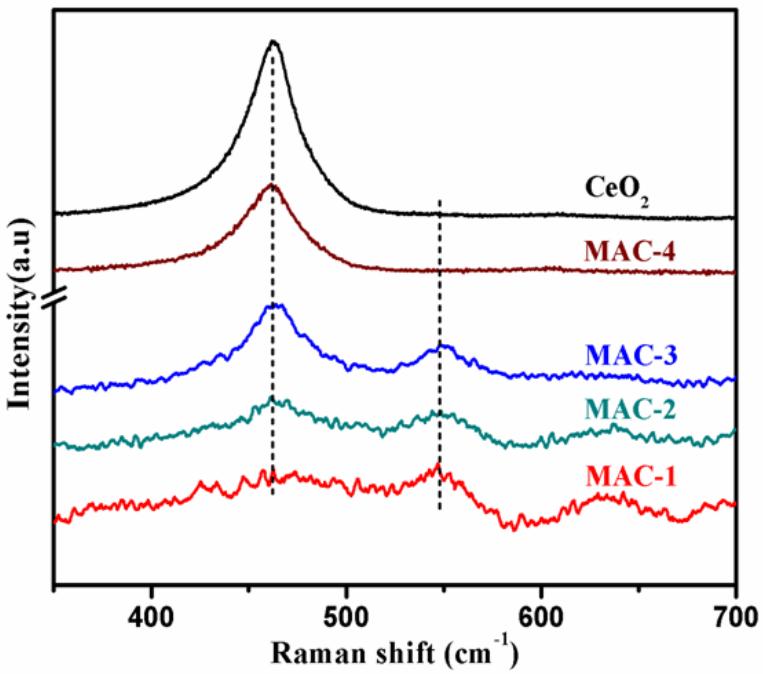

Fig. 4.5. Raman spectra of all catalysts showing the oxygen vacancy generated at lower loading of cerium

Fig. 4.7 c shows the Ce 3d core level spectrum in which multiple peaks corresponding to both Ce^{3+} and Ce^{4+} were observed which was deconvoluted by a peak fitting method with the Shirley background.[26,27] The peaks resulting from Ce^{4+} $3d_{3/2}$ appearing at 900.8 eV (u), 907.2 eV (u″) and 916.7 eV (u‴) and also the peaks due to Ce^{4+} $3d_{5/2}$ occurring at 882.4 eV (v), 888.8 eV (v″) and 898.1 eV (v‴) were observed.[26,28-30] The four peaks corresponding to Ce^{3+}, namely u′, v′, u_o and v_o [903.7, 884.7, 899.2 and 880.1 eV respectively],[26,31,32] were observed with lower intensity which is due to fewer defects in pure ceria. The same peaks were observed with the same BE for MAC-2 (**Fig. 4.7 d**) but the intensities corresponding to Ce^{3+} were comparatively more than

those for the pristine ceria, which shows the increase in the defects caused by the increase in Ce^{3+} in MAC-2.

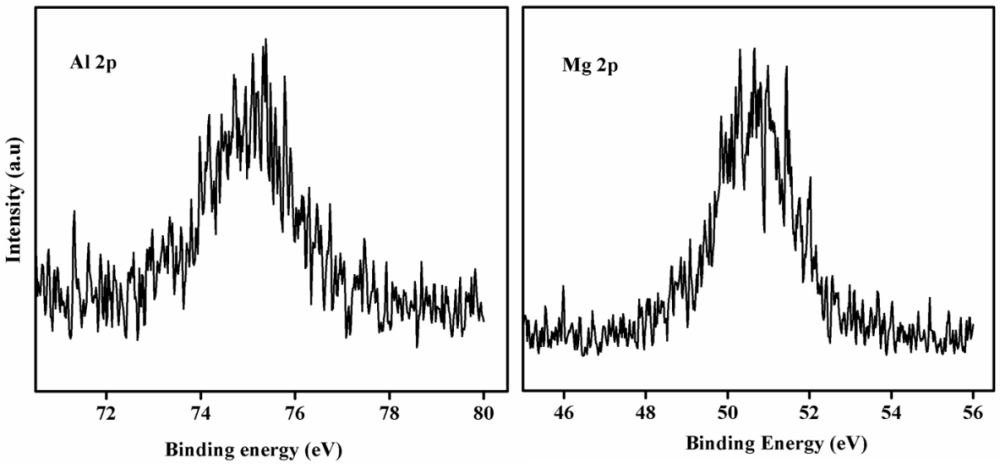

Fig. 4.6. XPS spectra: Al 2p and Mg 2p of MAC-2

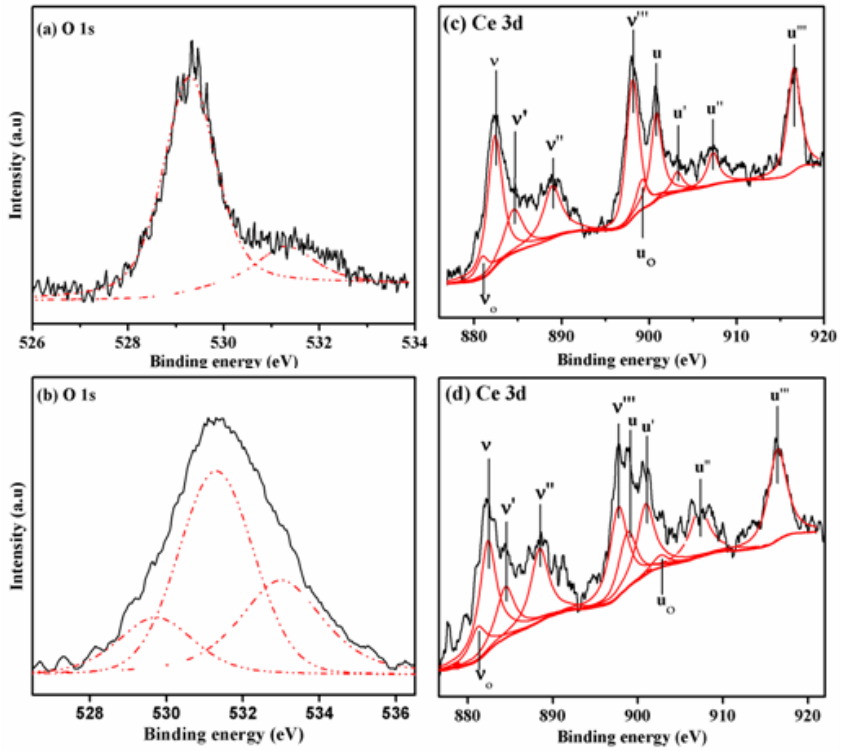

Fig. 4.7. XPS spectra: (a) O 1s of pure ceria, (b) O 1s of MAC-2, (c) Ce 3d of pure ceria and (d) Ce 3d of MAC-2. The black line represents the recorded spectra

4.4.1.5. Scanning Electron Microscopy (SEM)

The scanning electron micrographs of both calcined and uncalcined samples of MAC-2 were compared with Mg-Al mixed oxide derived from hydrotalcite as shown in **Fig. 4.8**. Mg-Al oxide exhibited hexagonal sheet like morphology as shown in **Fig. 4.8 a** and the presence of ceria

affects the sheet like morphology. Even though the uncalcined MAC-2 had a little flake like shape and this feature is completely lost after calcination and it didn't show any specific morphology **(Fig. 4.8 c).** EDAX analysis was used to measure the material composition as well as to find out the extent of homogeneity of the sample. **Fig. 4.9** is the elemental mapping with color coding for different elements. The data confirms that there is a homogeneous distribution of the metals in microscopic level.

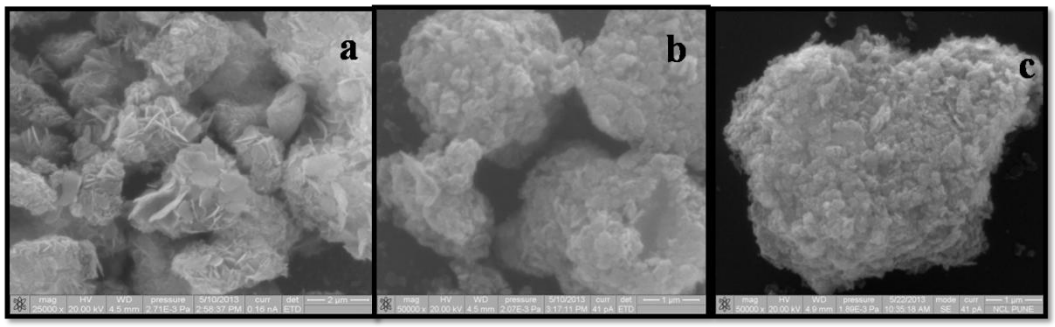

Fig. 4.8. SEM images of (a) Mg-Al mixed oxide (b) MAC-2 before calcination (c) MAC-2 after calcination

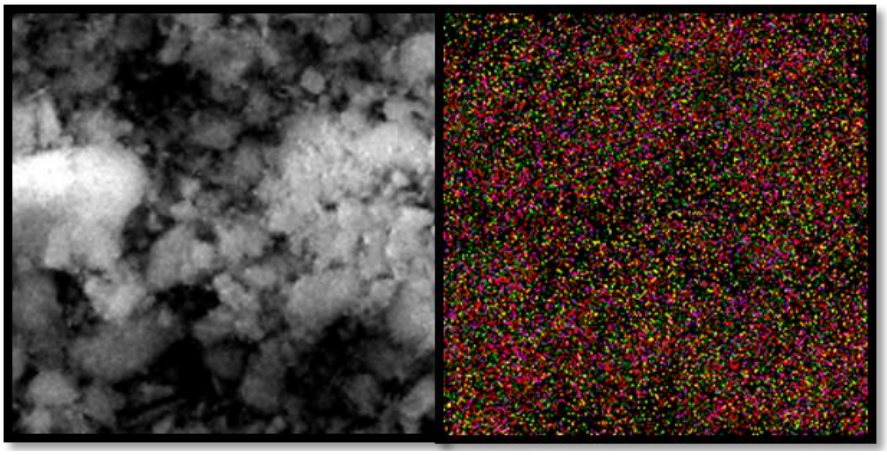

Fig. 4.9. Elemental mapping of MAC-2 (Mg–green, Al-blue, Ce-yellow, O-red)

4.4.1.6. Transmission electron microscopy (TEM)

Fig. 4.10 shows the TEM images of calcined catalysts, namely Mg(Al)O, a catalyst with maximum cerium (MAC-4) and a catalyst giving maximum conversion (MAC-2). Mg(Al)O shows a nanofibre or distorted sheet morphology **(Fig. 4.10 a)** which is usually observed for calcined hydrotalcites. However, upon introduction of a small amount of cerium to Mg(Al)O, a sheet like morphology is seldom seen. MAC-2 shows **(Fig. 4.10 b and c)** an even distribution of

ceria clusters on the basic framework of the catalyst. The same types of images were obtained for the MAC-1 and MAC-3 catalysts.

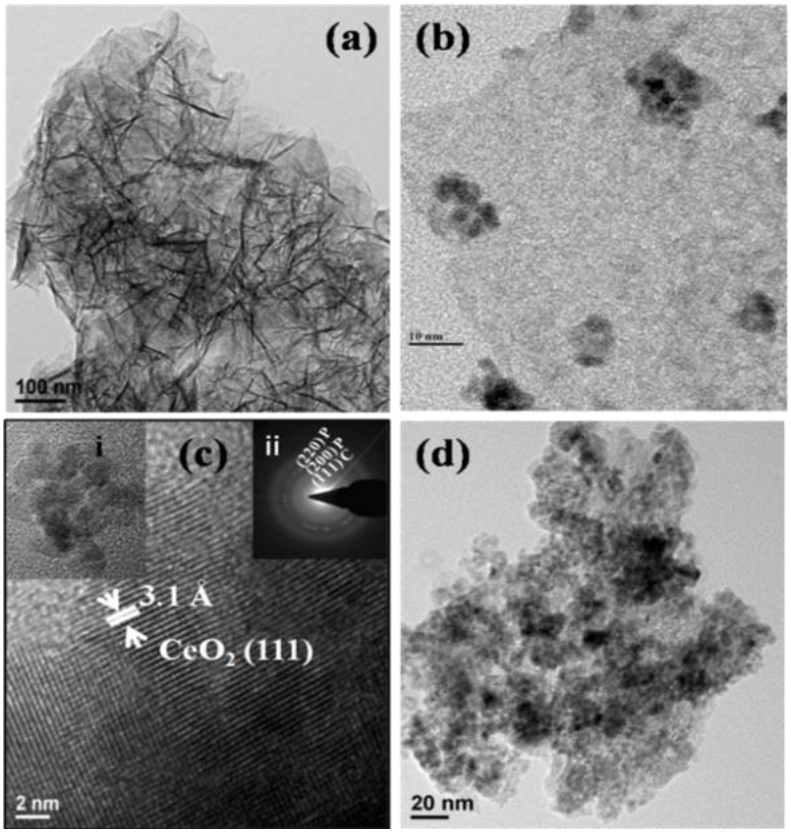

Fig. 4.10. TEM of (a) Mg(Al)O, (b) MAC-2 and (c) MAC-2-high resolution image of (i) individual ceria clusters. (ii) Diffraction (P - periclase and C - ceria) pattern. (d) MAC-4 showing aggregated ceria clusters.

4.4.2. Catalytic activity measurements

The activity of various hydrotalcite derived mixed oxide catalysts for the oxidative dehydrogenation of ethyl benzene to styrene with oxygen as oxidant was investigated. Due to the exothermic nature of the reaction and the presence of combustible reactants and products along with oxygen, caution must be taken during the course of the reaction. ODH was carried at 450 °C at atmospheric pressure over the hydrotalcite derived mixed oxide catalysts. The reaction was done over 1 mL catalyst and with LHSV 3 h^{-1} ethyl benzene and GHSV 1200 h^{-1} oxygen flow. Styrene is the major product whereas toluene, benzene, water and carbon oxides are the side products of the reaction. Reactant feed flow, oxidant flow and temperature variation studies were carried out in order to optimize the catalysts. Catalytic activities were tested for 12 hours time on stream and the reaction data are compared for every hour.

4.4.2.1. Effect of preparation method

The catalytic activity of MAC-4 prepared via co precipitation as well as co-precipitation followed by hydrothermal treatment was compared **(Fig. 4.11)** for 12 hours at 450 °C and LHSV of EB and O_2 at 3 h^{-1} and 1200 h^{-1} respectively. During the initial hours of TOS, co-precipitated catalyst showed higher conversion and as time on stream increases the activity started to decrease. The hydrothermally treated catalyst showed a better and stable activity when compared to the earlier. Thus co precipitation followed by hydrothermal treatment method was followed for further synthesis of the catalysts which was used for optimization studies.

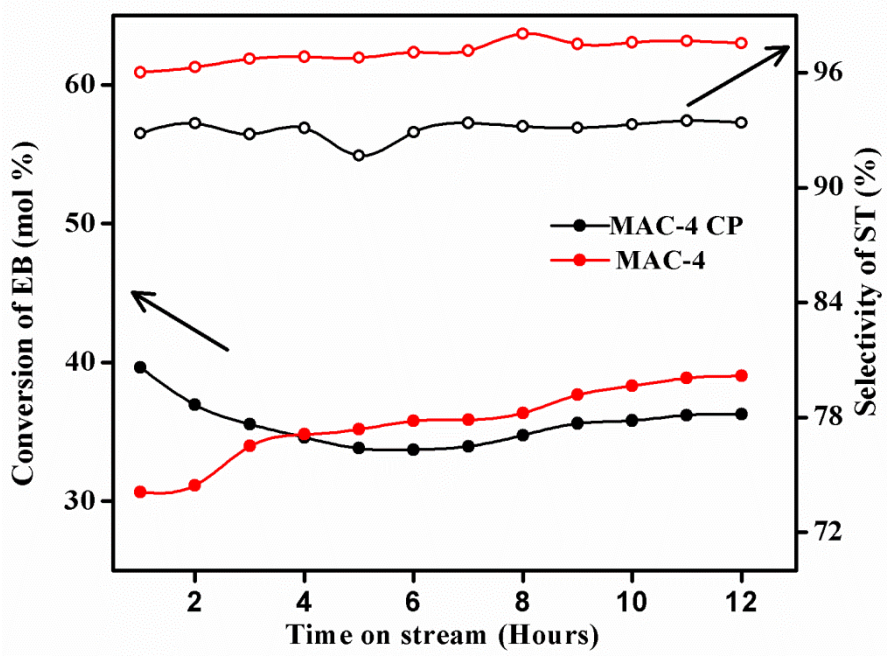

Fig. 4.11. Effect of Hydrothermal treatment for MAC-2

Reaction conditions: *450 °C, LHSV 3 h^{-1} with respect to EB, GHSV 1200 h^{-1} with respect to oxygen 1 atm.pressure, 1 mL catalyst*

4.4.2.2. Effect of oxygen flow

To understand the effect of oxidant (molecular oxygen) flow on catalytic activity, the reaction was carried out with three different flow rates of oxygen (GHSV 600, 1200 and 2400 h^{-1}), and the results are shown in **Fig. 4.12.** MAC-2 was employed as a catalyst and the reaction was measured at 450 °C and LHSV 3 h^{-1} with respect to EB flow. In ODH reactions the surface coke which forms in 2-3 hours of the initial reaction over the catalyst plays a vital role in increasing the catalytic activity. The thin coke layer helps in increasing the activity and the good oxygen transport of CeO_2 helps in long term stability of the catalyst.[33] The conversion increases as the

oxygen flow increases from GHSV 600 to 1200 h^{-1} wherein the maximum activity is observed with 1200 h^{-1}. However the selectivity remains stable at both the oxygen flow rates (600 and 1200 h^{-1}). At very high oxygen flow rate (2400 h^{-1}) the initial conversion was high and decreased as time progressed, which was due to cracking of EB and ST to over oxidized gaseous products mainly to CO_2, which was confirmed by the low mass balance of liquid products and in the spent catalyst analysis.

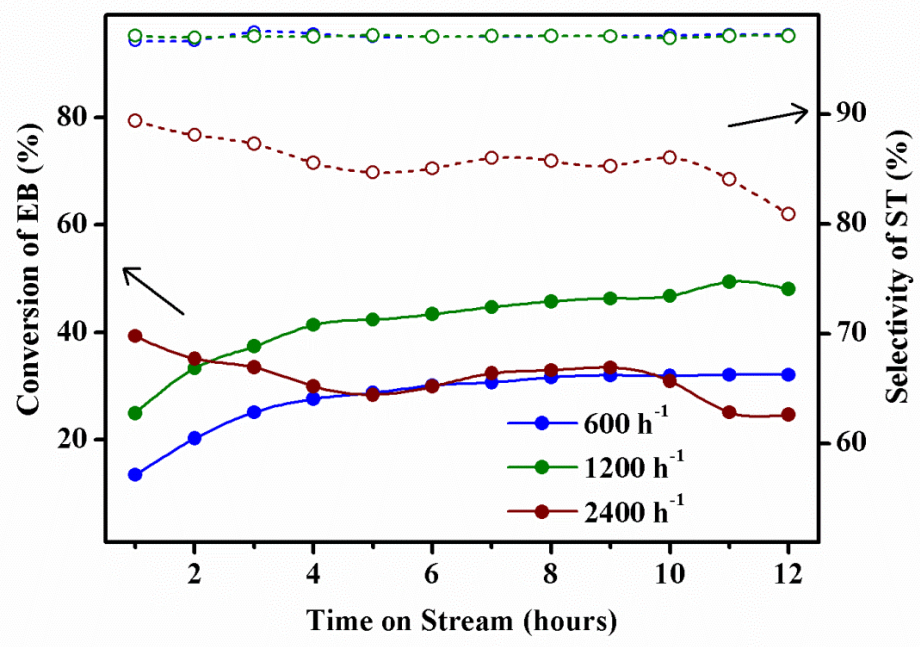

Fig. 4.12. Conversion of EB and selectivity of ST at different oxygen flow rates over MAC-2. ***Reaction conditions:*** *450 °C, LHSV 3 h^{-1} with respect to EB, 1 atm.pressure, 1 mL catalyst*

The initial high conversion at high oxygen flow rate suggests that at high oxygen flow, high oxygen mobility in ceria is observed, which directly helps in higher conversion. This is in contrast to the gradual increase in conversion from around 20 % at TOS 1 hour to optimum conversion at TOS = 4 hours for the two lower GHSV flow rates. Indeed an initial high flow rate is suggested to increase the conversion which would optimize the ST yield right from the beginning.

4.4.2.3. Effect of reaction temperature

Fig. 4.13 shows the EB conversion and ST selectivity as a function of temperatures (400-500 °C) with MAC-2 as the catalyst with 1200 h^{-1} GHSV oxygen flow and 3 h^{-1} LHSV EB flow. It is observed that conversion increases as the temperature increases. Higher conversion and selectivity are observed at 450 °C; moreover, the catalytic activity remains stable at this

temperature. At 500 °C the initial conversions increased and after 5 hours the conversion decreased which is mainly due to more coke deposition at higher temperatures because of over oxidation. This was confirmed by TGA analysis of the spent catalyst will be discussed later. Hence 450 °C was taken as an optimized reaction temperature for maximum conversion and stable yield of styrene.

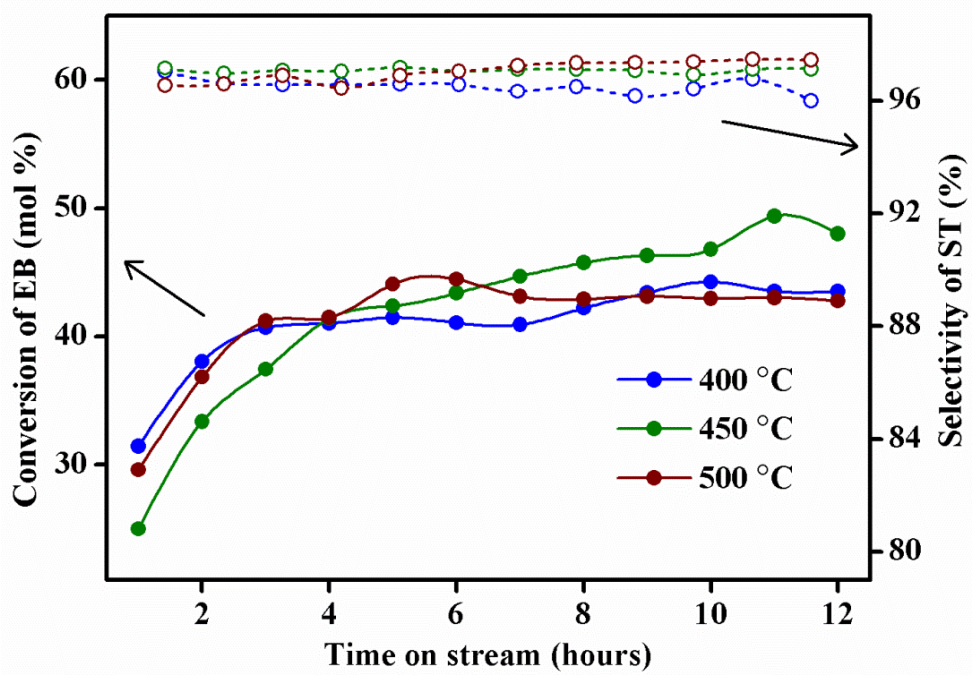

Fig. 4.13 Conversion of EB and selectivity of ST at various reaction temperatures over MAC-2.

Reaction conditions: *LHSV 3 h^{-1} with respect to EB and GHSV 1200 h^{-1} with respect to oxygen, 1 atm. pressure, 1 mL catalyst.*

4.4.2.4. Effect of ethyl benzene flow

Fig. 4.14 shows the EB conversion and ST selectivity as a function of EB flow rate (LHSV = 2, 3, 4, 6 h^{-1}). MAC-2 was employed as a catalyst and the reaction was measured at 450 °C and 1200 GHSV h^{-1} oxygen flow. At very low EB flow (LHSV = 2 h^{-1}) an interesting observation was made: the conversion of EB is stable and the selectivity towards styrene was decreased. This is due to the increased contact time over catalyst, which favors the decomposition of the styrene formed. At an appropriate LHSV 3 h^{-1} flow, the conversion increased steadily along with yield of styrene. Conversion and selectivity decreased as the flow rate increased (LHSV = 4 and 6 h^{-1}), which is due to less contact time between the catalyst and the reactants. Henceforth 3 h^{-1} (LHSV) was decided as the optimal flow of EB for further studies.

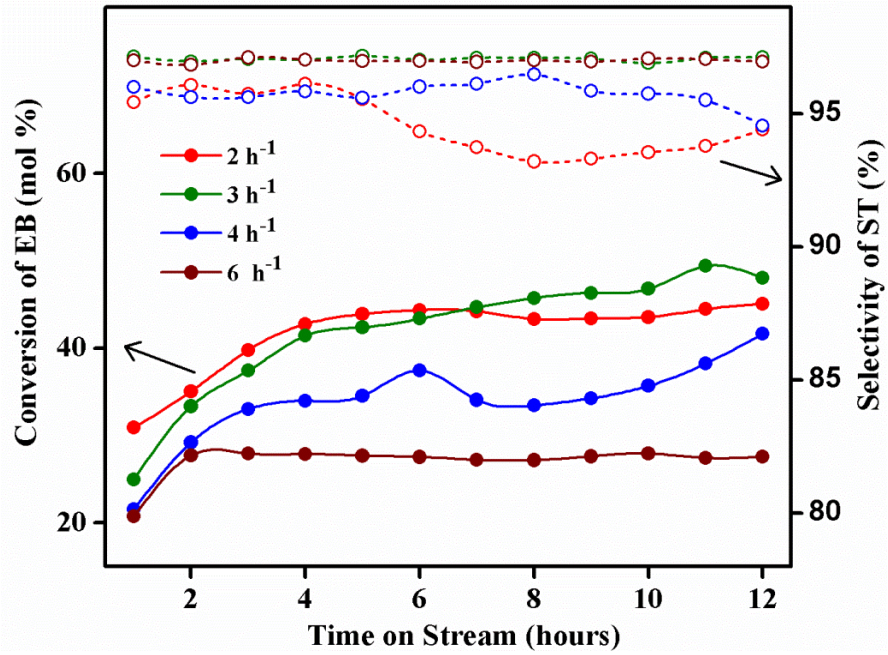

Fig. 4.14. Conversion of EB and selectivity of ST at various EB flow rates over MAC-2.

Reaction conditions: *450 °C, GHSV 1200 h^{-1} with respect to oxygen, 1 atm. pressure, 1 mL catalyst.*

4.4.2.5. Effect of cerium loading

A catalyst containing various amounts of cerium was prepared to optimize the nominal amount of cerium that is required for maximum conversion, which is shown in **Fig. 4.15**. Catalysts containing lower amounts of cerium (x = 0.01, 0.03, 0.05) gave better conversion when compared to higher cerium loading. Among the three catalysts, MAC-2 (x = 0.03) gave the maximum conversion of about 49.4 % with 97 % selectivity towards ST when compared to the other two catalysts. This amount of cerium was considered as the optimum amount to achieve high yield of styrene. At higher loadings (x = 0.1, 0.3, 0.5) the conversions decreased gradually because of agglomeration of ceria on the surface of the catalyst and poor dispersion. The conversion and selectivity profile of a higher amount (MAC-4) of cerium containing catalyst is given, which shows around 10 % decrease in the yield of styrene. For understanding the activity of cerium containing hydrotalcite derived oxide, reactions were performed with Mg-Al oxide and ceria **(Fig. 4.16)** which gave a maximum of 35 and 38 % conversion respectively with lower selectivity (92.8 and 87.8 % respectively) towards styrene than the cerium containing Mg-Al mixed oxide. This indicates that the higher activity associated with MAC is due to synergistic interaction of CeO_x and hydrotalcites, with ceria playing the role of an oxygen supplier.

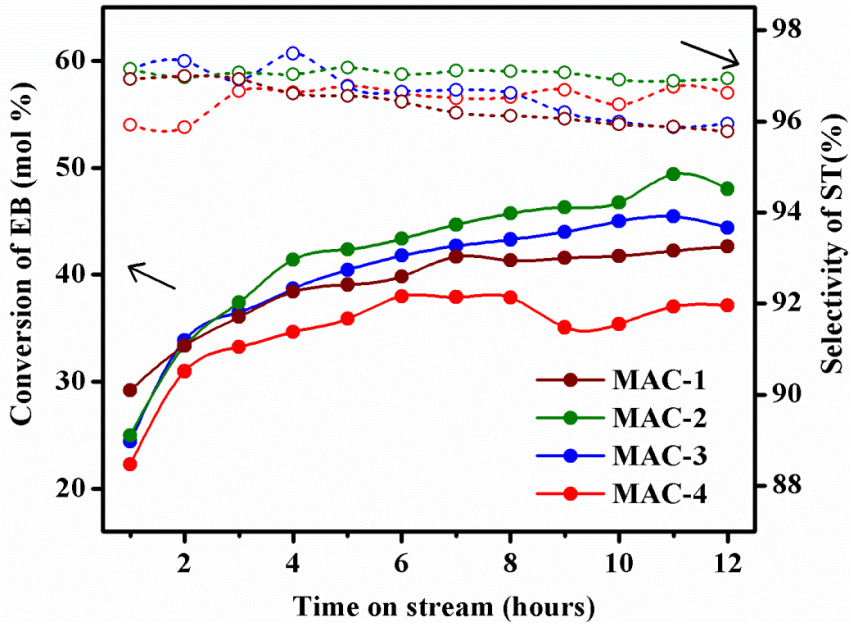

Fig. 4.15. Conversion of EB and selectivity of ST at various cerium loadings

Reaction conditions: *450 °C, LHSV 3 h^{-1} with respect to EB and GHSV 1200 h^{-1} with respect to oxygen, 1 atm. pressure, 1 mL catalyst.*

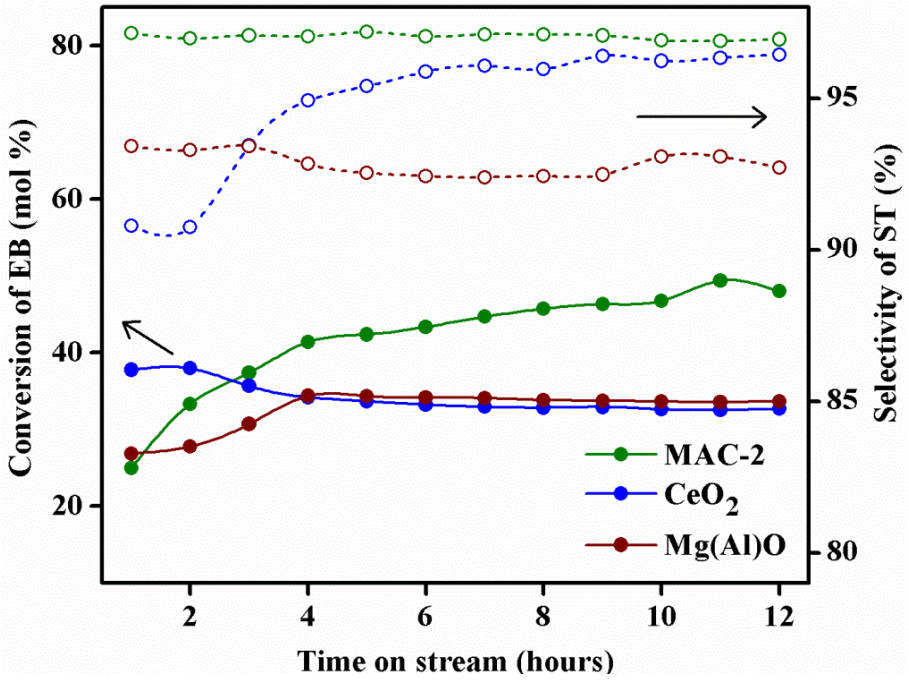

Fig. 4.16. Conversion of EB and selectivity of ST for i) MAC-2 ii) Ceria iii) Mg(Al)O.

Reaction conditions: *450 °C, LHSV 3 h^{-1} with respect to EB and GHSV 1200 h^{-1} with respect to oxygen, 1 atm. pressure, 1 mL catalyst.*

The atom economy for all catalysts employed was calculated using the equation - **4.3**.[33] The experimental efficiency was calculated by multiplying the yield of styrene obtained with the

theoretical yield. The atom economy of MAC-2 was more when compared with pure ceria. The turnover number (TON) and turnover frequency (TOF) decrease as the cerium loading increases (**Table 4.3**) which supports the claim that a lower amount of cerium has good dispersion which helps in obtaining good activity and stability.

$$\text{Theoretical atom economy} = \frac{\text{Mass of the required product}}{\text{Mass of all obtained products}} \qquad \textbf{4.3}$$

Catalyst	Turn over Number [a]	Turn Over Frequency [b] (s^{-1})	Atom Economy (%)
MAC-1	216	0.90	34.4
MAC-2	96.5	0.40	40.7
MAC-3	50.6	0.21	36.8
MAC-4	4.8	0.02	30.4
[a] calculated based on basicity and amount of ceria present in the catalyst [b] calculated at steady state reaction conditions			

Table.4.3. TON, TOF and Atom Economy values for all the catalysts studied

Entry (Mg:Al:Ce mole ratio)	Conv.of EB[a] (mol %)	Selectivity[a] (%)		Yield of styrene[a] (mol %)
		Styrene	Others[b]	
Mg(Al)O	33.6	93.1	6.8	31.3
MAC-1	42.2	95.9	4.0	40.5
MAC-2	49.4	97.0	2.9	47.9
MAC-3	45.5	95.8	4.0	43.4
MAC-4	37.0	96.7	3.3	35.8
CeO_2	32.5	96.3	3.6	31.3
[a] Conversion at steady state. ***Reaction conditions:*** *450 °C, LHSV 3 h^{-1} with respect to EB and GHSV 1200 h^{-1} with respect to molecular oxygen. Molar ratio (O_2/EB) = 2, 1 atm. pressure, 1 mL catalyst, Liquid mass balance obtained in each run ~2.9 mL.* [b] Toluene, benzene, benzaldehyde and styrene oxide				

Table.4.4. Conversion of EB and product selectivity comparison

4.4.2.6. Time on stream study

In order to study the stability of the catalyst, the optimized catalyst (MAC-2) was employed for longer (TOS) condition (72 hours) under optimized reaction conditions i.e. 450 °C, LHSV 3 h^{-1}

with respect to EB and GHSV 1200 h^{-1} with respect to molecular oxygen. The activity remained the same **(Fig. 4.17)** as mentioned earlier in the effect of cerium loading with maximum 49.4 % conversion and 97 % selectivity towards styrene. During 72 hr of TOS study it was observed that the catalytic activity remains more or less stable with only ~3 % decrease in conversion even after 72 hours.

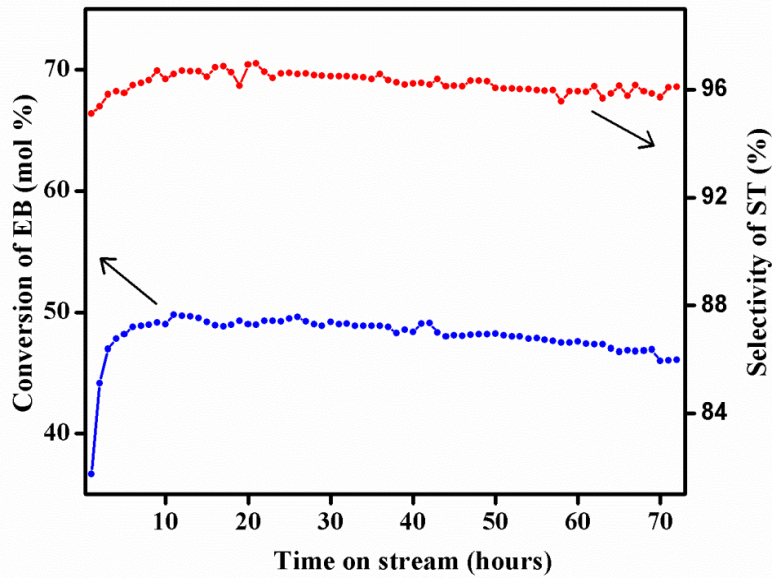

Fig. 4.17. 72 hours TOS study using MAC-2 as catalyst.

Reaction conditions: *450 °C, LHSV 3 h^{-1} with respect to EB and GHSV 1200 h^{-1} with respect to oxygen,1 atm pressure, 1 ml catalyst*

This is far better than pure ceria which shows a decrease of ~7 % in 12 hours of TOS. The activity was same as the initial maximum conversion when the catalyst was regenerated with 1200 h^{-1} oxygen flow at 450 °C. These features of the catalyst with long term sustainability and easy regeneration of catalyst at less working temperature than the commercial process[34] focuses on the energy efficiency which is an important aspect to be considered in developing a greener process. The yield of styrene is more when compared with pure mesoporous ceria[20] emphasized the importance of dispersing ceria in a particular mixed oxide system. The present catalyst retains its initial maximum activity which was not observed in vanadia based catalyst systems.[14,32] This is mainly due to good oxygen transport of ceria which in turn avoids excess coke formation to maintain the activity for more than 12 hours. Seldom literature reports demonstrated the activity for more than 20 hours with high selectivity. This stability was observed continuously for 72 hours which supports the high efficiency of our MAC- 2 catalyst.

4.4.3. Spent catalyst Analysis

PXRD pattern of spent catalyst was taken and compared with freshly calcined catalyst **(Fig. 4.18).** There is no phase transition of the spent catalyst during the studies which was corroborated by PXRD and also suggests that the catalyst is intact and stable even after reaction. The amount of coke deposited was evaluated for different reaction conditions using the data obtained from TGA of the spent catalyst. The following observations were made from TGA analysis, i) the highest weight loss was observed for the catalyst employed at 500 °C ii) the lowest was for the high oxygen flow (2400 h^{-1}) iii) also the catalyst employed at lower oxygen flow showed more weight loss. Based on these observations it can be concluded that, the high coke formation at very high temperatures and low oxygen flow deactivates the catalyst and also high oxygen flow decreases the coke formation by oxidizing the coke formed. Catalyst used at 400 °C showed less coke deposition and less activity when compared to optimized temperature (450 °C). So in order to have less coke and stable activity of the catalyst, an optimal temperature with a suitable flow of oxygen is required for good conversion and also in regenerating the catalyst during the reaction for longer time. Based on these observations the optimized reaction condition i.e. 450 °C and 1200 h^{-1} with respect to oxygen suits well for getting a better yield of ST and stable activity.

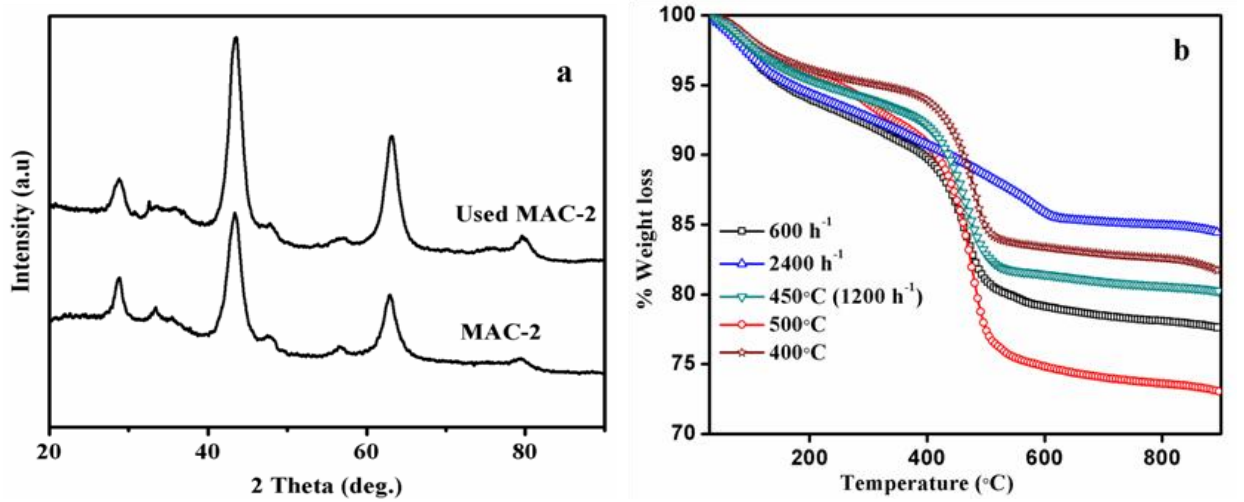

Fig. 4.18. a) PXRD of fresh and spent (MAC-2), b) TGA of spent catalyst (MAC-2) at various temperature and oxygen flow conditions

4.4.4. Conclusion

Systematic cerium containing mixed oxides from a hydrotalcite precursor were prepared with a high surface area which also shows a better catalytic activity for the conversion of EB to styrene.

The morphological studies show evenly distributed ceria crystallites at lower loading of cerium. The catalyst with 0.03 mol % of cerium shows the highest conversion when compared to all other compositions prepared. On increasing the cerium loading the catalytic efficiency decreased and at 0.5 mol % of cerium the activity is more or less similar to pure ceria. Stable catalytic activity for EB to ST under optimized reaction conditions was demonstrated continuously for 72 hours, which shows the sustainability and stability of the catalyst. The spent catalyst analysis proves the stability of the catalyst where there is no significant difference in catalyst characteristics even after the reaction. Interestingly there is no sintering or aggregation of ceria in spite of exothermic nature of the reaction. The basicity, reducibility, oxygen storage capacity and metal surface concentration were found to play a predominant role in this reaction.

PART-B

4.5. ODH of EB to ST over Manganese substituted Ca(Sr)TiO_3 perovskite type oxides

4.5.1. Catalytic activity

The perovskite type catalysts studied for ODH of ethane was studied for EB also. The catalyst codes/notations remain the same as earlier chapter. To understand the influence of calcium content in the activity of STM, calcium with three different molar ratios of calcium was prepared.

4.5.1.1. Effect of Manganese and Calcium in $SrTiO_3$

All the prepared catalysts [CT, CM, CTM, ST, STM and SCTM (0.25,0.5,0.75)] were tested for the oxidative dehydrogenation of ethylbenzene to styrene. The reaction conditions such that LHSV 3 h^{-1} with respect to EB, GHSV 1200 h^{-1} with respect to O_2 at atm. pressure, and 500 °C temperature was maintained for all the catalysts. Among all these catalysts $Sr_{0.5}Ca_{0.5}Mn_{0.1}Ti_{0.9}$ - SCTM 0.5(SC5TM) shows better activity and selectivity toward this reaction which is shown in the **Fig. 4.19**

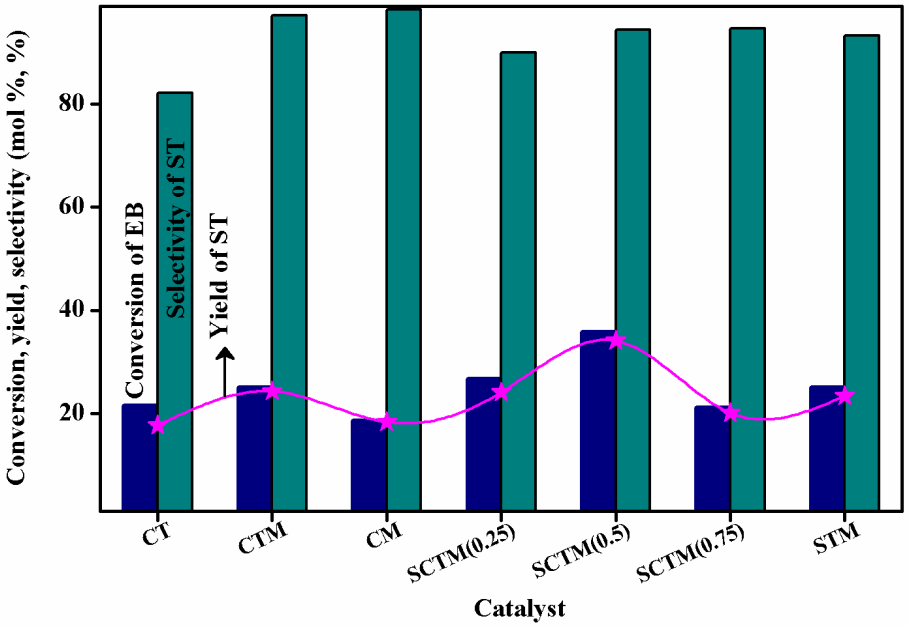

Fig. 4.19. Activity comparison for all the catalysts

Reaction conditions: *500 °C, LHSV 3 h^{-1} with respect to EB and GHSV 1200 h^{-1} with respect to oxygen,1atm pressure, 1 ml catalyst*

4.5.1.2. Effect of Preparation method

To compare the catalytic activity the perovskite catalyst $Sr_{0.5}Ca_{0.5}Mn_{0.1}Ti_{0.9}O_3$ (SC5TM) was prepared by both citrate-gel method and glycine combustion method which was investigated

under optimized reaction conditions such as LHSV 3 h^{-1} with respect to EB, GHSV 2400 h^{-1} with respect to oxygen at 1 atm. and 1 ml catalyst at 500 °C. The EB conversion and ST selectivity of both catalysts are shown in the **Fig. 4.20**. It was observed that the catalyst SC5TM prepared by glycine combustion method gave a better styrene yield than the catalyst which was prepared by the citrate gel method. For the optimization studies the catalyst prepared by glycine combustion method was employed.

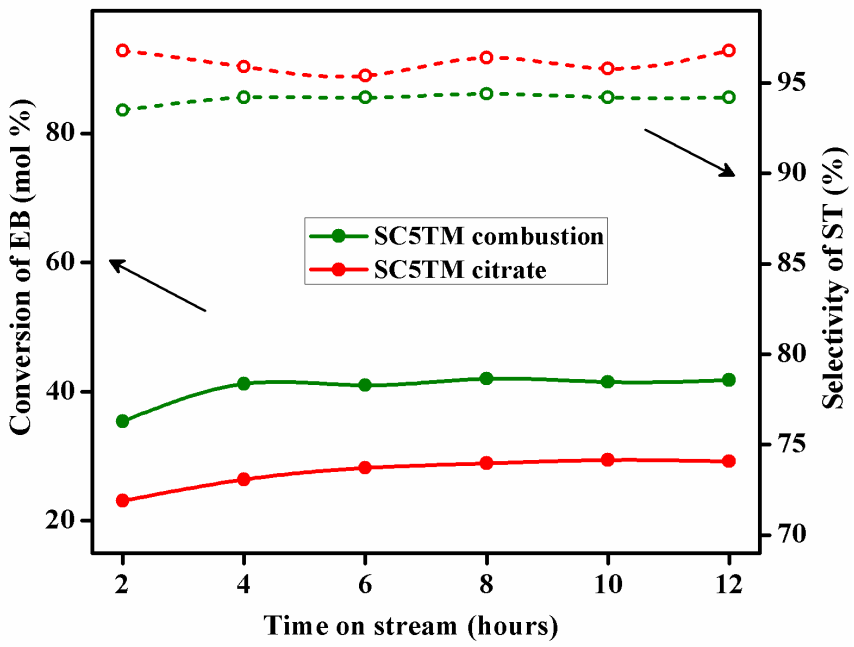

Fig. 4.20. Effect of preparation method for ODH of EB to ST

Reaction conditions: *500 °C, LHSV 3 h^{-1} with respect to EB and GHSV 2400 h^{-1} with respect to oxygen,1 atm pressure, 1 ml catalyst*

4.5.1.3. Effect of the reaction temperature

Fig. 4.21 depicts the effect of reaction temperature on ethyl benzene conversion (varied from 450 - 600 °C) on the optimized catalyst SC5TM at LHSV 3 h^{-1} with respect to EB, GHSV 2400 h^{-1} with respect to oxygen at 1 atm. pressure. As expected, EB conversion gradually increases with increasing reaction temperature which indicates that the ODH of EB is more favorable at higher temperature using this catalyst but it is found that above 500 °C conversion increases rapidly while selectivity decreases with increasing temperature it may be due to the cracking of EB at high temperature. Based on the overall activity (Conversion and selectivity) 500 °C was considered to be a better reaction temperature where highest selectivity was obtained. Hence, in remaining all our studies 500 °C was kept as the optimized temperature.

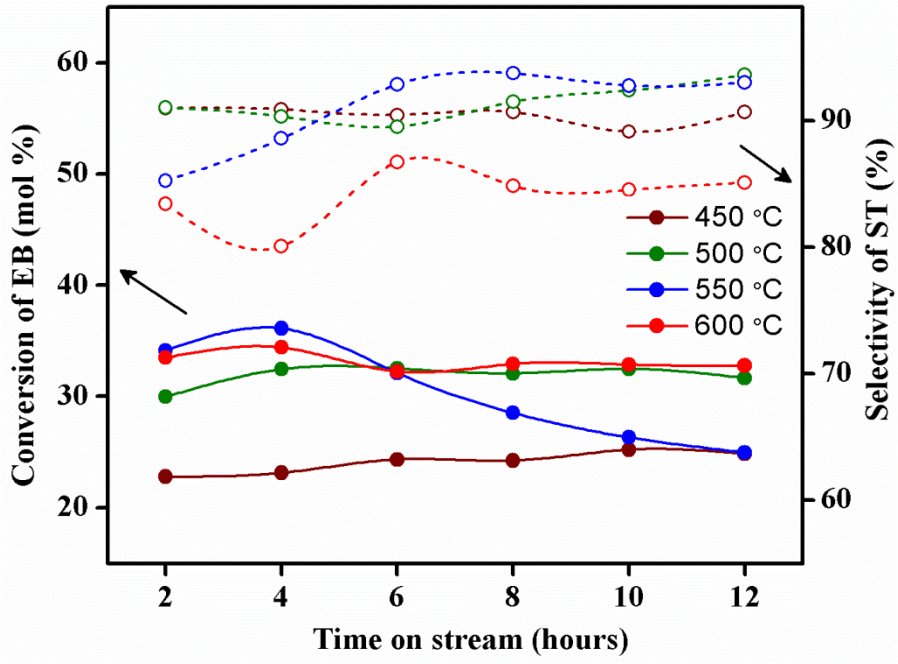

Fig. 4.21. Effect of temperature for ODH of EB to ST over SC5TM

Reaction conditions: *LHSV 3 h^{-1} with respect to EB and GHSV 2400 h^{-1} with respect to oxygen,1 atm pressure, 1 ml catalyst*

4.5.1.4. Effect of Oxygen flow

Ethyl benzene conversion was investigated with different oxygen flow rates and the other parameters were LHSV 3 h^{-1} of EB at 500 °C for 12 hours. The catalytic activity for 1200, 2400, 3600 and 4200 h^{-1} GHSV of oxygen is shown in the **Fig. 4.22**. It was observed that the ethylbenzene conversion initially increased with increasing time on stream up to 6 hours then a steady state catalytic activity was obtained in the case of 1200, 2400, 3600 h^{-1}. In the case of 4200 h^{-1} oxygen flow the conversion decreases after 6th hour which is prominently due to the very less contact time of EB over the catalyst. These results reveal that the 2400 h^{-1} oxygen flow exhibited high styrene yield for the catalysts with stable conversion. Selectivity towards styrene decreases with increase in oxygen flow rate. Slight excess of cracking products such as toluene and benzene was also observed in higher oxygen flow which evidences the cracking of EB at higher flow.

4.5.1.5. Effect of O_2 to EB ratio

Fig. 4.23 shows the EB conversion and ST selectivity as a function of EB flow rate (LHSV = 1.8, 2.4, 3 h^{-1} which corresponds to O_2/EB - 3.3, 2.5 and 2 respectively) over SC5TM as a catalyst and the reaction was done at 500 °C and GHSV 1200 h^{-1} oxygen flow.

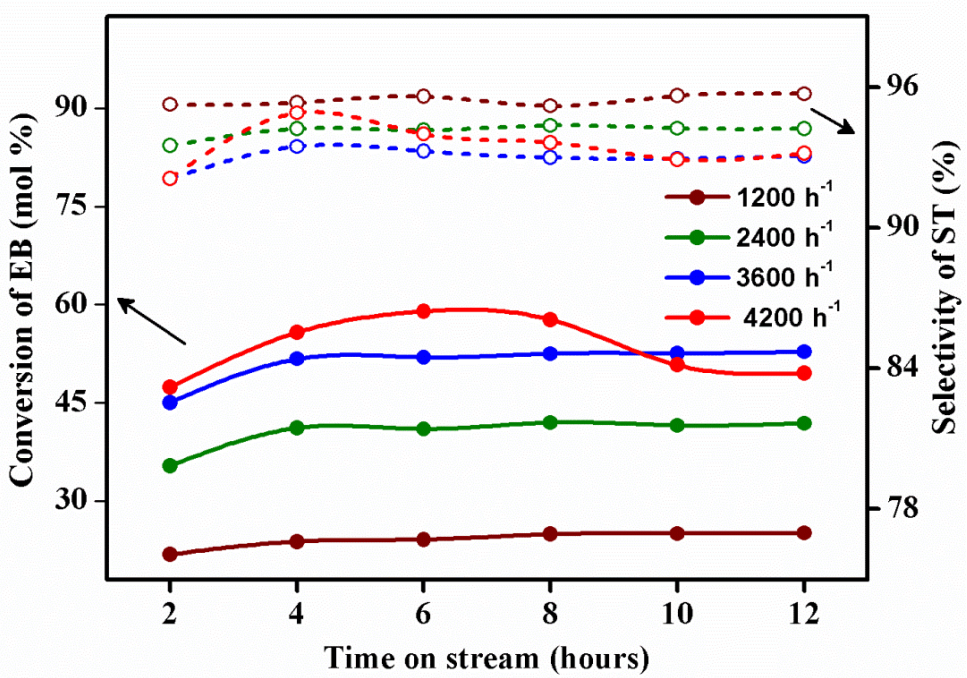

Fig. 4.22. Effect of oxygen flow for ODH of EB to ST over SC5TM

Reaction conditions: *500 °C, LHSV 3 h^{-1} with respect to EB, 1 atm pressure and 1 ml catalyst*

From these data it was evident that EB conversion reaches the maximum of 33.1 % with 95.6 % selectivity to styrene over the catalyst when the oxygen to EB ratio is 3.3. The selectivity towards styrene is independent of EB flow which is almost same in all cases. This conversion enhancement at this oxygen to EB ratio is due to the high contact time of EB over the catalyst and this ratio was maintained as an optimized condition for getting better activity.

4.5.2. Spent catalyst analysis

The spent catalysts (STM, CTM and SC5TM) were subjected to Thermogravimetric analysis from room temperature to 800 °C. It was observed that the CTM showed a higher weight loss when compared to other catalysts which was also observed for ODH of ethane due to more electrophilic oxygen species been formed on this catalyst surface. SC5TM showed minimal weight loss when compared to STM and CTM which supports the reason for better activity towards ODH of EB to ST also. Based on this study it is evident that the electrophilic oxygen species when present in nominal amounts helps in driving the reaction and when the concentration of these species increases total oxidation happens due to which coke is also formed which decrease the overall activity of the catalyst.

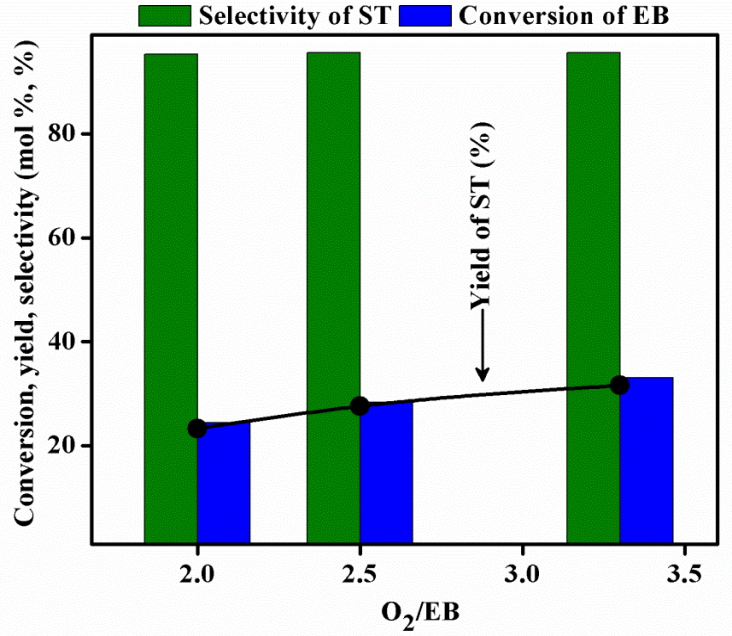

Fig. 4.23. Effect of O_2/EB ratio for ODH of EB to ST over SC5TM

Reaction conditions: *500 °C, GHSV 2400 h^{-1} with respect to oxygen,1 atm pressure and 1 ml catalyst*

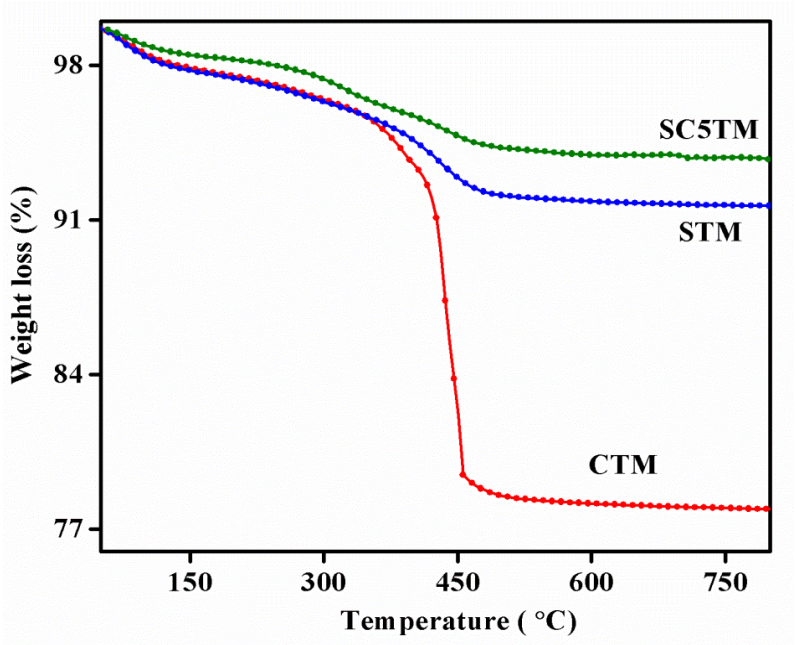

Fig. 4.24. TGA analysis of SC5TM,STM and STM

4.5.3. Conclusion

From these studies, Manganese and Strontium substituted on $CaTiO_3$ type perovskites (CT, ST, STM, CM, CTM and SC5TM) were prepared by facile citric acid sol-gel method. After optimizing the metal ratios among the catalytic studies the best catalyst was SC5TM which

showed a better activity when it was prepared by glycine combustion method. In conclusion, we demonstrated that the SC5TM prepared by glycine combustion exhibited both high activity and selectivity in oxidative dehydrogenation of ethylbenzene to styrene in presence of oxygen as oxidant. For the active catalyst that obtained from initial screening was investigated under varying reaction conditions like temperature, reactant flows, oxidants, different metal proportions. The best results observed for the ODH of EB on the catalyst SC5TM (0.5:0.5:0.1:0.9) were prepared by glycine combustion and tested under steady EB flow LHSV 3 h^{-1} and GHSV 2400 h^{-1} with respect to oxygen at 500 °C and at atmospheric pressure. The PXRD patterns shown a homogenous and pure phase formation of Perovskite type oxides for all the materials prepared. The spent catalyst analysis showed a minimal amount of coke formation when compared to other catalysts studied.

4.6. References

1. Chemicals and petrochemicals manufacturer's association of India (CPMAI).
2. O. Shekhah, W. Ranke, R. Schlogl, *J. Catal*., 225 (2004), 56 - 68.
3. F. Cavani, F. Trifiro, *Appl. Catal. A*, 133 (1995), 219-239.
4. D. E. Stobbe, F. R. van Buren, A. J. van Dillen and J. W. Geus, *J. Catal*., 135 (1992) 533- 548
5. T. Hirano, *Appl. Catal*., 26 (1986) 81
6. T. Hirano, *Appl. Catal*., 28 (1986) 119.
7. T. Imai, US 4 418 237 (1983).
8. T. Imai, US 4 435 607 (1984).
9. J. Romatier, M. Bentham, T. Foley and J.A. Valentine, Proc. *Dewitt Petrochem. Rev*., Houston, Texas, 1992, p. K1.
10. U.S. Pat. 3,351,635 (Nov. 7, 1967), J. Kollar (to Halcon International, Inc.).
11. U.S. Pat. 4,066,706 (Jan. 3, 1978), J. P. Schmidt (to Halcon International, Inc.).
12. D. L. Trent, DOW e-library, *The Dow Chemical Company*
13. B. M. Reddy, K. N. Rao, G. K. Reddy, A. Khan and S. E. Park, *J. Phys. Chem. C*,111 (2007), 18751-18758.
14. K. Sivaranjani, A. Verma and C. S. Gopinath, *Green Chem*.,14(2012), 461-471.

15. L. Wang, J. Delgado, B. Frank, Z. Zhang, Z. Shan, D. S. Suand F. S. Xiao, *ChemSusChem*, 5(2012), 687-693.
16. Y. Ohishi, T. Kawabata, T. Shishido, K. Takaki, Q. Zhang,Y. Wang, K. Nomura and K. Takehira, *Appl. Catal. A* ,288(2005), 220-231.
17. N. R. Shiju, M. Anilkumar, S. P. Gokhale, B. S. Rao, C. V. V. Satyanarayana, *Catal. Sci. Technol*., 1(2011), 1262-1270.
18. E. Heracleous, A. A. Lemonidou, *J. Catal.*, 237(2006), 175-189.
19. R. J. Balasamy, B. B. Tope, A. Khurshid, Ali A. S. Al-Ali, L. A. Atanda, K. Sagata, M. Asamoto, H. Yahiro, K. Nomura, T. Sano, K. Takehira, S. S. Al-Khattaf, *Appl. Catal., A*, 398 (2011), 113-122.
20. J. Xu, L. C. Wang, Y. M. Liu, Y. Cao, H. Y. He and K. N. Fan, *Catal. Lett.*, 133 (2009), 307-313.
21. J. Xu, B. Xue, Y. M. Liu, Y. X. Li, Y. Cao and K. N. Fan, *Appl.Catal. A*, 405 (2011), 142-148.
22. E. S. Gnanakumar, C. J. Jino, T. Raja and C. S. Gopinath, *J. Nanosci. Nanotechnol*., 13(2013), 2682-2688.
23. M. Guo, J. Lu, Y. Wu, Y. Wang and M. Luo, *Langmuir*, 27 (2011), 3872-3877.
24. B. Murugan and A. V. Ramaswamy, *J. Am. Chem. Soc*., 129 (2007), 3062-3063.
25. L. Chmielarz, M. Rutkowska, P. Kustrowski, M. Drozdek,Z. Piwowarska, B. Dudek, R. Dziembaj and M. Michalik, *J. Therm. Anal. Calorim.*,105(2011), 161-170.
26. A. E. Nelson and K. H. Schulz, *Appl. Surf. Sci*., 210(2003),206-221.
27. C. S. Gopinath, S. G. Hedge, A. V. Ramasamy and S. Mahapatra, *Mater. Res. Bull*., 37(2002), 1323-1332.
28. L. Jiang, H. Zhu, R. Razzaq, M. Zhu, C. Li and Z. Li, *Int. J. Hydrogen Energy*, 37(2012), 15914-15924.
29. B. Murugan, A. V. Ramaswamy, D. Srinivas, C. S. Gopinath, and V. Ramaswamy, *Chem. Mater*., 17(2005), 3983-3993
30. A. Pfau and K. D. Schierbaum, *Surf. Sci*., 321(1994), 71-80.
31. F. Zhang, P. Wang, J. Koberstein, S. Khalid and S. W. Chan,*Surf. Sci*., 563(2004), 74-82.
32. K. N. Rao, B. M. Reddy, B. Abhishek, Y.-H. Seo, N. Jiang, and S.-E. Park, *Appl. Catal., B*, 91(2009), 649-656.

33. R. A. Sheldon, *Green Chem*., 9(2007), 1273-1283.

34. E. H. Lee, *Catal. Rev. Eng. Sci*., 8(1973), 285-305

Chapter 5 : Oxidative dehydrogenation of 1-butene to 1,3-butadiene

Synopsis

- In $CeVO_4$, the transition elements Cr, Mn, Fe and Co were substituted in cerium site by a simple pH controlled precipitation followed by the hydrothermal treatment

- The formation of CeO_2 crystallites on the surface of $CeVO_4$ was evidenced by PXRD and Raman spectroscopy studies

- The surface ratio of Ce^{4+}/Ce^{3+} was calculated after deconvolution of Ce 3d core X-ray photoelectron spectra of pure $CeVO_4$ and with 'Mn' substitution

- Catalytic activity towards ODH of 1-butene for all the transition metal substituted $CeVO_4$ were carried at optimized reaction conditions in which the 'Mn' substituted catalyst gave a better activity

- Further activity studies were carried out to optimize the manganese loading and catalytic activity of optimized composition which was compared with manganese impregnated $CeVO_4$

5.1.Introduction

1,3-butadiene (BD) is one of the important platform chemical which is employed in the production of many fine chemicals and commercial end products. The potential of BD to form rubber like polymers was identified in the earlier days of 20th century and its production was more during the World War II in Germany and in the United States. After the discovery of Ziegler Natta catalysts which were based on organometallic which was used to get high quality rubbers from BD.[1] It is an important building block chemical which is used to synthesize a variety of polymers like SBR(styrene-butadiene rubber), polybutadiene (PB), Styrene butadiene latex, Acrylonitrile-butadiene-styrene (ABS) resins, adiponitrile and nitrile rubber. **Fig.5.1** shows the ratio of chemicals produced from BD. Among this the SBR finds more usage as these are used for the manufacture of tyres and along with that it is also used production of adhesives, sealants, coatings, and other rubber articles such as shoe soles, etc.[2,3]

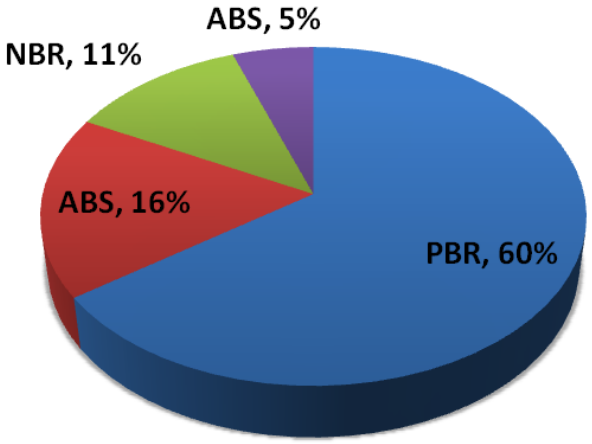

Fig. 5.1. Commercially important products from BD[3]

5.2. Production of 1,3-butadiene

In 1920-1930 when the synthetic rubber was produced from BD industries had their own way and source of synthesis. For example in Russia, BD was synthesized from the grain ethanol using a single step process which was called as Lebedev process.[1,4,5] Germany under the brand name "Buna-S" produced BD from the acetylene that was obtained from coal. This acetylene process was prevalent those days by two ways of synthesis which are (i) Aldol process and (ii) Reppe process. In the Aldol process the acetylene from coal is converted to acetaldehyde which is converted to 1,3-butanediol by aldol reaction and this on dehydration forms BD. In the Reppe process formaldehyde is reacted with acetylene to form 1,4-butynediol which on hydrogenation

gives 1,4-butanediol and this on partial dehydration via tetrahydrofuran, BD was obtained.[6] Due to the supply demand factors and operational costs both the routes were abandoned. The emergence of fossil fuels fuelled many pathways as it was a remarkable source for many of the platform chemicals and fine chemicals. Due to the decline in acetylene, BD was obtained during the naphtha cracking process and till date around 98 % of the global BD is obtained from the C4 raffinates which are extracted from naphtha cracking.(**Fig. 5.2**) Generally the separation of BD is from the C4 stream and it requires an exhaustive and expensive extractive distillation with a selectivity of only 4-5 % due to formation of azeotropic mixture with butane. In addition to this the C4 fraction itself is greatly dependent on cracking severity. Due to the invention of shale gas and the ethane only steam cracking process which has lower operating costs and increased selectivity towards ethene, the production of BD by naphtha cracking does not satisfy the demands of the growing BD market. Due to this restrictions on the availability of BD, high BD prices are likely to occur in near future.[7]

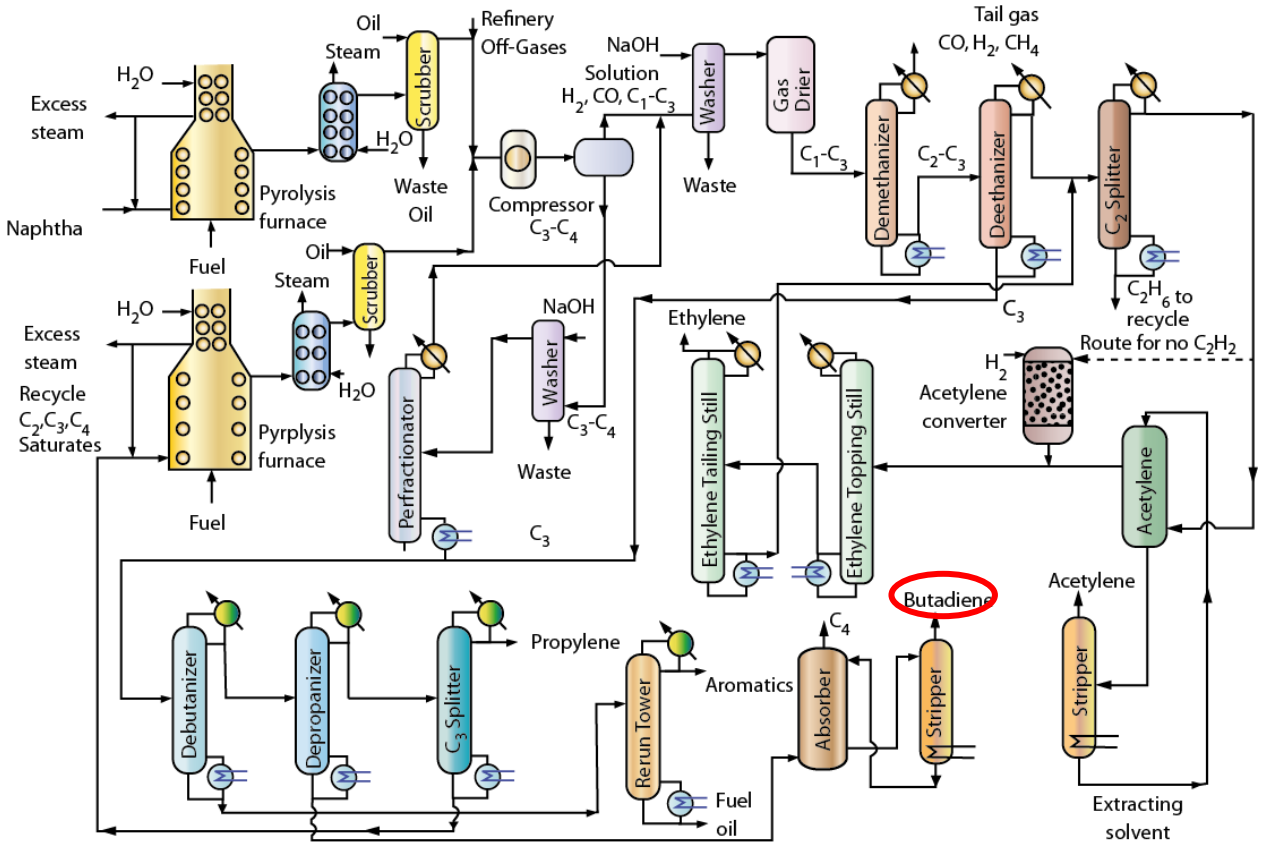

Fig. 5.2. Naphtha Cracking process with extraction chambers[8]

5.3. Dehydrogenation of butanes and butenes

The dehydrogenation of butane and butene is another pathway for the production of BD. As shown in **Scheme-5.1** the dehydrogenation process is highly endothermic and requires high temperature for a reasonable conversion of butane. Due to the high endothermicity and the coke formation the yield of BD is less and to overcome this Le chatelier's principle can be applied wherein the reaction can be carried out with little vacuum or in presence of steam. This has three advantages, i) reduced coke deposition, ii) provides additional heat for the reaction, and iii) steam can be easily separated and recycled during reaction

$$C_4H_8 \rightarrow C_4H_6 + H_2 \quad \Delta H° = 110 kJmol^{-1} \qquad \textbf{5.1}$$

In 1943 Houdry-Catadiene process was developed wherein the dehydrogenation was carried out in single step over 20 % Chromium oxide loaded on Aluminium oxide. This process is carried out at high temperatures from 600-700 °C due to which coking is more and frequent regeneration is required.[8-9] Phillips petroleum developed a two step process wherein the first step butane is dehydrogenated to butene over Cr_2O_3-Na_2O-Al_2O_3 and in second step butene is dehydrogenated to BD over Fe_2O_3-K_2O-Al_2O_3 catalysts.[10] Due to the regeneration drawbacks and high endothermicity there are very less reports in open literature for dehydrogenation of butane and butene.

5.4. Oxidative dehydrogenation of butane and 1-butene

Oxidative dehydrogenation (ODH) overcomes all the drawbacks of dehydrogenation where the thermodynamic limitations can be reduced by oxidizing the hydrogen formed using an oxidant and coke is also removed by oxidizing it to CO_x. The exothermic oxidation of hydrogen to water helps in partially covering the heat requirements of the endothermic dehydrogenation reaction. The catalysts that are active for ODH of n-butane are classified as Zn and Mn ferrites, supported vanadium oxide, vanadates (mainly magnesium vanadate), molybdates, and nickel-based oxides.[11] Many catalytic systems have been studied for ODH of n-butane but still a convincing productivity is not obtained as even in the best-tested catalysts owing to high reactivity of alkenes, the yields for total dehydrogenation products are limited. Butenes which are obtained from refining and naphtha cracking units serve as the starting materials for conversion into butadiene through a single-stage process. Oxo-D process of Petro-Tex (1965) and OXD process of Phillips was developed wherein steam was used in the process with steam/butene molar ratio of 12/1.

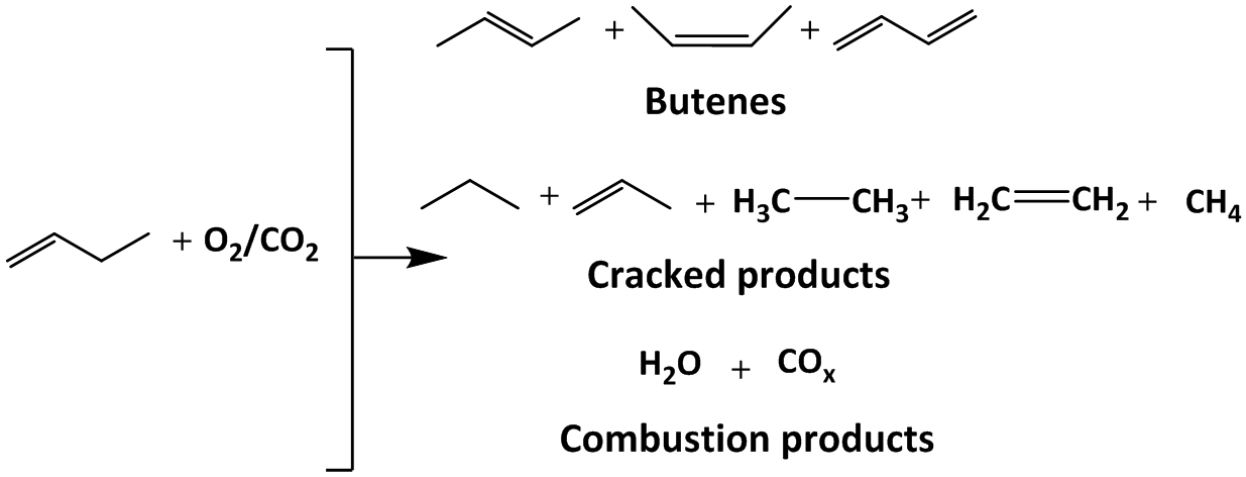

Fig. 5.3. Reaction scheme for ODH of 1-butene

Among the materials investigated for ODH of 1-butene to 1,3-butadiene bismuth molybdates are the widely studied oxide systems[12-14] and a few noble metal based systems[15-17] are also been reported till date in open literature. Bismuth molybdates are extensively studied systems but in pure form it exhibits low performance in ODH reaction. To improve catalytic performance metals like Co, Ni, Fe, La,V, Ce was incorporated and investigated.[18-23] In all these processes steam or $CO_2$was employed as diluent to increase the selectivity of BD.

5.5. Results and discussion

5.5.1. Catalyst Characterization

5.5.1.1. Powder X-ray Diffraction

PXRD patterns of all the catalysts synthesized are shown in **Fig. 5.4**. In the PXRD pattern of $CeVO_4$ the peaks of tetragonal phase $CeVO_4$ (JCPDS. No. 12-0757) were predominant with additional peaks of cubic CeO_2 (JCPDS. No. 78-0694) as impure phase. In the $CeVO_4$ when the transition elements Cr, Mn, Fe and Co was incorporated in cerium site there was an increase in the intensity of the peaks corresponding to CeO_2 (**Fig. 5.4 a**). In case of 'Co' incorporated catalyst the peaks corresponding to ceria phase were predominant which is mainly due to the blocking of ceria which is agglomerated on the surface of the catalyst. Based on the catalytic activity of $CeVO_4$ with three different molar ratios of 'Mn' was incorporated and the peaks corresponding to CeO_2 increased as the loading of the 'Mn' increased (**Fig. 5.4 b**). In all the catalysts peaks corresponding to polymeric V_2O_5 were not found.

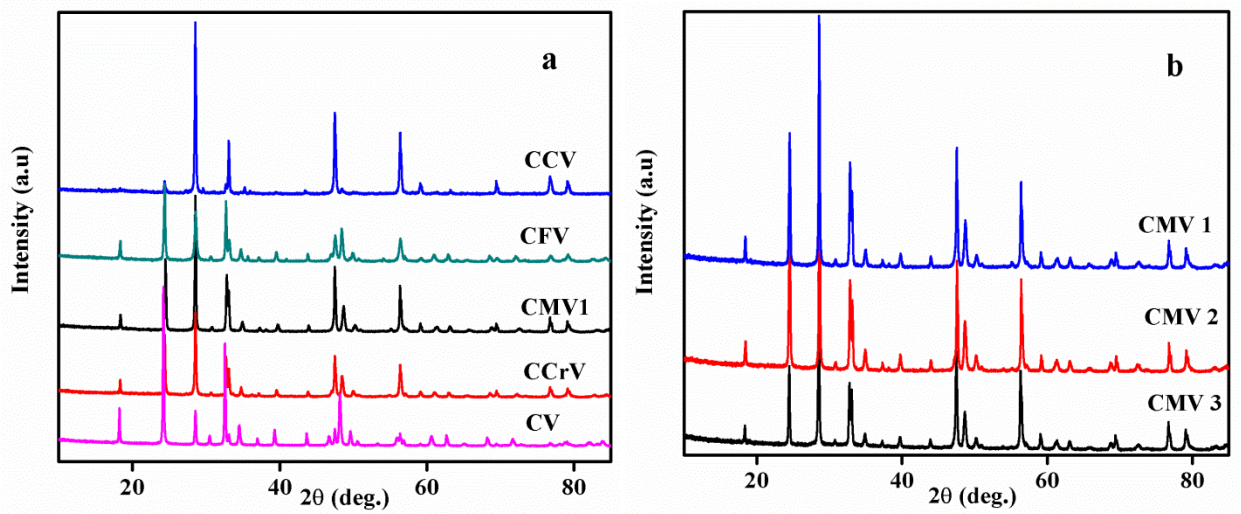

Fig. 5.4. PXRD pattern of $CeVO_4$ with a) different transition metals and b) different loadings of Manganese

Surface area of all the catalysts were calculated by using Brunauer-Emmett-Teller (BET) equation and the results are shown in **Table.5.1**. The surface area of all the samples were low which are characteristic for these type of materials.[24] The low surface area of these samples were due to the crystal growth and agglomeration of particles during calcination at 600 °C.

S.No	Catalyst (molar ratio)	Code	Surface area (m^2/g)
1	$CeVO_4$ (1:1)	CV	6.7
2	$CeCrVO_4$ (0.8:0.2:1)	CCrV	5.9
3	$CeMnVO_4$ (0.8:0.2:1)	CMV1	5.7
4	$CeMnVO_4$ (0.88:0.12:1)	CMV2	6.2
5	$CeMnVO_4$(0.94:0.06:1)	CMV3	6.3
6	$CeFeVO_4$ (0.8:0.2:1)	CFV	4.8
7	$CeCoVO_4$(0.8:0.2:1)	CCV	4.5

Table.5.1. BET surface area of all the catalysts synthesized

5.5.1.2. Transmission electron microscopy (TEM)

TEM images shown in **Fig 5.5** depict the morphology of the crystallites of CMV2 which were mostly cylindrical and spherical structures both measuring 20-50 nm. In HRTEM it was

observed that there was a homogeneous distribution of CeO_2 over the $CeVO_4$ matrix and separate clusters of CeO_2 were not observed. In addition to that the lattice fringes of MnO_2 or polymeric V_2O_5 species were not observed. The lattice fringes of both $CeVO_4$ and CeO_2 were observed and these d-spacing matched well with the value obtained from PXRD pattern.

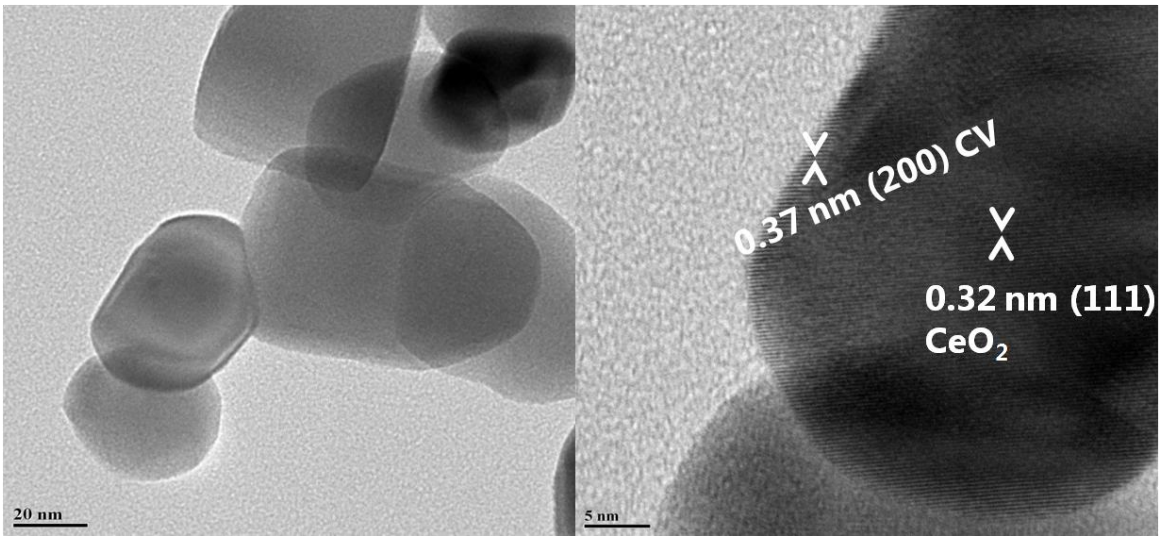

Fig. 5.5. TEM images of CMV2 showing the morphology and lattice fringes

5.5.1.3. Raman Spectroscopy

Raman spectra of all the catalysts are shown in **Fig 5.6**. In the case of $CeVO_4$ bands at 223, 258, 368, 460, 783, 796 and 858 cm^{-1} were observed. The Raman band at 858 cm^{-1} corresponds to symmetric stretching of vanadate species (A_{1g}), peaks at 796 and 783 cm^{-1} corresponds to the antisymmetric stretching of vanadates (E_g and B_{2g}) and 460 and 368 cm^{-1} to deformations of B_{2g} and B_{1g}.[25-27] The peak corresponding to vibrational mode of the cubic fluorite (F2g) CeO_2 lattice[28] at 460 cm^{-1} increases as transition metals were incorporated in the $CeVO_4$ lattice. In addition, the incorporation of transition metals in 'Ce' site decreased the intensity of peaks corresponding to $CeVO_4$. Raman band corresponding to VO_x species from polymeric V_2O_5 at 995 cm^{-1} were not observed on the spectra of any of the samples taken for the study. In case of manganese incorporated $CeVO_4$ at higher loadings of manganese the bands corresponding to Mn-O stretching vibration of MnO_2 was observed at 578 cm^{-1}.[29]

5.5.1.4. X-ray photoelectron spectroscopy (XPS)

To explore the electronic and surface properties of CV and CMV2, both the catalysts were subjected to XPS analysis. O 1s spectra of CV and CMV2 are shown in **Fig. 5.7.** in which a prominent peak at 529.1 eV was observed which corresponds to the lattice oxygen of the $CeVO_4$

and CeO_2.[28,30,31] In case of CMV2 the O 1s peak was slightly broad due to the surface hydroxyl impurities at 530.1 eV. V 2p spectra are shown in **Fig. 5.8.** in which two peaks corresponding to V $2p_{3/2}$ (516.4 eV) and V $2p_{1/2}$(524.1 eV) were observed.[30,32]

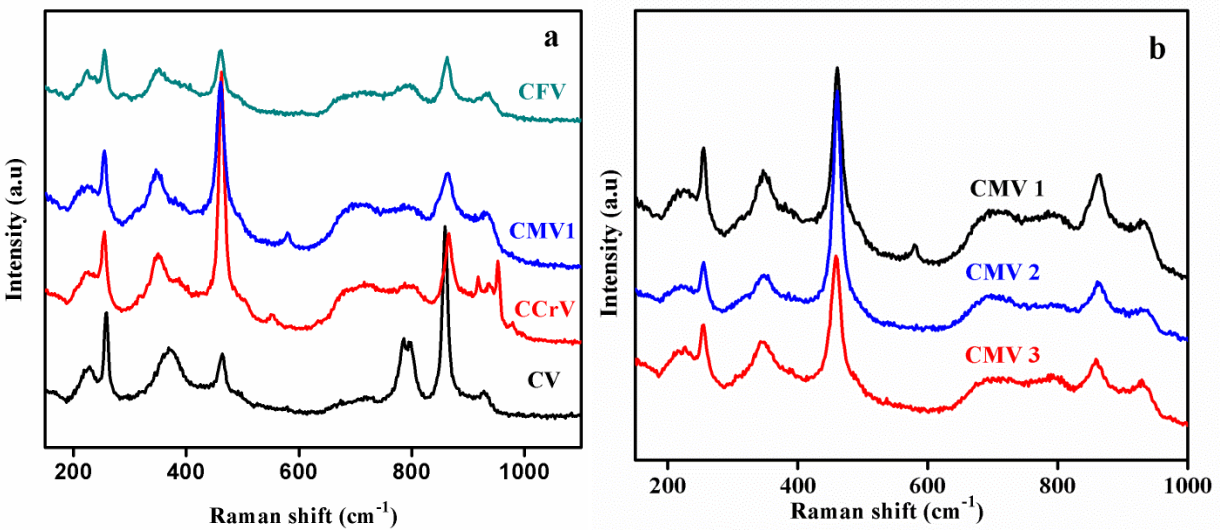

Fig. 5.6. Raman spectra of $CeVO_4$ with a) different transition metals and b) different loadings of Manganese

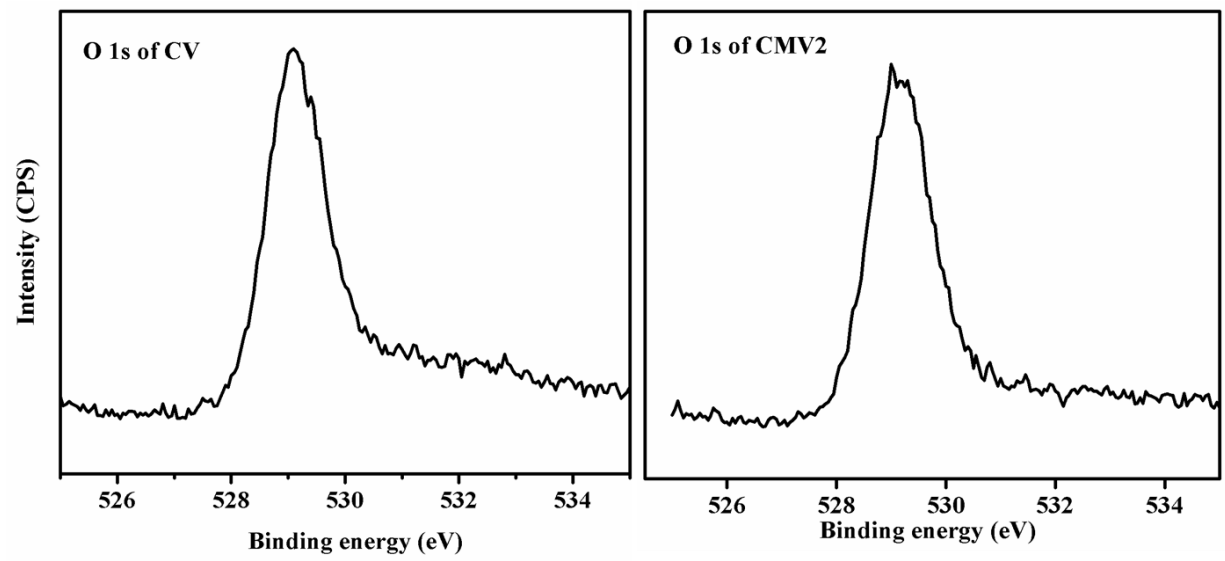

Fig. 5.7. O 1s XPS spectra of CV and CMV2

To understand the changes in surface Ce^{4+}/Ce^{3+} ratio in CV after substituting 'Mn' the Ce 3d core level spectra was taken (**Fig. 5.9**). The curve fitting were carried out by using CASA software and Shirley background subtraction was employed for background removal. In Ce 3d core level the peaks resulting from Ce^{4+}at 900.8 eV (u), 907.2 eV (u″) and 916.7 eV (u‴), 882.4 eV (v),

888.8eV (ν″) and 898.1 eV (ν‴) and four peaks corresponding to Ce^{3+} at 903.7 eV (u′), 884.7 eV(ν′), 899.2 eV (u_o) and 880.1 eV (ν_o)[28,31] were observed in both CV and CMV2.

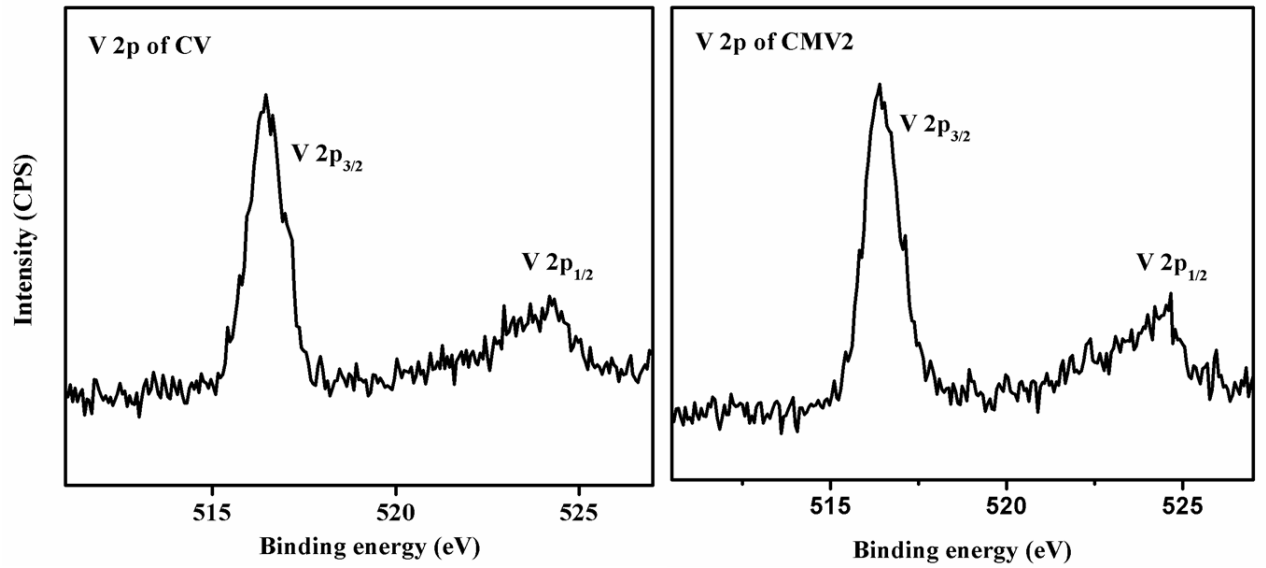

Fig. 5.8. V 2p XPS spectra of CV and CMV2

Due to the activation in $CeVO_4$ surface the concentration of Ce^{4+} was slightly higher than expected (**Table.5.2**). After 'Mn' substitution, as observed in PXRD in XPS also it was evident that the ratio of Ce^{4+} also increased. This increase in ratio of Ce^{4+} helps in increasing the selectivity of BD which will be discussed in catalytic activity discussion. In CMV2 catalyst the spectra of Mn 2p was recorded (**Fig. 5.10**) in which low intense and broad peaks corresponding to $2p_{3/2}$ (Mn^{3+}-641.3 and Mn^{4+}-642.6 eV) and $2p_{1/2}$(653 eV) were observed.[33,34]

Catalyst	**Peak area[a] (%)**	
	Ce^{3+}	**Ce^{4+}**
CV	43	57
CMV2	30	70
a - calculated from area under the curve after curve fitting		

Table.5.2. Peak area % of $Ce^{(4+ \text{ and } 3+)}$ after deconvolution

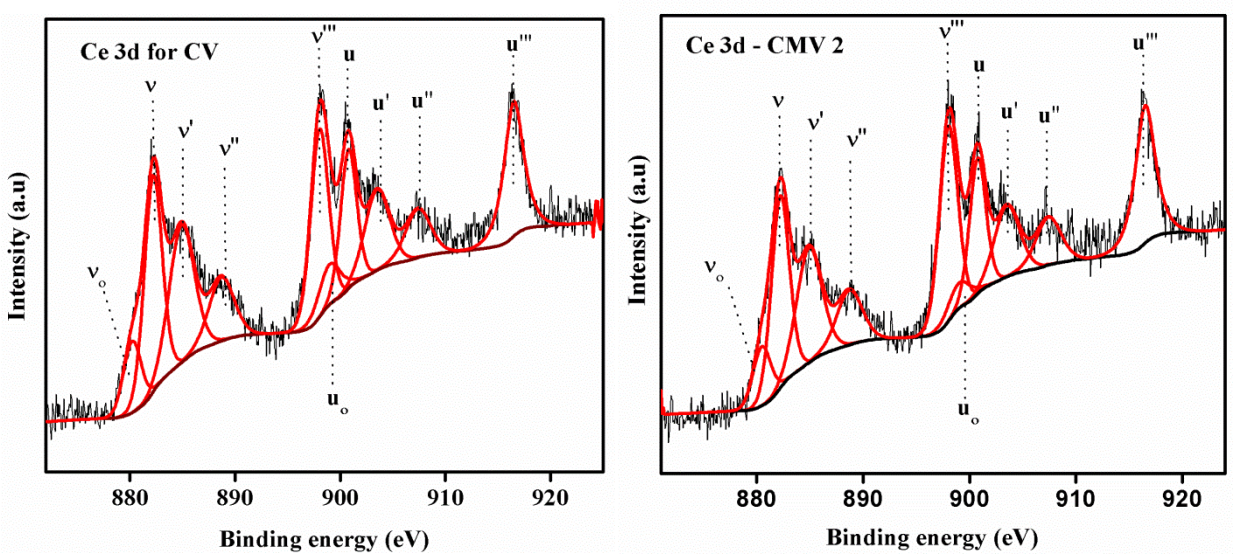

Fig. 5.9. Ce 3d XPS spectra of CV and CMV2

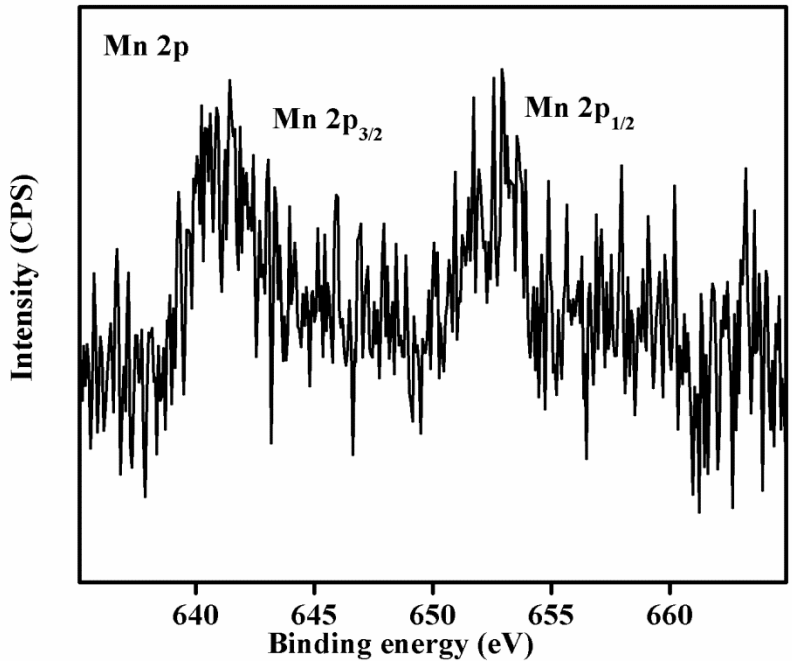

Fig. 5.10. Mn 2p XPS spectra of CMV2 catalyst

5.5.2. Catalytic activity

5.5.2.1. Effect of transition metal substitution in $CeVO_4$

To understand the role of transition metals substitution in $CeVO_4$ for ODH of 1-butene to 1,3-butadiene, 'Cr,Mn,Fe,Co' were substituted in 'Ce' site (**Fig. 5.11**). All the catalysts were tested with the reactant flow 6000 h^{-1} (Ar:1-butene:O_2 - 8:1:1), at 400 °C and atmospheric pressure. With $CeVO_4$ 37 % conversion of 1-butene and 41 % selectivity towards 1,3-butadiene was

obtained. Among the first row transition metals Cr, Mn, Fe, Co are known to be catalytically active for oxidative dehydrogenation reactions. In order to investigate their role in enhancing the activity of $CeVO_4$ towards ODH of 1-butene to 1,3-butadiene 0.2 molar ratio of these metals were substituted in the 'Ce' site. Among the four transition metals substituted $CeVO_4$, Manganese substituted catalyst showed an increased conversion and selectivity when compared to other metal substituted catalyst. In case of CMV1 1-butene conversion of 54 % and 44 % selectivity towards 1,3-butadiene was obtained. FCV which contains 'Fe' substitution showed a similar selectivity as CMV1 but the conversion of 1-butene was lower than that of CV. Based on the catalytic activity, it was found that 'Mn' substituted catalyst is better when compared to other three catalyst and further studies were made to optimize the reaction parameters and manganese loading.

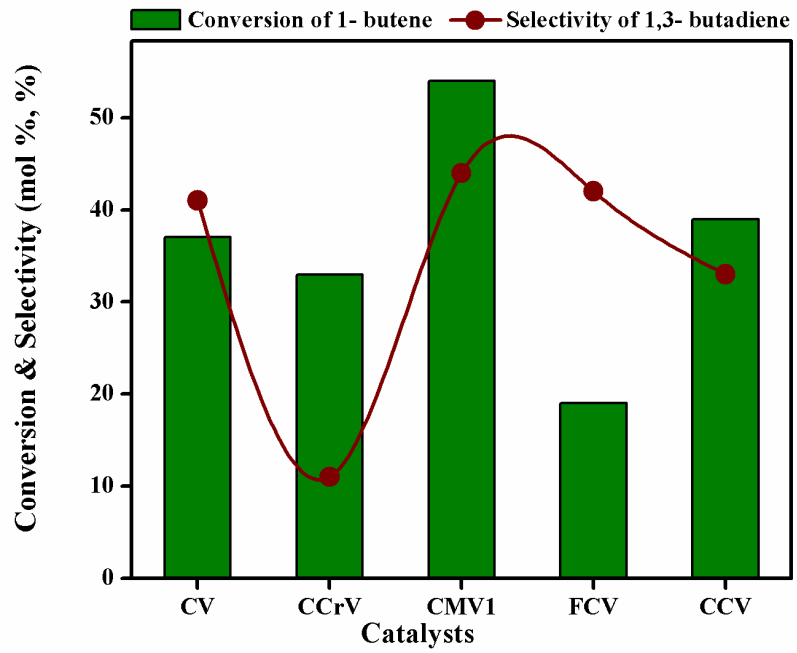

Fig. 5.11. Effect of transition metal substitution in $CeVO_4$ for ODH of 1-butene to 1,3-butadiene
Reaction conditions*:Total reactant flow 6000 h^{-1} (Ar:1-butene:O_2 - 8:1:1), at 400 °C and atmospheric pressure*

5.5.2.2. Effect of manganese loading

To optimize the amount of manganese loading in $CeVO_4$ three molar ratios (0.2,0.12,0.06-CMV1, CMV2, CMV3 respectively) of manganese substituted $CeVO_4$ was prepared and investigated for ODH of 1-butene (**Fig. 5.12**). All the catalysts were tested with the reactant flow 6000 h^{-1} (Ar:1-butene:O_2 - 8:1:1), temperature range between 350-450 °C and atmospheric

pressure. As the loading of manganese increased the conversion of 1-butene increased (at 400 °C) which is due to the increase of active redox sites of 'Mn' for reaction. Initially the selectivity towards 1,3-butadiene increased when the manganese loading was increased from 0.06 to 0.12 molar ratio and when the loading was further increased the selectivity towards 1,3-butadiene drastically decreased. This trend was also observed in other two temperatures (350 and 450 °C). At 400 °C with CMV2 as the catalyst a nominal conversion of 1-butene (50.5 %) and 70 % selectivity towards 1,3-butadiene was obtained. The product distribution at all temperatures for CMV2 is shown in **Fig. 5.13**, in which as the temperature increases the selectivity towards BD increases proportionally as conversion increases. The selectivity for 1,3-butadiene decreases with increase in temperature above 400 °C which is due to the total oxidation of 1-butene to CO_2 at higher temperatures which was evident from the increase in the selectivity of CO_2. Based on these studies it was observed that the optimized condition for increased activity for ODH of 1-butene using CMV as catalyst is 0.12 molar ratio loading of Mn and temperature 400 °C with 6000 h^{-1} total flow of reactants.

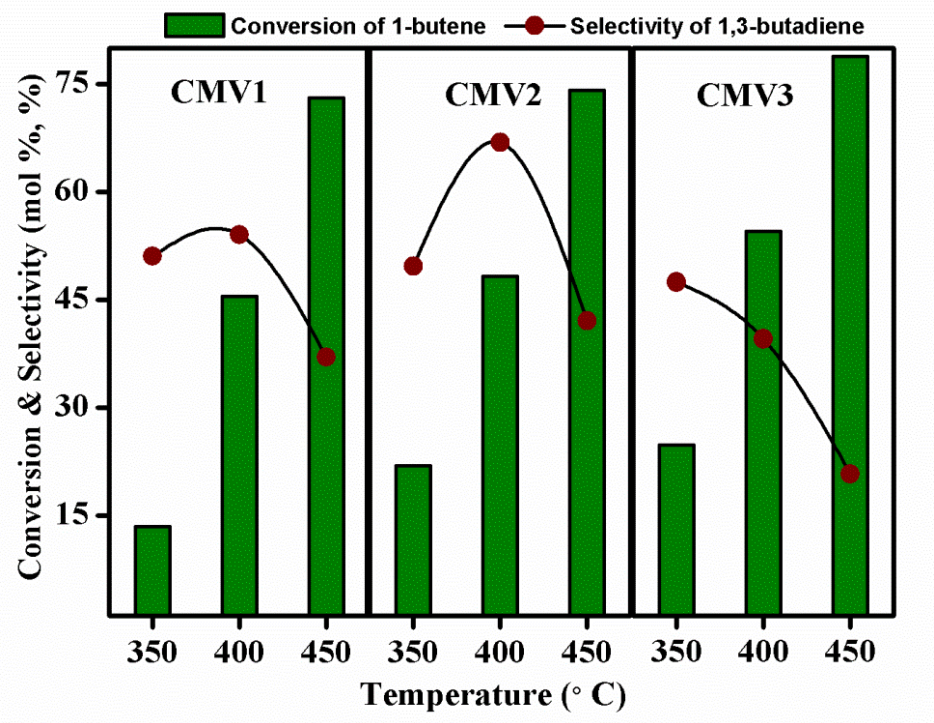

Fig. 5.12. Effect of manganese loading on ODH of 1-butene

Reaction conditions*:Total reactant flow 6000 h^{-1} (Ar:1-butene:O_2 - 8:1:1), at 350-450 °C and atmospheric pressure*

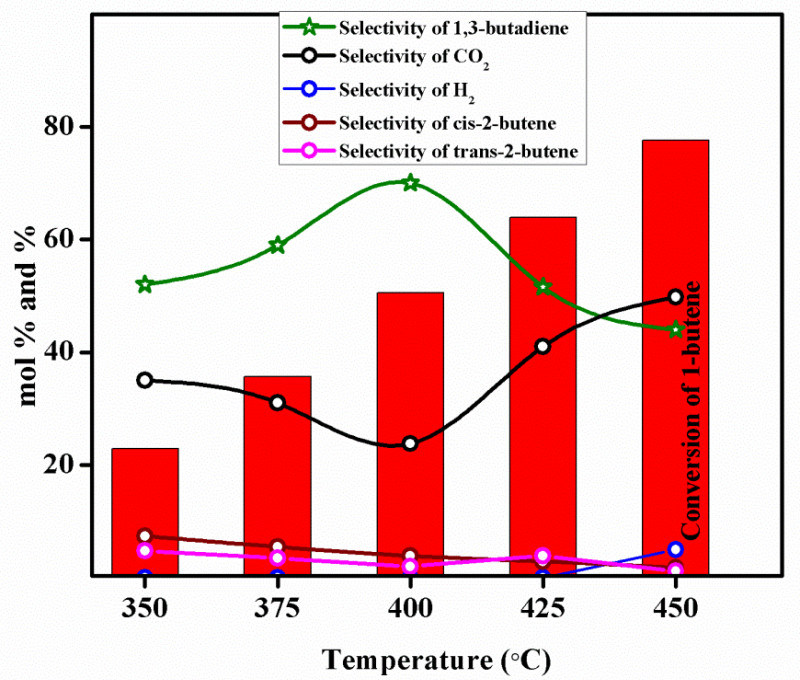

Fig. 5.13. Product distribution for ODH of 1-butene over CMV2 catalyst

Reaction conditions:*Total reactant flow 6000 h^{-1} (Ar:1-butene:O_2 - 8:1:1), at 350-450 °C and atmospheric pressure*

5.5.2.3. Effect of method of preparation

In order to emphasize the effect of method of preparation of CMV2, 'Mn' impregnated $CeVO_4$(Mn-imp $CeVO_4$) was prepared with the same loading of Mn that was substituted in $CeVO_4$. Both the catalysts were tested at same reaction conditions, the reactant flow 6000 h^{-1} (Ar:1-butene:O_2 - 8:1:1), at 400 °C and at atmospheric pressure. When CMV2 catalyst was employed the selectivity towards BD was higher than the combustion products like CO_2 and H_2.(**Fig. 5.14**) When the 'Mn' impregnated $CeVO_4$ was employed as a catalyst the selectivity towards total combustion products were higher when compared with CMV2 catalyst. As shown in **Fig. 5.14**, it is evident that the hydrogen selectivity from 1 % in CMV2 increases to 25 % in case of Mn-imp $CeVO_4$. This difference in activity is due to the formation of more CeO_2 crystallites on the surface of the CMV2 catalyst when compared to Mn-impregnated $CeVO_4$. The synergistic interaction of MnO_x and CeO_2 enables the formation of a -Mn-O-Ce- bond which greatly reduce the oxygen vacancies formed on the surface of the catalyst.[35] When the oxygen vacancies are reduced the over oxidation of hydrocarbons are minimized which in turn increases

the selectivity towards desired dehydrogenated products. This character of CMV2 helps in achieving an increased selectivity towards 1,3-butadiene with a nominal conversion of 1-butene.

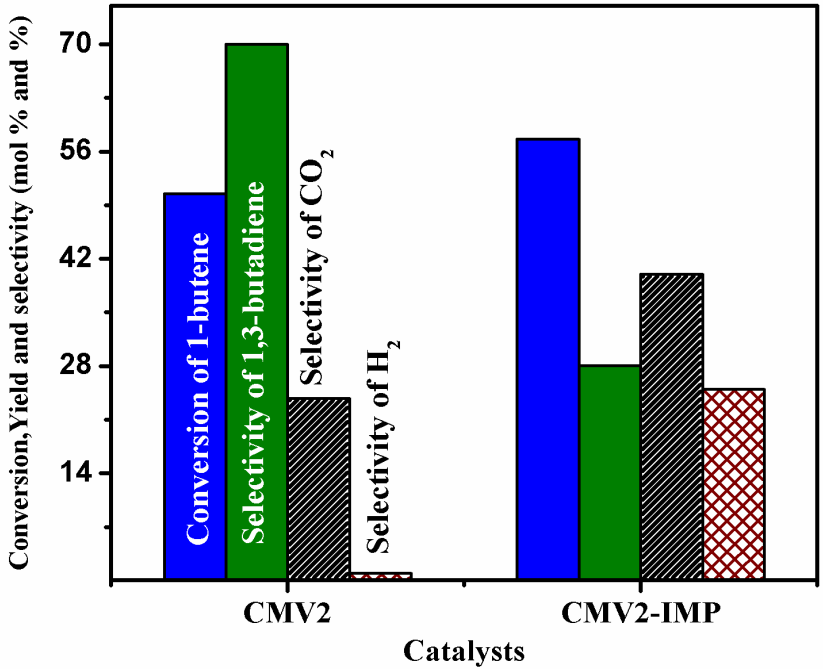

Fig. 5.14. Product distribution for ODH of 1-butene over CMV2 catalyst and Mn-impregnated $CeVO_4$

Reaction conditions**:** *Total reactant flow 6000 h^{-1} (Ar:1-butene:O_2 - 8:1:1), at 400 °C and atmospheric pressure.*

5.5.2.4. Spent Catalyst - TGA Analysis

To investigate the amount of coke deposited on the spent catalyst the catalyst after reaction was subjected to TGA analysis from room temperature to 800 °C in presence of air (**Fig. 5.15**). FCV showed a highest weight loss of 2.5 % when compared to all other catalysts that was studied. CMV catalysts showed lower weight loss when compared to all the other transition metal substituted $CeVO_4$ which supports the activity profile where the selectivity towards CO_2 was low. The CMV catalysts showed a weight gain which is likely due to the oxidation of Ce^{3+} which also suggests that there was very less coke deposition on these catalysts which was not even detectable. This supports the superior activity performance of the CMV2 catalyst when compared to other transition metal containing $CeVO_4$. Spent catalyst PXRD was also taken in which the $CeVO_4$ phase was intact with slight increase in the intensity of peaks corresponding to CeO_2.

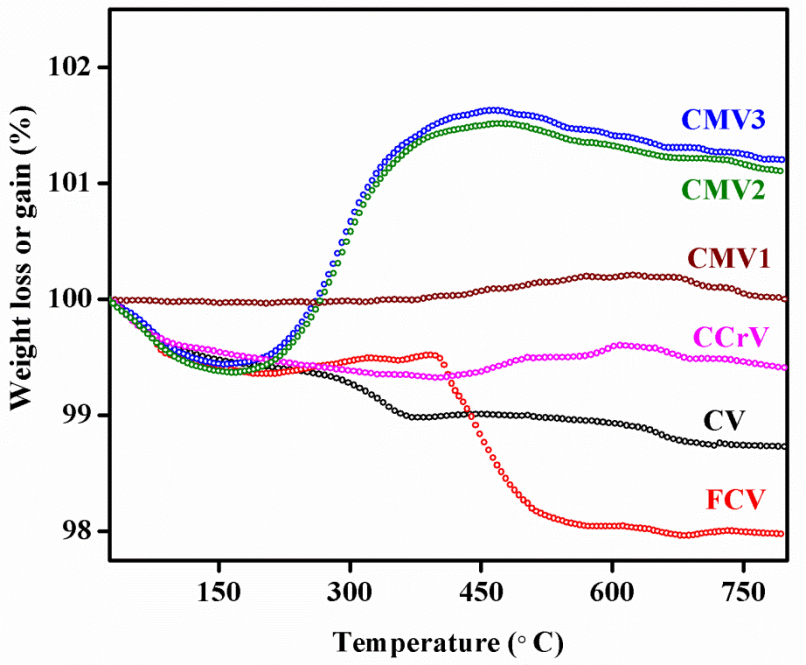

Fig. 5.15. TGA analysis of spent catalysts

5.6. Conclusions

$CeVO_4$ with various transition metals substituted in 'Ce' site were prepared by simple pH controlled precipitation followed by hydrothermal treatment. From PXRD it was evident that due to substitution, CeO_2 was formed on the surface of $CeVO_4$ which was very less in pure $CeVO_4$. Raman bands and transmission electron microscopy also support the information obtained from the PXRD pattern. From X-ray photoelectron spectroscopy the surface ratio of Ce^{4+}/Ce^{3+} was calculated for $CeVO_4$ and 'Mn' substituted $CeVO_4$ in which the ratio of Ce^{4+} is higher after incorporation of manganese. The $CeVO_4$ with 'Mn' showed a superior catalytic activity for ODH of 1-butene to 1,3-butadiene when compared to other transition metal substituted $CeVO_4$. From the optimization studies it was found that catalyst with 0.12 molar ratio of manganese gives a better selectivity (70 %) towards 1,3-butadiene at 400 °C. In this study a better activity was obtained compared to other catalysts reported for ODH of 1-butene and the improved selectivity in this process is achieved without usage of steam.

5.7. References

1. G. S. Whitby: Synthetic Rubber, John Wiley & Sons, New York, 1954, Chapter 2.
2. W.C. White, *Chem. Biol. Interact.,* 166 (2007) 10-14.
3. Chemicals and Petrochemical Manufacturer's Association, India.
4. G. Egloff, G. Hulla, *Oil Gas. J*.,41 (1942), 40.
5. A. Talalay, M. Magat, Synthetic Rubber from Alcohol, Interscience, New York 1945.
6. R. F. Goldstein and A. L. Waddams, The petroleum chemicals industry, E.&F.N. Spon LTD, London, 1967.
7. E V. Makshina, M Dusselier, W Janssens, J Degreve,P A. Jacobsa, B F. Sels, *Chem. Soc. Rev.*, 43(2014), 7917-7953
8. R. G. Craig, J. M. Duffalo, *Chem. Eng. Prog*.75 (1979), 62.
9. R. G. Craig, E. A. White, *Hydrocarbon Process*. 59 (1980), 111.
10. K. K. Kearby: "Catalytic Dehydrogenation,"in: Catalysis, vol. 3, Reinhold, New York 1955.
11. F Cavani, F Trifiro, Selective Oxidation of C4Paraffins.*Catalysis*; Specialist Periodical Report; Royal Society of Chemistry: Cambridge, 11(1994), 246-317
12. J. C. Jung, H. Lee, H. Kim, Y.M. Chung, T. J. Kim, S. J. Lee,S. H. Oh, Y. S. Kim, Song, *J. Mol. Catal. A*, 271(2007), 261-265.
13. A. P. V. Soares, L. D. Dimitrov, M. C. R. A. de Oliveira, L. Hilaire, M. F. Portela, R. K. Grasselli, *Appl. Catal. A*, 253(2003), 191-200.
14. Ph. A. Batist, C. G. M. van de Moesdijk, I. Matsuura, G.C. A. Schuit, *J. Catal*., 20 (1971), 40-57.
15. S Furukawa, M Endo, T Komatsu, *ACS Catal.*, 4(2014), 3533-3542.
16. Y. She, J. Han, Y. H. Ma, *Catal. Today*, 67 (2001), 43-53.
17. K. Fujimoto, T. Kunugi, *Ind. Eng. Chem. Prod. Rd.*, 20(1981),319-323.
18. J. C. Jung, H. Lee, J. G.Seo, S. Park, Y-M. Chung, T. J. Kim, S. J. Lee, S-H Oh, Y. S. Kim, I. K. Song, *Catal. Today*,141 (2009) 325-329.
19. J-H Park, H Noh, J W Park, K Row, K D Jung, C-H Shin, *Appl. Catal. A*, 431-432 (2012) 137-143.
20. J-H Park, K Row, C-H Shin, *Catal. Comm*., 31 (2013), 76-80.
21. C Wan, D-gCheng, F Chen, X Zhan, *Chem. Eng. Sci*.,135(2015), 553-558.
22. J-H Park, C-H Shin, *Appl. Catal. A*, 495 (2015), 1-7.

23. C Wan, D-g Cheng, F Chen, X Zhan, *Catal. Today*, 264 (2016) 180-184.
24. SGillot, J-PDacquin, CDujardin, P Granger, Top Catal., 59 (2016), 987-995.
25. F Luo, C-J Jia, R Liu, L-D Sun, C-H Yan, *Mater. Res. Bull.*, 48 (2013) 1122-1127.
26. C. C. Santos, E. N. Silva, A. P. Ayala, I. Guedes, P. S. Pizani, C.-K. Loong, L. A. Boatner, *J. Appl. Phys*., 101 (2007), 053511.
27. T. Hirata, A. Watanabe, *J. of Solid State Chem*., 158 (2001), 264-267.
28. A K Venugopal, A T Venugopalan, P Kaliyappan, T Raja, *Green Chem*., 15(2013), 3259-3267
29. H Lee, J Kang, M S Cho, J-B Choi, Y Lee, *J. Mater. Chem*., 21(2011),18215-18219.
30. J Hou, H Huang, Z Han, H Pan, *RSC Adv*., 6(2016), 14552-14558
31. P Ju ,Y Yu , M Wang, Y Zhao, D Zhang, C Sun, X Han, *J. Mater. Chem*. B, 4(2016), 6316-6325
32. A. Pfau and K. D. Schierbaum, *Surf. Sci.*, 321(1994), 71-80.
33. T.V. Choudhary, S. Banerjee, V.R. Choudhary, *Appl. Catal. A*, 234(2002), 234, 1-23.
34. J S Yoon, Y-S Lim, B H Choi, H J Hwang, *Int. J. Hydrogen Energy*, 39(2014), 7955-7962
35. P Zhang, H Lu, Y Zhou, L Zhang, Z Wu, S Yang, H Shi, Q Zhu, Y Chen, S Dai, *Nature Comm*., Article.No. 8446 (2015)

Chapter 6: Summary and Conclusions

At the end of all chapters in a dissertation it is obligatory to summarize the research work undertaken for the advantage of the reader. Hence, this chapter summarizes the conclusions reached based on the experimental results during these investigations. Understanding the structure activity relationship is a key phenomenon in development of a catalytic processes. Physicochemical characterizations and surface sensitive techniques helps in identifying the properties of the catalyst which can be tailored to increase or tune the efficiency of the catalytic activity. This thesis has covered the synthesis and characterization of three different catalytic systems and their workability for the ODH of three different substrates. Specific properties of the catalyst which drives in the overall activity was understood and discussed.

Chapter 1: Introduction

This chapter provides a general and brief introduction about catalysis and its history. The current processes used for production of olefins from respective hydrocarbons that are carried out commercially are discussed with their shortcomings. The importance of ODH is been put forth along with their benefits when compared to conventional and existing processes. A detailed overview of the mixed metal oxide systems that was employed for our studies with their structure and synthesis pathways is discussed.

Chapter 2: Catalyst synthesis and experimental techniques for characterization

The catalyst synthesis methods and the physicochemical techniques used to evaluate the catalysts are discussed in detail. The catalysts that were synthesized are perovskite type mixed oxides, mixed oxide derived from hydrotalcite and transition metal substituted cerium orthovanadates. The characterization studies used for studying these materials were carried out by Powder X-ray diffraction, BET surface area measurement, TPD, TGA, XPS, EDAX etc. For each technique, theory and experimental procedure have been described.

Chapter 3: Oxidative dehydrogenation of ethane to ethylene over Manganese substituted $Ca(Sr)TiO_3$ perovskite type oxides

In this chapter the commercial importance of ethene and the existing processes for production are discussed in brief with illustrations. Literature overview for ODH of ethane to ethylene with

pros and cons of reported catalytic systems. An exhaustive investigation of the $Ca(Sr)TiO_3$ perovskite type catalyst using various characterization techniques to study their structure and morphology. Various molar ratios of manganese substituted $Ca(Sr)TiO_3$ perovskites were prepared by simple citric acid gel method. Structural refining and lattice parameters were derived for all the synthesized samples. XPS was used to find the surface changes at various temperatures and extending it to correlate with the activity profile obtained. From XPS analysis of $Sr_{0.5}Ca_{0.5}Ti_{0.9}Mn_{0.1}$(SC5TM), it was evident that the 'Mn' species exist in lower oxidation state at the temperature range of 450-550 °C which drive for more of total combustion of ethane which was also evidenced in catalytic activity. SC5TM shows a stable catalytic activity up to 24 hours without any significant loss. Spent catalyst TGA analysis was also done to correlate the long term stability of the optimized catalyst.

Chapter 4: Oxidative dehydrogenation of ethyl benzene (EB) to styrene (ST)

Literature background of the commercial and existing catalytic systems for ODH of EB to ST along with the commercial importance of ST and its polymers was elaborately discussed.

Part A of this chapter deals with understanding the role of basicity, reducibility, oxygen storage capacity and metal surface concentration in obtaining a better activity for ceria incorporated mixed oxide derived from hydrotalcites. Cerium containing mixed oxides derived from a hydrotalcite precursor was prepared from a simple co-precipitation followed by hydrothermal treatment. The morphological studies show evenly distributed ceria crystallites at lower loading of cerium. The catalyst with 0.03 mol % of cerium shows the highest conversion (49.4 %) when compared to all the compositions prepared and showed 72 hours stable activity at optimized reaction conditions. The spent catalyst TGA analysis was done to demonstrate that to have less coke and stable activity of the catalyst, an optimal temperature with a suitable flow of oxygen is required for good conversion and also in regenerating the catalyst during the reaction for longer time.

Part B of this chapter emphasizes the role of manganese in $Ca/SrTiO_3$ perovskites for obtaining a fairly better activity towards EB to ST. $Sr_{0.5}Ca_{0.5}Ti_{0.9}Mn_{0.1}$(SC5TM) prepared by glycine combustion showed slightly higher activity when compared to citrate gel method prepared SC5TM. For the active catalyst that obtained from initial screening was investigated under varying reaction conditions like temperature, reactant flows, oxidants, different metal proportions and other metal substitution. The best results observed for the ODH of EB on the

catalyst SC5TM (0.5:0.5:0.1:0.9) were prepared by glycine combustion and tested under steady EB flow LHSV 3 h^{-1} and GHSV 2400 h^{-1} with respect to oxygen at 500 °C and at atmospheric pressure.

Chapter 5: Oxidative dehydrogenation of 1-butene to 1,3-butadiene over Cerium orthovanadates

In this chapter the importance of 1,3-butadiene and the drawbacks of the reported catalysts was discussed. Synthesizing and systematically studying the role of hetero cations like Cr, Mn, Fe and Co in cerium orthovanadates in promoting the activity of the catalyst. The formation of CeO_2 crystallites on the surface of $CeVO_4$ was evidenced by PXRD and Raman spectroscopy studies. The surface ratio of Ce^{4+}/Ce^{3+} was calculated after deconvolution of Ce 3d core X-ray photoelectron spectra of pure $CeVO_4$ and with 'Mn' substitution. Understanding the role of 'Mn' in improving the activity of orthovanadates and tuning other parameters for better and selective activity for ODH of 1-butene to 1,3-butadiene. Further activity studies were carried out to optimize the manganese loading and catalytic activity of optimized composition which was compared with Manganese impregnated $CeVO_4$.

The synthesis of catalytic system with tailored properties for specific substrate is required in ODH reaction as those specific properties tune and drive the catalytic activity. By understanding this concept we were fairly successful in increasing the energy efficiency, as the reaction were carried out with a comparatively lower temperature than the commercial process with a long term stable catalytic activity.

Scope for Future research

The present work summarizes the development of catalysts for the ODH of hydrocarbons with oxygen as the oxidant. Among the oxidants used for oxidants oxygen is preferred, as it serves dual purpose: for driving the reaction and rejuvenating the catalyst by burning the coke formed on the surface. However in some processes oxygen induces cracking of hydrocarbon at high temperatures. In order to overcome this drawback soft oxidants like CO_2 and N_2O can be employed, as these oxidants do not induce cracking and the usage of these green house gases is also an environment benign pathway.

List of publications

- Oxidative dehydrogenation of ethyl benzene to styrene over hydrotalcite derived cerium containing mixed metal oxides

  Ashok Kumar V, Aswathy T V, Periyasamy K and T Raja, *Green Chem*., 15(2013), 3259-3267

- Probing the structure activity relationship of Manganese substituted $Ca(Sr)TiO_3$ perovskites for Oxidative dehydrogenation of ethane to ethene

  Ashok Kumar V, Aswathy T V, T Raja

  (***communicated***)

- Renewable fuels from biomass-derived compounds: Ru-containing hydrotalcites as catalysts for conversion of HMF to 2,5-dimethylfuran

  Atul S. N, **Ashok Kumar V**, Nishita L, M Manikandan, Raja T and Satyanarayana C, *Catal. Sci. Technol*., 5(2015), 1463-1472

- An efficient robust fluorite $CeZrO_{4-\delta}$ oxide catalyst for the eco-benign synthesis of styrene

  K Periyasamy, Aswathy T V, **V Ashok kumar**, M Manikandan, R Shukla, A K. Tyagi and T Raja, *RSC Adv*.,5(2015), 3619-3626

- Promotional effect of Fe on performance of supported Cu catalyst for ambient pressure hydrogenation of furfural

  M Manikandan, **Ashok Kumar V**, Atul S. N, Satyanarayana C and T Raja, *RSC Adv*., 6(2016), 3888-3898

- Role of surface synergistic effect on the performance of Ni-basedhydrotalcite catalyst for highly efficient hydrogenation of furfural

  M Manikandan, **Ashok Kumar V**, K Prabu, R K Jha, T Raja, *J. of Mol. Catal. A*, 417 (2016) 153-162

- Effective and selective oxidation of 2-butanol over Mn supported catalyst systems

  K Prabu, M Prabu, **Ashok Kumar V**, Aswathy T V, W.V.Y. S Sandilya, C S. Gopinath, T Raja, *Appl. Catal. A*, 525(2016) 237-246.

List of patents

- Ni containing anionic clays as hydrogenation catalysts , T Raja, M Manikandan, **Ashok Kumar V,** Patent No. WO2015198351A2
- Novel improved process for conversion of Alkanes to Alkenes, T Raja, **Ashok Kumar V,** Aswathy T V, M Prabu, K Prabu.**(**Patent filed- Provisional filing no. 201611038068**)**